

6-17-2019

Neurostimulator with Waveforms Inspired by Nature for Wearable Electro-Acupuncture

Jose Aquiles Parodi Amaya
Louisiana State University and Agricultural and Mechanical College

Follow this and additional works at: https://repository.lsu.edu/gradschool_dissertations



Part of the [Alternative and Complementary Medicine Commons](#), [Bioelectrical and Neuroengineering Commons](#), [Biomedical Devices and Instrumentation Commons](#), [Electrical and Electronics Commons](#), [Other Analytical, Diagnostic and Therapeutic Techniques and Equipment Commons](#), and the [Small or Companion Animal Medicine Commons](#)

Recommended Citation

Parodi Amaya, Jose Aquiles, "Neurostimulator with Waveforms Inspired by Nature for Wearable Electro-Acupuncture" (2019). *LSU Doctoral Dissertations*. 4969.
https://repository.lsu.edu/gradschool_dissertations/4969

This Dissertation is brought to you for free and open access by the Graduate School at LSU Scholarly Repository. It has been accepted for inclusion in LSU Doctoral Dissertations by an authorized graduate school editor of LSU Scholarly Repository. For more information, please contact gradetd@lsu.edu.

NEUROSTIMULATOR WITH WAVEFORMS INSPIRED BY NATURE FOR WEARABLE
ELECTRO-ACUPUNCTURE

A Dissertation

Submitted to the Graduate Faculty of the
Louisiana State University and
Agricultural and Mechanical College
in partial fulfillment of the
requirements for the degree of
Doctor of Philosophy

in

The Division of Electrical and Computer Engineering

by

Jose Aquiles Parodi Amaya
B.Sc., Louisiana State University, 2013
M.Sc., Louisiana State University, 2015
August 2019

ACKNOWLEDGEMENTS

This thesis is dedicated to God, my beautiful and supportive wife Maria, and my parents. They have supported me throughout all my studies and have been there for me through thick and thin. They have always been a refuge for me when times were tough, and have shown me the amazing life that waits for me after graduation.

I also want to thank Dr. Jin-Woo Choi for taking me in as a graduate student with a risky idea. He taught me all the lessons related to a doctoral study, and was instrumental in my professional development as a scientist. With his support I was able to continue my professional development at LSU, and for that I am immensely grateful.

I would also like to give a special thanks my colleagues and labmates: Tallis Huther da Costa, Glenn Shin, Hamed Shamkhalichenar, Pedro Chacon, Eddie Austin, Jong-Joon Park, Ryan Tortorich, and Dr. Edward Song. I know that your future careers are bright, and the work we all have done in this lab will be a testament to our commitment to unsurpassed quality, resolute integrity, and unparalleled potential.

TABLE OF CONTENTS

ACKNOWLEDGEMENTS.....	ii
LIST OF TABLES.....	v
LIST OF FIGURES.....	vi
ABSTRACT.....	viii
1. INTRODUCTION.....	1
1.1. Motivation.....	1
1.2. Objectives.....	4
1.3. Dissertation Outline.....	7
2. EFFECTS OF WAVEFORM PARAMETERS ON NEUROSTIMULATION OUTCOMES.....	8
2.1. Introduction.....	8
2.2. Overview of Neurostimulation and Neuromodulation.....	8
2.3. Transcranial Electrical Stimulation.....	10
2.4. Deep Brain Stimulation.....	21
2.5. Vagus Nerve Stimulation.....	22
2.6. Electro-Acupuncture.....	26
2.7. Conclusions.....	28
3. PULSE GENERATION CIRCUIT FOR NOVEL STIMULATION WAVEFORMS.....	32
3.1. Introduction.....	32
3.2. Review of State-of-the-Art.....	33
3.3. Circuit for Pulse Generation.....	34
3.4. Circuit Analysis.....	40
3.5. Power Analysis.....	44
3.6. Characterization Procedures of the Pulse Generator.....	46
3.7. Measured Results.....	48
3.8. Conclusions and Improvements for Circuit.....	59
4. WEARABLE SMARTPHONE-COMPATIBLE ELECTRO-ACUPUNCTURE NEUROSTIMULATOR FOR ENHANCED CLINICAL AND SCIENTIFIC OUTCOMES.....	62
4.1. Introduction.....	62
4.2. Acupuncture Background and Design Problem.....	62
4.3. Design of Electro-Acupuncture Circuit.....	64
4.4. Measurement Results and Discussion.....	68
4.5. 2-Channel Implementation.....	74
4.6. Conclusions.....	77
5. ARDUINO SOFTWARE AND HARDWARE AND ANDROID STUDIO SOFTWARE.....	80

5.1.	Introduction	80
5.2.	Arduino Programming.....	80
5.3.	Android Programming.....	84
5.4.	Conclusions	86
6.	SUMMARY AND CONCLUSIONS.....	88
6.1.	Review of Neurostimulation Literature Focusing on Waveforms and Parameters.....	88
6.2.	A Pulse Generation Circuit for Novel Stimulation Waveforms.....	90
6.3.	Wearable Smartphone-Compatible Electro-Acupuncture Neurostimulator for Enhanced Clinical and Scientific Outcomes	90
6.4.	Arduino and Android Studio Software.....	91
7.	SUGGESTIONS FOR FUTURE WORK.....	93
7.1.	Biphasic Signal Generation.....	93
7.2.	Improvements to Electro-Acupuncture Stimulator System	93
	APPENDIX A: CAT STUDY PROTOCOL IACUC APPROVAL.....	97
	APPENDIX B: FIGURE PERMISSIONS.....	98
	REFERENCES	105
	VITA.....	119

LIST OF TABLES

Table 2.1. tACS studies showing brain oscillation entrainment.	16
Table 2.2. tACS studies showing contradictory results to brain oscillation entrainment.	17
Table 2.3. tRNS studies showing observed stimulation outcomes.	20
Table 3.1. Circuit characterization components.	48

LIST OF FIGURES

Figure 2.1. Comparison between stimulation waveforms used in TES for tDCS, tACS, and tRNS.	11
Figure 2.2. Detail of stimulation waveforms used in various studies.	13
Figure 2.3. Detail of stimulation waveforms used in various studies and their approximate time derivatives (dashed).....	14
Figure 2.4. Phase shifted tACS protocols utilized by Vossen [76].....	18
Figure 2.5. Efficient neurostimulation waveforms produced by genetic algorithm in Wongsarnpigoon [45].....	23
Figure 2.6. Simulated effects of tissue capacitance on stimulation voltages and nerve activation thresholds.....	24
Figure 2.7. Anatomical tissue computational model developed by Mourdoukoutas [98] to simulate current paths from VNS applied using surface electrodes.....	26
Figure 2.8. Tissue voltage waveform comparison between ideal implantable pulse generator (Ideal), and an adjusted implantable pulse generator model (IPG).....	30
Figure 3.1. Overview of an envisioned circuit that allows different pulse outputs depending on circuit design.	35
Figure 3.2. Overview of pulse generator circuitry and pulse generation phases.	38
Figure 3.3. An example input and output signal.....	41
Figure 3.4. Circuit models for analysis.....	41
Figure 3.5. Charging phase equivalent circuit for power analysis.....	45
Figure 3.6. Simulations of component effects on input power consumption.	47
Figure 3.7. Circuit output showing circuit voltages and four operational phases.	50
Figure 3.8. Characterization results for increasing C_2 or as κ is decreased.	51
Figure 3.9. Circuit output signal with increasing R	52
Figure 3.10. Characterization results of circuit output pulse with increasing Rp	53
Figure 3.11. Measured results for the circuit with a variable output pulse frequency.....	54
Figure 3.12. Characterization results for increasing load capacitance.....	55

Figure 3.13. Characterization results for increasing load resistance.	56
Figure 3.14. Characterization results for increasing C_2 in PBS solution.	57
Figure 3.15. Characterization results for increasing R in PBS solution.....	58
Figure 4.1. Comparison between features of proposed system, and problems with current commercial stimulators.	64
Figure 4.2. Electro-acupuncture circuit design.	65
Figure 4.3. Stimulation pulse output circuits showing boost converter and HV switch layout, and microprocessor I/O.	66
Figure 4.4. Design of PCB and case.	67
Figure 4.5. Smartphone app images.....	69
Figure 4.6. Output voltage measurements using smartphone control via Bluetooth.	69
Figure 4.7. Stimulation measurements using smartphone control via Bluetooth over a range of stimulation frequencies.	70
Figure 4.8. Output voltage measurement with acupuncture needles as electrodes and PBS 1X as load.....	72
Figure 4.9. Animal experimental results of using reduced doses of atipamezole hydrochloride and acupuncture for anesthesia recovery.	74
Figure 4.10. Multi-channel device block diagram.	75
Figure 4.11. 2-channel device design.	77
Figure 4.12. Oscilloscope voltage measurements and calculated 2-channel system output.....	78
Figure 5.1. Software and hardware block diagrams showing serial communications between the microprocessor and Bluetooth module, and wireless communications between the smartphone and Bluetooth module.....	81
Figure 5.2. Android layout for 2-channel device.....	86

ABSTRACT

The work presented here has 3 goals: establish the need for novel neurostimulation waveform solutions through a literature review, develop a neurostimulation pulse generator, and verify the operation of the device for neurostimulation applications.

The literature review discusses the importance of stimulation waveforms on the outcomes of neurostimulation, and proposes new directions for neurostimulation research that would help in improving the reproducibility and comparability between studies.

The pulse generator circuit is then described that generates signals inspired by the shape of excitatory or inhibitory post-synaptic potentials (EPSP, IPSP). The circuit analytical equations are presented, and the effects of the circuit design components are discussed. The circuit is also analyzed with a capacitive load using a simplified Randles model to represent the electrode-electrolyte interface, and the output is measured in phosphate-buffered saline (PBS) solution as the load with acupuncture needles as electrodes. The circuit is designed to be used in different types of neurostimulators depending on the needs of the application, and to study the effects of varying neurostimulation waveforms.

The circuit is used to develop a remote-controlled wearable veterinary electro-acupuncture machine. The device has a small form-factor and 3D printed enclosure, and has a weight of 75 g with leads attached. The device is powered by a 500 mAh lithium polymer battery, and was tested to last 6 hours. The device is tested in an electro-acupuncture animal study on cats performed at the Louisiana State University School of Veterinary Medicine, where it showed expected electro-acupuncture effects. Then, a 2-channel implementation of the device is presented, and tested to show independent output amplitude, frequency, and stimulation duration per channel.

Finally, the software and hardware requirements for control of the wearable veterinary electro-acupuncture machine are detailed. The number of output channels is limited to the number of hardware PWM timers available for use. The Arduino software implements PWM control for the output amplitude and frequency. The stimulation duration control is provided using software timers. The communications protocol between the microcontroller board and Android App are described, and communications are performed via Bluetooth.

1. INTRODUCTION

1.1. Motivation

Neurostimulation is a growing field that applies knowledge from the historically distinct fields of engineering, medicine, and biology to enhance the lifestyle of individuals. Neurostimulation has applications in prosthetic limb control, rehabilitation and physical therapy, neural pacemaker and control, and recently in cognitive enhancements and treatment of neurological conditions such as Alzheimer's, Parkinson's, and epilepsy. Neurostimulation has been regarded to be in the future of medical treatments [1-3]. The myriad applications and variety of technology and fields involved in neurostimulation has sparked interest in the scientific community to study how to improve neurostimulation devices and methodologies, and to discover new applications. Neurostimulation devices range from implantable pacemakers and vagal nerve stimulators, to transcutaneous electrical nerve stimulation devices and wireless stimulators. Studies in methodologies seek to find the optimal stimulation parameter combinations for treatment of specific conditions, and how these specific stimulation parameters affect treatment outcomes. Stimulation parameters include signal waveform, amplitude, frequency of stimulation, and duration of stimulation. In this work we seek to make a contribution to this field by developing a device that implements a novel stimulation waveform, and we carry out a preliminary study into the applications for this novel waveform.

Neurostimulation is a multidisciplinary field that focuses on delivering controlled signals to the nervous system for therapy or enhancement. Neurostimulation treatment has several advantages over conventional pharmacological treatment: specificity, reduced side-effects, and novel solutions to chronic conditions such as hypertension, epilepsy, and rheumatoid arthritis [1]. The methods for neurostimulation include mechanical, ultrasound [4], optogenetics [5], and electrical [3]. Electrical neurostimulation has been the subject of intense research in the 20th and

21st centuries. Electrosleep, a form of transcranial electrical stimulation, was proposed in 1902 to cause patients to fall asleep [6]. In 1938 the vagus nerve of cats was stimulated in an effort to visualize the coordinated activity of the brain [7]. As early as 1957, electrical stimulation was being used in patients to allow for external cardiac pacing, and later in 1958 the first wearable and implantable cardiac pacemakers were successfully tested [8]. Transcranial electrical stimulation on several areas of the brain was carried out in healthy subjects in a report from 1980 [9]. In recent years, electrical neurostimulation has been posited as the future of comprehensive medical treatment under the umbrella term “electroceuticals” [1-3, 10].

Neurostimulation has demonstrated capabilities to alter the compound action potentials and long-term potentiation behavior of complex neural networks even at low stimulation intensities [11] via an effect termed neuromodulation. Neuromodulation has been observed at all levels, from individual nerve cells to brain regions, including the synapses [12]. Neuromodulation has shown promise in the fields of neuroprostheses, where it can be used to enhance the learning rate of the use of neuroprosthetic devices [13, 14], and cognitive enhancement, where a person can achieve improved learning rates of complex tasks [15, 16]. This effect is thought to arise from action potentials (APs) that are modulated as they propagate through individual nerve cells depending on the nerve cell’s properties at the level of the soma, [17], axon [18], and transmembrane proteins [19]. This modulation can be enhanced or inhibited with neurostimulation [16]. Modulation of AP firing rate and the AP waveform at the presynaptic cell such that the excitatory and inhibitory postsynaptic potentials (EPSPs and IPSPs) are changed allows for modulation of excitatory and inhibitory transmission at the postsynaptic cell [19, 20].

The challenges of stimulation waveform design involve the diverse options and requirements for each anatomical stimulation target [21], the undetermined long-term effects of

neurostimulation, the diversity of tissue, organ, and patient-level reactions, the unknown neural mechanisms involved [22], and the unknown side effects of stimulation methodology [23]. Additionally, differences in stimulation waveforms [24], the polarity of current and direction [25], electric field shape and direction [26], and the temporal pattern of stimulation [27] have been shown to have effects on the outcome of stimulation. We do not address all these challenges in this work, and we limit our approach to specific problems related to neurostimulation device design that affect stimulation waveform. The parameters of electrical stimulation waveforms such as the waveform type, amplitude, width and frequency of stimulation have been shown to affect prosthetic sensory information in the vestibular nerve [28], the rate of excitation of individual nerves [29] and nerve bundles [30], and the spatial selectivity within the bundles [31].

Our review found a diversity of effects in transcranial electrical stimulation (TES) using direct current, alternating current, or random noise as stimulation signal [32-35]. This could indicate that the rate of change of the stimulation waveform is a factor in the outcomes of stimulation. This effect may not be apparent in single neuron measurements, as TES is used on intact brains, although [36] briefly discusses voltage rate of change as being a parameter in the degree of activation of sodium channels in subthreshold synaptic potentials. Furthermore, we found replicate studies by different groups which led to different outcomes in TES effects where the primary difference between experimental procedures was stimulation waveform shape [37-39]. Stimulation waveforms have been studied for their effects in neurostimulation. These include square or rectangular [31, 40], exponential, ramp [41], sinusoidal [26, 42, 43], triangle, and Gaussian [44, 45] waveforms. To the best of our knowledge, there have not been any devices specifically designed to output signals that have waveforms with shape inspired by nature. We think EPSPs may provide an advantage over other signal waveforms such as square and

rectangular due to their constant rate of change throughout the duration of the pulse. Additionally, there have been few *in-vivo* or *in-vitro* studies verifying the effects of waveforms with shapes inspired by nature. What we have found in previous literature is an *in-vitro* study showing evidence that stimulation with signals that look like EPSPs affects transmembrane proteins kinetics [36]. Furthermore, there is a lack of sufficient scientific evidence on the role that stimulation waveforms and patterns play on neuromodulation and plasticity [24, 25, 27], such that there is a need for novel stimulation waveforms to determine the effects and capabilities of electrical stimulation. Thus, we choose to design a pulse generator that produces signals with shape inspired by nature and are similar to the shape of EPSPs for investigation of the effect of different waveforms on neurostimulation.

1.2. Objectives

The objective of this work is to present a novel type of neurostimulator device, and test its application as a neurostimulation solution. This work has three main parts: establish the need for novel stimulation waveforms through a comprehensive literature review, development of a neurostimulation device, and verification of the operation of the device for neurostimulation applications. The specific work performed in each part is described in the following sections.

1.2.1. Review of Waveform Parameters and Their Effects in Neurostimulation

The selection of the stimulation waveform will determine the design of the neurostimulator device. First, the effects of different stimulation waveforms on the outcomes of stimulation must be determined. We narrow the field of review to epidermal stimulation methods, transcutaneous methods, and implantable or direct contact nerve stimulation methods.

State-of-the-art reports and studies on transcranial electrical stimulation (TES), deep brain stimulation (DBS), vagal nerve stimulation (VNS), and electro-acupuncture (EA) are reviewed for evidence of waveform effects. The interest of the scientific community on the effects of stimulation

parameters on outcomes are assessed. The use of simulations and computer models are also important, since it is impossible to study each combination of stimulation parameter and physiological condition. The current state-of-the-art of computer models utilized for studying stimulation parameters is reviewed. Lastly, electro-acupuncture will be reviewed from the perspective of neurostimulation.

1.2.2. Development of Pulse Generator Circuit

The first step in developing a neurostimulator is to review the state-of-the-art to assess drawbacks of current technology to improve on them. We first assess the challenges of neurostimulator design, and determine we can provide a novel approach for scientists that are not experts in electronics by implementing a circuit with few design components while still maintaining versatility in stimulation signal design.

The circuit analytical equations are derived to allow accurate design of output pulse signals for diverse applications. Equations are derived to find the output pulse amplitude, output pulse width or duration, and approximate the limit of stimulation frequency. The analytical expressions are compared with mathematical equations found in the literature that define voltage waveforms found in nature. The analytical expressions were also derived for a circuit output when the load is a simplified Randles model representative of electrode-electrolyte interface.

The device is then characterized to verify the accuracy of the analytical expressions, and to verify the role of the design components in modifying the stimulation parameters: output pulse amplitude, output pulse width, and stimulation frequency. The circuit output was also measured in phosphate-buffered (PBS) saline solution with acupuncture needles as electrodes.

1.2.3. Neurostimulator for Remote-Controlled Wearable Veterinary Electro-Acupuncture

We considered electro-acupuncture a viable target for our pulse generator design. Commercial machines for electro-acupuncture (EA) are large, benchtop devices that can be improved with modern wireless technology and smartphone compatibility. These machines are acceptable for human electro-acupuncture, as human patients are compliant and can readily follow instructions. The case is different for veterinary applications where an animal may feel stressed in a different environment, and may react unexpectedly to EA procedures. In this case, it is better for the EA stimulator to be small and wearable by the animal, so that the animal can move around and be relaxed during EA treatment.

We determine that the neurostimulator must be implemented in a small and light-weight format to allow for small animals such as cats to wear the device. The commercial device operation is measured and we used this to design the stimulation waveform parameters: maximum amplitude, frequency band, and waveform width. A boost converter with voltage output control via pulse-width modulation (PWM) was used as the input source for the neurostimulator, and a high-side switch was utilized to allow for the gating the high-voltage input to the neurostimulator pulse generator. The neurostimulator signal parameter controls are coupled to a microcontroller which manages communication to a Bluetooth module for control via smartphone. The device was tested in an EA study conducted at the Louisiana State University School of Veterinary Medicine to verify operation as an EA stimulator. The device was constructed in a 2-channel implementation, and independent output amplitude, stimulation frequency, and stimulation duration control was verified using the current electronic design.

1.3. Dissertation Outline

Chapter 2 contains the literature review performed to identify the need for research in stimulation waveforms. The evidence showing the diverse effects of various stimulation waveforms is discussed, and the interest in the field for stimulation parameter studies and tissue models. Chapter 3 presents the development of a pulse generator circuit for neurostimulator device applications. The analytical equations are presented for accurate waveform design for specific applications. Chapter 4 discusses the application of the neurostimulator for EA, and addition of features that allow for wireless control of the device for wearable applications. Chapter 5 discusses the software and hardware requirements of the neurostimulator device. The last chapter summarizes the main contributions of this work and proposes future directions for this work.

2. EFFECTS OF WAVEFORM PARAMETERS ON NEUROSTIMULATION OUTCOMES

2.1. Introduction

As previously discussed in chapter 1, neurostimulation technology has applications in treatment of medical conditions, rehabilitation, and cognitive enhancement. The challenges of neurostimulator design were briefly discussed, and it was mentioned that stimulation waveform and stimulation parameters play a significant role in neurostimulation outcomes. A review of neurostimulation research with a focus on stimulation waveform and stimulation parameters is presented in this section. In this manner we establish the stimulation waveform selection and design of neurostimulator device. Transcranial electrical stimulation (TES), deep brain stimulation (DBS), vagal nerve stimulation (VNS), and electro-acupuncture (EA) research is evaluated.

2.2. Overview of Neurostimulation and Neuromodulation

The primary purpose of neurostimulators for medical treatment (electroceuticals) is to fine-tune organ and systemic function by tapping into the natural nerve pathway between the brain and the organs. Research in neural recording and better understanding of neural signaling allowed for electrical neurostimulation techniques to develop into broadly two categories according to electrode placement: invasive and non-invasive [46]. Non-invasive methods include transcranial direct current stimulation (tDCS) [47], transcranial magnetic stimulation (TMS) [48], and peripheral nerve stimulation [49], while invasive methods include deep brain stimulation (DBS) [50], some types of vagus nerve stimulation (VNS), and electro-acupuncture (EA) [51].

Neurostimulation techniques employ different methodologies and technologies; however, they all pursue the same objective: use electrical stimuli to elicit action potentials from nerve tissue in a predictable manner to cause neuromodulation. Neuromodulation is the change in response of nerve tissue to biological or external stimuli. The effects of stimulation protocols such as

stimulation frequency, duration, and modality on action potential recruitment have been well documented [13, 14, 24, 50, 52, 53]; however, the effects of the stimulation waveform on the outcome of the treatment method have not been thoroughly established [40, 41, 45]. In this review we performed a literature search of tDCS, transcranial alternating current stimulation (tACS), transcranial random noise stimulation (tRNS), DBS, VNS, and EA papers that addressed problems in neurostimulation. We looked for papers that accurately described the stimulation waveform utilized throughout the study so we can compare their findings with other similar papers. In this way we categorize the literature that studies electrical stimulation in a new way that emphasizes the effects of stimulation waveform, and propose that electrical stimulation waveform plays a significant role in treatment outcome for transcranial electrical stimulation (TES).

This review will explore TES, DBS, VNS, and EA with special emphasis in the literature that studies the effects of stimulation waveforms. We also look at current problems and trends in neurostimulation to identify new research directions. In this manner we will show the current state-of-the-art of electrical neurostimulation. We propose 4 main topics for furthering neurostimulation research:

- Comprehensive parametric studies that include standardized methodological reporting. To aid in this approach we suggest utilizing graphical figures to show the stimulation pulse parameters and settings.
- Consideration of complete electrical models for pulse generation studies that include pulse generator circuits and tissue capacitance.
- Study of effects of various stimulation pulse waveforms and their effects on stimulation outcomes.
- Consideration of some electro-acupuncture treatments as peripheral nerve stimulation.

2.3. Transcranial Electrical Stimulation

2.3.1. Overview

Transcranial electrical stimulation (TES) is one of the primary neuromodulation methods in the current state of the art. TES treatments have already moved from the laboratory setting to the clinical and commercial settings [54]. TES encompasses several methodologies for which the main purpose is to cause neurostimulation to the brain using devices outside the skull. TES that is applied by placing electrodes on the skin – dermal TES – and driving different stimulation waveforms through them. The general types of stimulation are classified by waveforms used, and include transcranial direct current stimulation (tDCS), alternating current stimulation (tACS), and random noise stimulation (tRNS) [55, 56] (Figure 2.1).

TES methods have been reliably shown to cause neuromodulation; however, the precise mechanisms through which TES causes neuromodulation remain a topic of debate and require further study [57-60]. Additionally, each type of dermal TES is thought to elicit different neuromodulatory effects. Mechanisms that have been proposed include:

- promotion of long-term potentiation (LTP) or long-term depression (LTD) for tDCS [32, 33],
- modulation of brain oscillations for tACS [34],
- and repetitive opening of sodium channels for tRNS [35].

2.3.2. Transcranial Direct Current Stimulation

The study of tDCS has boomed in recent years. This is mainly due to the ease with which stimulation can be applied, and the plethora of effects that have been achieved with tDCS. Procedures can be conducted without hospitalization or surgical intervention. tDCS can be combined with various imaging techniques to see the direct effects of stimulation on the intact brain [55]. These effects include cognitive enhancements [61] and physical rehabilitation [58, 62].

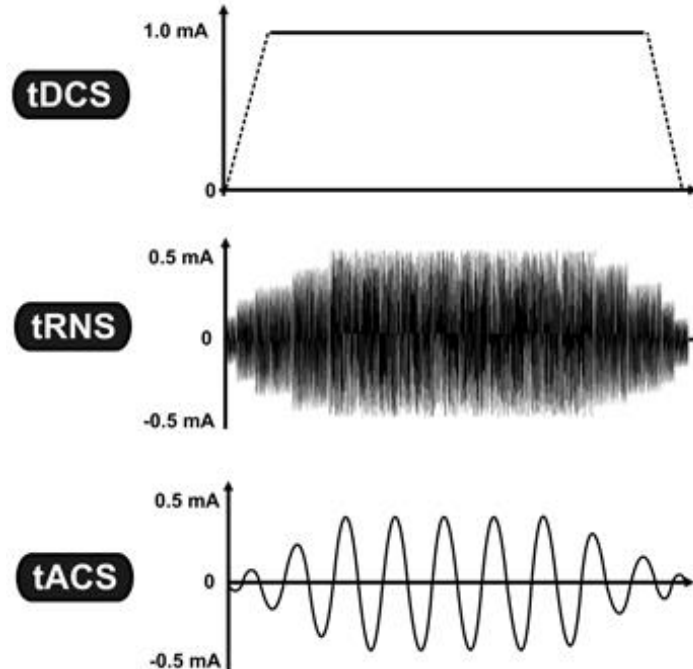


Figure 2.1. Comparison between stimulation waveforms used in TES for tDCS, tACS, and tRNS. Adapted from Saiote [56]. Used under the Creative Commons Attribution 4.0 International License.

The main neuromodulatory effect from tDCS appears to be the selective promotion of LTP or LTD [32]. However, we focus our review on the unknown effects of neurostimulation waveforms on the outcome of tDCS. Then, we examine review papers and outline the main recommendations for future tDCS research. We end this section by looking at the need for improved neurostimulation models.

The direct evidence we found that relates the effect of stimulation waveform on the outcome of tDCS treatment is from the study by Marshall et al. [37], and the follow-up verification studies performed by Eggert et al. [39] and Sahlem et al. [38]. Marshall [37] showed a group of medical students improve declarative memory by applying slow-oscillating (0.75 Hz) voltages. However, Eggert in 2013 [39] repeated the study in elderly subjects and obtained contradicting results showing no improvement, and Sahlem in 2015 [38] rigorously repeated the study with medical students which also obtained results showing no improvement. Sahlem recognized the only

difference between their study and Marshall's was the stimulation waveform. Eggert also mentioned the waveforms are different, but also proposed that the age difference in subjects may be a confounding factor. The premise lies in that all three studies performed virtually identical stimulation procedures except for the stimulation waveform, and in the case of the Eggert study a much older population. Figure 2.2 shows the stimulation waveforms utilized in each study.

The waveforms shown in Figure 2.2 share some differences and similarities. The similarities is that they are all 0.75 Hz waveforms, and they apply a current density of 0.517 mA cm⁻² except with the waveform from Eggert which applies 0.331 mA cm⁻². However, the difference lies in the temporal characteristics of the waveforms, or their rate of change with respect to time. Figure 2.3 shows the waveforms and the representative time rate of change.

We believe the temporal dynamic characteristics play an important role in the outcomes of stimulation because of the capacitive component of tissue and nerve models [36, 63, 64]. It should also be noted that the waveform used by Eggert is very similar to low-frequency AC waveforms, and that despite the DC offset, the time rate of change component becomes negative.

Several reviews have been presented that study stimulation waveforms. Paulus [59] presented a review of TES methodologies for tDCS, tACS, and tRNS. Paulus describes what stimulation parameters mean and how to properly define them, and stresses that stimulation parameters provide a large design space. Brunoni et al. [57] discuss the limitations of current tDCS scientific studies, and propose several improvements that will aid in translating scientific research into clinical research. Grill discusses computational models and their required use in developing novel stimulation waveforms in [65], where he concludes that further research is required that not only focuses on the energy efficiency of stimulation waveforms, but also considers the outcome of clinical treatments. Guleyupoglu et al. [6] discusses the history of TES and stimulation

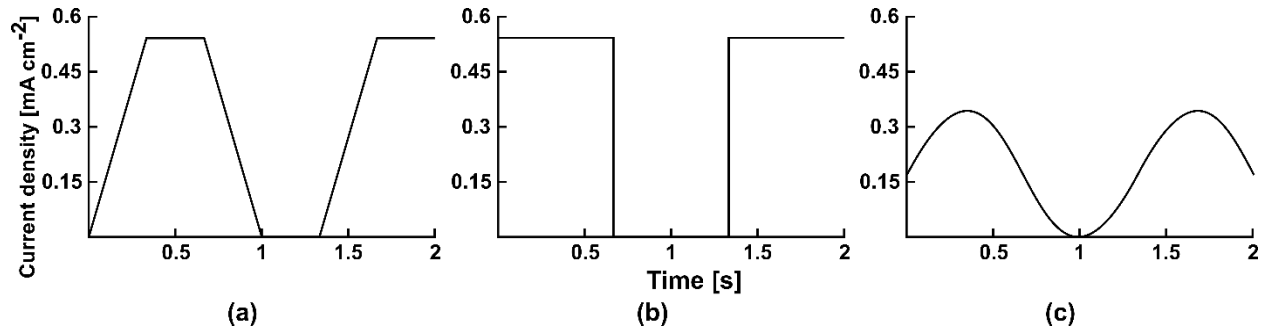


Figure 2.2. Detail of stimulation waveforms used in various studies: (a) trapezoidal waveform used by Marshall [37], (b) square wave used by Sahlem [38], and sinusoidal waveform used by Eggert [39].

parameters and waveforms should be carefully defined in future research. Guleyupoglu stresses that standardization of reporting methods is key for improving reproducibility of results. We found that the review papers in tDCS (and TES) emphasize the low reproducibility of results due to a lack of standardization in terminology and reporting techniques. We think this problem arises in part due to the lack of consensus in reporting methods for stimulation parameters, specifically stimulation waveforms.

Modeling the brain is a valid approach to further understanding tDCS and TES, as it may be possible to apply different waveforms and parameters to models and simulations. Bikson [66] discussed the importance of computational models in 2012; arguing that tDCS models may help address the problem of properly dosing a patient without extensive trial and error. The models can be used to hypothesize dose and methodologies to improve clinical outcomes and validate tDCS neural mechanisms. Kunze [67] implemented in 2016 a large-scale brain network model in order to study the membrane dynamics of neural populations. Kunze suggests that non-invasive brain stimulation may affect brain dynamics by analyzing how functional subnetworks interact with each other. It is important that models be used to guide further research, since the design space of stimulation waveforms is large [27]. Adequate microscopic and macroscopic models will be needed to verify and guide future research in this field.

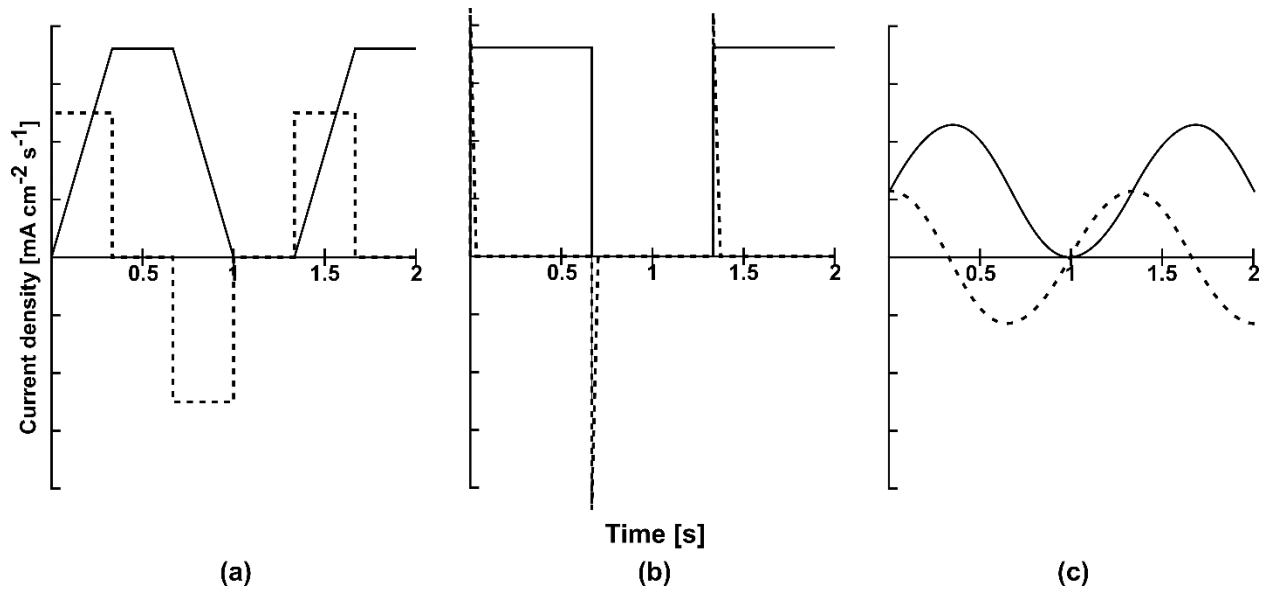


Figure 2.3. Detail of stimulation waveforms used in various studies and their approximate time derivatives (dashed): (a) trapezoidal waveform used by Marshall [37], (b) square wave used by Sahlem [38], and sinusoidal waveform used by Eggert [39]. Time derivative and waveforms not drawn to scale.

2.3.3. Transcranial Alternating Current Stimulation

The tACS field has grown along with tDCS, and for similar reasons. Application of tACS utilizes similar equipment as tDCS, and the electrodes are also placed on the skin. Many of the procedural advantages of tDCS are shared by tACS. In this section we discuss how the difference between applying AC waveforms instead of DC waveforms yields different results in TES. The main tDCS neuromodulatory effect of LTP and LDP promotion presented by Cohen Kadosh [33] and Kronberg [32], contrasts with the entrainment of brain oscillations reported to be the outcome of tACS [34, 68, 69]. However, there is conflicting research that proposed that spike-timing dependent plasticity (STDP) is the mechanism behind the observed effects of tACS. Lastly, some recent studies have used individual patient alpha frequencies for tACS instead of fixed frequency tACS, and it is important to watch the development of this new method to determine which is more effective.

There is recent evidence that the neuromodulatory effect of tACS is entrainment of brain oscillations [34, 68-74]. Kanai [70] studied the effects of tACS with fixed frequencies and found that 20 Hz tACS modulates cortical excitability more strongly than other frequencies. Neuling [34] showed that neuromodulation after-effects from tACS is dependent on brain states. Helfrich [69] studies the application of simulated current flow predictions with EEG in behavioral testing, and shows that entrainment is frequency-specific. Helfrich observes that effects can last longer than stimulation (after-effects). Pahor and Jaušovec [73, 74] studied the effects of tACS on performance of various tasks. They show that tACS affected performance in specific difficulties, and changed resting brain oscillations in some brain areas. Pahor proposes that this is because tACS affects rhythmic activity of local brain networks. However, the study did not perform recordings of EEG data before stimulation, so it is difficult to determine if the results were direct effects of tACS. Voskuhl [68] uses brain-oxygen level dependent (BOLD) fMRI imaging to study the effects of tACS on brain oscillations and their correlation with brain metabolism and activity. Voskuhl also presents a summary of how brain oscillations are associated with brain function. In particular he summarizes:

- theta frequency associated with memory,
- alpha frequency associated with perception,
- beta frequency associated with motor function, and
- gamma frequencies are also associated with perception.

Santaracchi [71] applied tACS at gamma frequencies (40 Hz) and studied its effects on task performance. tACS stimulation was found to affect fluid intelligence, with participants showing increased performance only on tasks that involve logical reasoning. Subjects with lower base performance showed greater improvements than individuals with higher base performance.

Witkowski [72] demonstrated direct measurement of entrained brain oscillations by performing magnetoencephalography during tACS. A summary of studies showing brain oscillation entrainment observations is shown in Table 2.1.

Table 2.1. tACS studies showing brain oscillation entrainment.

Refs.	tACS Stimulation	Experimental Target	Observation
[34]	IAF for 20 min	High/low endogenous alpha power	Low endogenous alpha power can be modulated
[68]	IAF or 1 Hz for 18 min, varying intensity	BOLD signals measured during task	Alpha tACS lowers BOLD response during task
[69]	10 Hz for 20 min	EEG during tACS while performing task	tACS modulates alpha band brain oscillations
[70]	5, 10, 20, 40 Hz with TMS	Phosphene induction via TMS	tACS affects visual cortex excitability
[71]	5 Hz, 40 Hz, and HF tRNS	Fluid intelligence and working memory	Improvement based on individual ability
[72]	Amplitude modulated tACS	MEG during tACS	Entrained brain oscillations measured during tACS
[73]	Theta tACS based on IAF for 15 min	EEG measurement while performing task	Increased fluid intelligence after tACS
[74]	Theta tACS based on IAF for 15 min	EEG measurement while performing task	Working memory improved after tACS

IAF: individual alpha frequency, BOLD: blood-oxygen level dependent, HF: high frequency.

On the other hand, Brignani [75] studied effects of tACS on Gabor patch detection and discrimination and found a reduction in performance, contradicting the notion of brain oscillation entrainment. Vossen [76] also found contradicting evidence. Vossen applied phase dependent tACS protocols (Figure 2.4) and studied α -aftereffects under phase-continuous and phase-discontinuous conditions. They concluded that α -aftereffects could be explained by STDP. Lafon [77] recreates Marshall [37] and obtains contradicting results where slow-oscillation tACS does not lead to brain oscillation entrainment. They confirm that thalamocortical sleep spindle power is modulated with the endogenous slow-wave rhythm. It is difficult to explicitly confirm that tACS leads to long-lasting brain oscillation entrainment with contrasting evidence, however, Witkowski

[72] presents a strong argument for brain oscillation entrainment during tACS with direct measurement of the signals. A summary of studies contradicting brain oscillation entrainment is shown in Table 2.2.

Table 2.2. tACS studies showing contradictory results to brain oscillation entrainment.

Refs.	tACS Stimulation	Experimental Target	Observation
[75]	6, 10, 25 Hz	Task performance during tACS	tACS does not entrain local stimulation sites
[76]	IAF for 11 – 15 min	EEG measured during tACS and task	tACS induces brain plasticity
[77]	0.75 and 1 Hz during NREM sleep or awake	iEEG measured during tACS	tACS did not entrain sleep spindles

IAF: individual alpha frequency, iEEG: implantable electro-encephalograph.

Another interesting point of contention is the adoption of patient individualized tACS frequencies over fixed frequency tACS. Several papers performed a procedure to determine the exact alpha frequency of a subject, and used this individual frequency to derive any other frequencies utilized in the study [68, 69, 74, 76].

2.3.4. Transcranial Random Noise Stimulation (tRNS)

Transcranial random noise stimulation is a relatively novel form of TES [78]. tRNS shares many of the advantages of tDCS and tACS, however, as a novel field the precise mechanisms and properties of tRNS have not been extensively studied yet. The neuromodulatory mechanism difference between tDCS and tRNS has been proposed to be neurochemical with tDCS being NMDA-receptor protein dependent, and tRNS being voltage-gated sodium channel dependent [79]. We will look at evidence of the different effects of tDCS compared to tRNS [80, 81], and the effects of tRNS on learning [82-84], memory [85, 86], and perception [87-89].

The basic neurochemical mechanism of TES are not well understood. Chaieb [79] found evidence that tRNS effects are dependent on different neurochemical mechanisms than tDCS. Chaieb found evidence that tRNS motor-evoked potentials are not affected by NMDA-receptor

Intermittent tACS-protocols

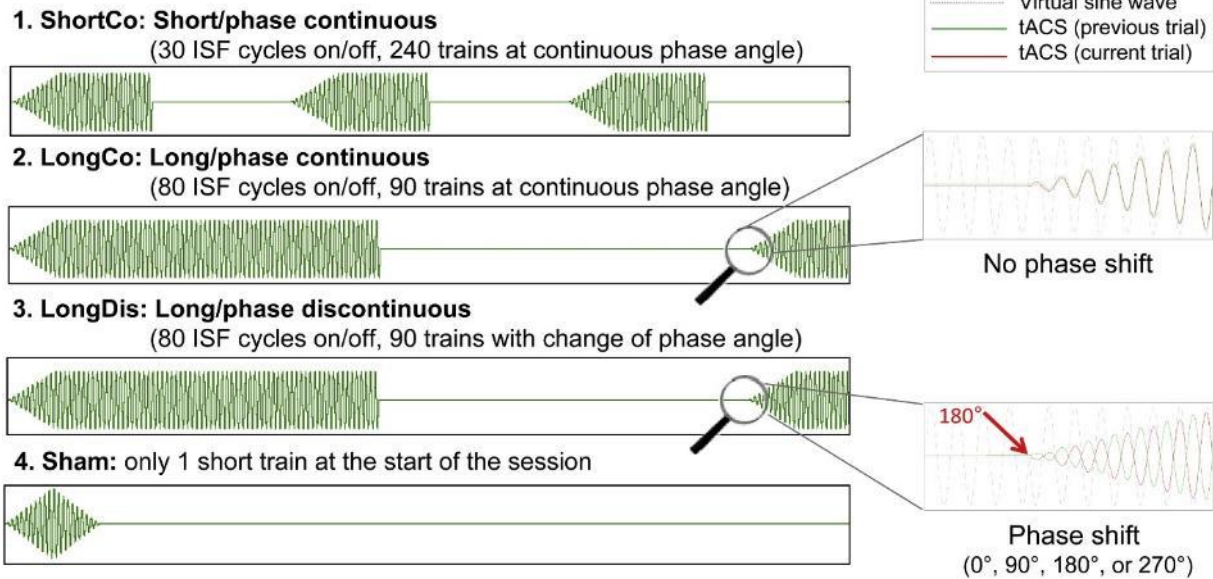


Figure 2.4. Phase shifted tACS protocols utilized by Vossen [76]. Used under the Creative Commons Attribution 4.0 International License.

antagonists (dextromethorphan), but were inhibited by GABA agonists (lorazepam). They conclude that tRNS after-effects are mediated by voltage-gated sodium channels.

tDCS and tRNS have different effects on neuromodulation, and direct comparisons are useful to better understand the differences between them. Ambrus [80] studied perception thresholds using tDCS and tRNS, and found that tDCS perception threshold was at 400 μA , compared with 1200 μA with tRNS. Prichard [81] studied the differences of tDCS and tRNS on motor skills learning with stimulation of the M1 cortex. Both tDCS and tRNS showed improvements when compared to sham stimulation, but tDCS showed effects immediately after stimulation, and tRNS showed effects much later after stimulation.

tRNS studies have shown neuromodulatory effects on learning. Snowball [82] applied tRNS to the dorsolateral prefrontal cortex to study its effects on mathematics performance. Snowball found evidence of both increase speed of calculation and memory-recall mathematics learning, and this effect was seen directly after stimulation and maintained after 6 months. Snowball

concludes that tRNS enhances neuroplasticity and allows for more efficient learning. Popescu [83] performed a study that focused on the learning process of mathematics and found that tRNS improved learning of difficult problems, but no improvement was shown for learning easy problems. Van Koningsbruggen [84] performed a study where tRNS was applied to the occipital and frontal cortex while participants were rewarded for recognizing a specific color. The second part of the study involved identifying other colors, but this time with no reward. The study found that tRNS stimulation caused the original color associated with the reward to become distracting, and in this way showed that tRNS improved learning of value-driven conditions.

Memory and how it's affected by tRNS has also been studied. Holmes [85] studied the effects of tRNS on working memory while subjects performed the Cogmed Working Memory Training, and found no evidence that tRNS improved working memory. However, Mammarella [86] studied tRNS and its effects on the process of memory creation in the brain. Mammarella found that tRNS improved the ability of participants to discriminate between fabricated and real memories (reality monitoring), and that this effect was more prominent in older adults. These results indicate that tRNS may have effects for specific types of memory processes, or that it may affect various brain substructures differently.

Perception and how tRNS influences it is another topic of interest. Van Doren [87] looks at how tRNS affects auditory steady state responses, and found that participants showed increased excitability when stimulated with tRNS. Romanska [88] applied tRNS to the lateral occipitotemporal cortices and measured the effects on facial perception. Romanska was able to determine that tRNS produced task-specific and site-specific enhancements to facial perception. Van der Groen and Wenderoth [89] studied how stochastic resonance from tRNS improved detection of visual stimuli. They determined that noise appears to increase subthreshold nerve

potentials, and allowing them to become suprathreshold more easily. A summary of the observed effects of tRNS is shown in Table 2.3.

Table 2.3. tRNS studies showing observed stimulation outcomes.

Refs.	tRNS Stimulation	Experimental Target	Observation
[79]	0-640 Hz for 10 min	Cortical excitability effects from pharmaceuticals	NMDA receptors do not affect tRNS effects
[80]	0-640 Hz for 31 s, and tDCS with 200-2000 μ A,	Perception threshold for stimulation	tRNS has higher threshold than tDCS
[81]	100-640 Hz for 20 min	Motor skill learning during and after tDCS or tRNS	tRNS improved learning more gradually than tDCS
[82]	100-600 Hz for 20 min	Math learning and hemodynamic response during and after tRNS	Increased math learning and local hemodynamic response
[83]	100-640 Hz for 20 min, \pm 500 μ A amplitude	Math learning during and after tRNS	Increased difficult math learning
[84]	100-640 Hz for 20 min, 1 mA amplitude	Color visual attention capture during tRNS	Increased reward associated capture
[85]	101-640 Hz for 20 min, 1 mA intensity	Working memory training during tRNS	tRNS did not improve working memory tasks
[86]	100-600 Hz for 22 min, 1 mA intensity	Reality monitoring during tRNS	Increased reality monitoring
[87]	101-640 Hz for 20 min, 2 mA amplitude	EEG measurement of auditory steady state response	Increased auditory cortex excitability
[88]	High frequency for 20 min, with 1 mA	Facial identity and trustworthiness perception after tRNS	Increased facial identity perception
[89]	100-640 Hz, random intensity 0-1.5 mA	Visual detection during tRNS	Increased visual stimulus detection

The study of tRNS as a TES method is less than a decade in the making. There are many applications of tRNS that have been found so far, and many more fields to explore. The effects of TES methodologies have been found to be different according to stimulation waveform; be that direct-current, alternating current, or random noise. The stimulation methods differentiated mainly by the waveform of stimulation show unique properties and mechanisms of neuromodulation.

2.4. Deep Brain Stimulation

2.4.1. Overview

Deep brain stimulation is a neurostimulation method where electrodes are placed directly on the brain tissue and stimulation is then applied. Given the requirement for surgical intervention, deep brain stimulation research is more difficult to perform. For this reason, more emphasis is placed on determining efficient stimulation parameters. We found that there is interest in looking at the effects of the following stimulation parameters: frequency [90], pulse pattern [27], number of pulses [91], and waveform [41, 44, 45, 63].

2.4.2. Stimulation Parameters

There is great interest in determining the precise effects of stimulation parameters on the outcome of DBS. Cooper [90] performed a study in order to determine the effects of stimulation parameters on patients with essential tremor. They looked at stimulation frequency, voltage, and pulsewidth. They found that DBS effects were highly dependent on frequency, with low frequency stimulation making tremors worse, and high frequency stimulation coupled with voltage control reduced tremors. The optimal parameters for each individual were different. Cassar [27] studied the effects of using unique temporal patterns of stimulation instead of fixed frequencies. Cassar used a model-based approach with genetic algorithm optimization. The model results were tested in a deep brain stimulation model neural networks, and showed results that suggest that the new temporal patterns could be more effective than current clinical methods. This study suggests that using fixed frequencies to achieve DBS physiological effects may not be the best approach. Wongsarnpigoon and Grill [91] studied the effects of frequency, burst number of pulses, polarity, and electrode location on motor cortex DBS to determine what combinations led to better stimulation outcomes. They found several relations between stimulation parameters and

stimulation outcomes, showing that stimulation parameters have to be carefully chosen in order to obtain correct results.

2.4.3. Stimulation Waveforms

Stimulation waveform is also a topic of interest in DBS studies. This field has been studied by the Grill [41, 45] and McIntyre [44, 63] groups. Wongsarnpigoon [41] studied the efficiency of waveforms for stimulation of nerves. They studied 4 waveforms: square, and rising or decaying exponentials. Wongsarnpigoon concluded that none of the studied waveforms were optimal for all metrics: energy, charge, and power. They also noted that efficiency had a dependency on pulse width. In a different paper, Wongsarnpigoon and Grill [45] utilized a genetic algorithm to find an energy-efficient waveform for neurostimulation. The algorithm produced waveforms that looked like Gaussian curves (Figure 2.5). The shape of the waveforms was dependent on the pulse width limit that was set in the algorithm. Foutz and McIntyre [44] used computer models to test 8 different waveforms on their energy consumption. They concluded that the triangular pulse was the most efficient at stimulating populations of axons. Additionally, they studied the effects of tissue capacitance on the tissue waveform shape and simulated energy required for nerve bundle activation (Figure 2.6). As previously discussed, Lempka [63] studied the circuit models used for neurostimulation and concluded that ideal models did not present a complete picture when finding the expected voltage across tissue.

2.5. Vagus Nerve Stimulation

2.5.1. Overview

Vagus nerve stimulation (VNS) is a growing field because it allows for both transcutaneous and implantable stimulation methods. The vagus nerve controls many physiological processes and it is thought that several metabolic conditions may be treated with VNS. We found that stimulation

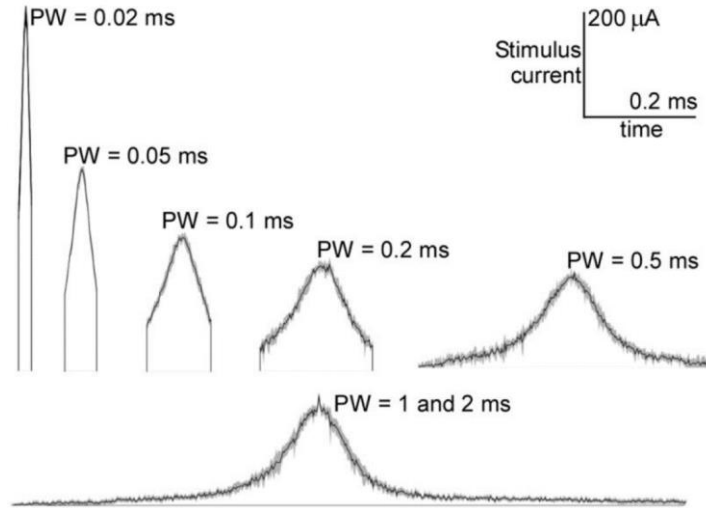


Figure 2.5. Efficient neurostimulation waveforms produced by genetic algorithm in Wongsarnpigoon [45]. Journal of Neural Engineering by Institute of Physics (Great Britain) Reproduced with permission of IOP Publishing in the format Thesis/Dissertation via Copyright Clearance Center.

parameters were a topic of interest in the field [92-97], and also that the effects of stimulation waveforms are difficult to study because of a lack of devices that can apply different stimulation waveforms. We found 5 papers that used a commercial VNS machine, 4 of which were identified [92, 95-97], and 1 where the machine was not identified [93].

2.5.2. Stimulation Parameters

Studies of VNS stimulation parameters try to find the given parameter settings that will allow for specific neuromodulatory effects. Labar [92] looked at how VNS output current affected patients' tolerance when VNS devices were replaced due to batteries discharging. Labar found that 21 out of 28 patients could not tolerate the same current level that they had utilized before device replacement. 17 out of 28 patients could not tolerate current settings one year after device replacement. Labar could not find a reasonable explanation for this phenomenon, but they proposed that long-term VNS alters the sensibility of the vagus nerve. Manta [96] studied the effects of several stimulation parameters on the firing activity of dorsal raphe neurons in the rat. They found that there was an optimal level for each parameter: frequency, current intensity, pulse

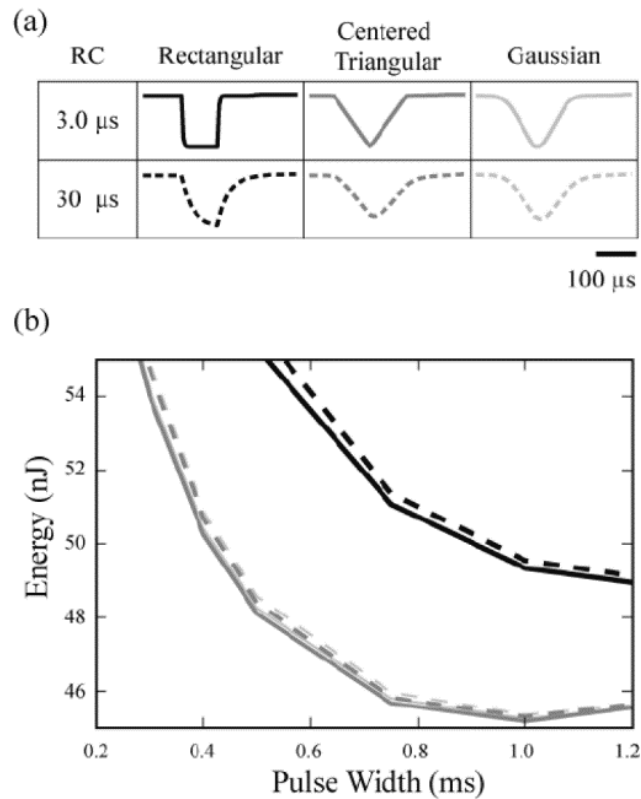


Figure 2.6. Simulated effects of tissue capacitance on stimulation voltages and nerve activation thresholds: (a) applied voltage waveform after passing through a low-pass RC filter, (b) Voltage applied on a DBS electrode and nerve activation energy modeled. Adapted from Foutz [44]. Journal of Neural Engineering by Institute of Physics (Great Britain) Reproduced with permission of IOP Publishing in the format Thesis/Dissertation via Copyright Clearance Center.

width, and time between stimulation. Interestingly, they also found that increasing intensity can lead to a decrease in firing activity. Manta also shows that optimal parameters can be found for specific cases and treatments using VNS. Shan-Shan [97] studied optimal parameters for VNS treatment of heart attacks in rat models. Shan-Shan concluded that optimal parameters for guaranteeing beneficial effects were difficult to determine. In this case, this study shows that VNS treatments may not have specific optimal stimulation parameters, and effects have to be considered on a case-by-case basis. Ghani [94] performed a review of VNS treatment for epilepsy specifically studying the effects of stimulation parameters on acute response. Ghani was able to identify 3 major trends with respect to stimulation levels. They show that high stimulation levels are more

effective in adults, while children were responsive to both high and low stimulation levels. However, adverse effects were more prevalent in groups with high stimulation. High and low stimulation levels refer to a combination of stimulation parameters. Borland [93] studied the effects of VNS intensity on plasticity of the sensory and motor cortices. Borland confirmed previous reports that VNS intensity and cortical plasticity show a non-monotonic relationship; which is that increasing VNS intensity does not cause increasing cortical plasticity all the time. Borland showed that current intensities of 0.4 mA and 0.8 mA were the most effective in increasing cortical plasticity. They discuss that the therapeutic effects of VNS are a likely combination of several cerebral subnetworks being stimulated. Hulseley [95] performed a parametric study of VNS stimulation parameters and its effects on the locus coeruleus. They found several relations between parametric ranges and specific locus coeruleus effects including phasic firing, increased firing rate, timing of phasic firing, and pulse-locked neural activity. The previous studies required direct stimulation on the vagus nerve in order for effects to be elicited, however, there is also a need for stimulation methods that do not require surgery.

2.5.3. Computer Models

Mourdoukoutas [98] developed a comprehensive 3D computational model of the anatomical structures surrounding the vagus nerve, and simulated current paths through the tissue if they were applied via electrodes on the skin (Figure 2.7). The simulation models anatomical structures and tissues, and takes into account their effects on the paths of stimulation current. Mourdoukoutas concludes that A- and B- fibers can be recruited via external electrodes, however C- fibers would not be recruited. The authors mention that the model can be applied to spinal cord nerves, deep brain stimulation, and cranial and peripheral nerve models.

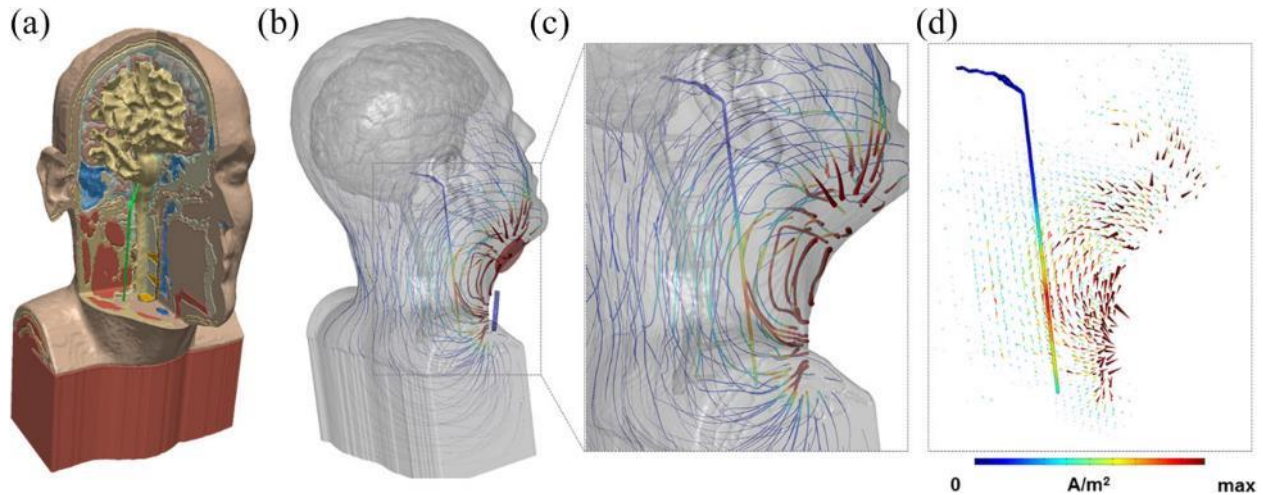


Figure 2.7. Anatomical tissue computational model developed by Mourdoukoutas [98] to simulate current paths from VNS applied using surface electrodes: (a) model derived using MRI data with vagus nerve highlighted in green, (b) surface electrode placement and current paths around tissue, (c) magnification around vagus nerve showing current paths, (d) arrow plot showing current density. Copyright 2017 International Neuromodulation Society.

2.6. Electro-Acupuncture

2.6.1. Electro-Acupuncture as Neurostimulation

Acupuncture is a methodology which consists of stimulation of specific anatomical points in order to treat various conditions [99]. Acupuncture stimulation can be performed in several manners, including electrical stimulation. Acupuncture through electrical stimulation is referred to as electro-acupuncture (EA). EA can be used to treat several medical conditions including pain management, musculoskeletal, neurological, obstetric, gastrointestinal, and surgical anesthesia [100, 101]. We propose that EA is a form of neurostimulation in some cases. This is because the proposed physiological mechanisms of acupuncture indicate that acupuncture points lie on nerve pathways [102], and are areas that contain excitable muscle, skin, and nerve complexes [103]. It has also been shown that acupuncture stimulation affects afferent nerve fibers [104]. Another study performed a comprehensive explanation of the neurobiological mechanisms that could be present in neurostimulation, and their physiological effects [105]. Recently, another study looked at the relationship between acupuncture points and the receptive fields of neurons [106]; indicating that

stimulation at acupuncture points is indeed neurostimulation. However, not all acupuncture points and acupuncture methods should be considered neurostimulatory. This is because there are hundreds of acupuncture points, and not all of them are associated with nerves.

2.6.2. Electro-Acupuncture Research Issues

Electro-acupuncture has similar advantages to TES in that stimulation does not require surgical intervention because the electrodes used are dry needles. A trained acupuncturist performs an evaluation on the patient, and then decides on the acupuncture treatment methodology. After transcutaneous insertion of the needles at the desired acupuncture points, the acupuncturist connects the needles to a pulse generator in order to cause stimulation [100]. Stimulation can be applied by variation of several parameters: frequency, temporal pattern, and intensity [107]. One of the issues with EA research is that there are no widely used reporting standards and comparison standards [108]. This causes research results to be difficult to reproduce, and later compare. Langevin [108] discusses that EA and manual acupuncture should be carefully compared, since in many cases direct comparisons are made without taking into account technical differences in stimulation. Langevin also points out that sometimes scientifically important factors are neglected such as physiological mechanisms and measurements. Langevin concludes that acupuncture studies should emphasize performing manual acupuncture and EA for the same duration, since this would allow a strong comparative basis between treatments. Zhao [52] discusses findings in EA, and proposed that differing results in EA research are probably due to the variety of stimulation parameters used in different studies.

2.7. Conclusions

2.7.1. Effects of Differing Waveforms on Stimulation Outcomes in Transcranial Electrical Stimulation

The variety of outcomes from one method (TES) used with different stimulation waveforms – direct current, alternating current, and random noise – demonstrates that stimulation waveform should be considered a key parameter in TES. Further complicating the matter, it also appears that specific waveform shape also plays a role in stimulation outcome. In tDCS this can be seen in the previous discussion about the studies by Marshall [37], Eggert [39], and Sahlem [38]. In tACS, the specific mechanisms of neuromodulation are still debated, as several papers show different conclusions. Specifically, the entrainment of brain oscillations has been proposed as a probable neuromodulatory mechanism [34, 68-73], and STDP has been proposed as a different mechanism that could explain the neuromodulatory effects [76]. tRNS is a young field where several applications have been found, and for which the specific effects on the brain are still being studied. Early studies, however, show that the neuromodulatory mechanisms of tRNS and tDCS are different [80, 81]. The study of TES methods still has yet to definitely establish the neuromodulatory mechanisms of stimulation, and it can be seen that stimulation waveform may play a role that has not been previously considered.

Lempka [63] performed a study in order to adjust biological electrical models to better account for the effect of the stimulation device and neural interface, although this paper focuses on the perspective of DBS (Figure 2.8). Howell [64] studied the effect of stimulation frequency on membrane capacitance of stimulated cells. Based on these studies, we propose that the temporal dynamics of stimulation waveforms may have significant effects that have not been previously studied. These unknown effects could help explain the differences in neuromodulation outcomes for TES methods (tDCS, tACS, tRNS).

The topic of safety was not considered for this review. However, there are significant safety concerns that must be addressed during TES such as skin injuries and possible nerve damage [109]. Ethical concerns should also be addressed in the study design phase [110].

The reviewed papers show a consensus that thorough standard reporting procedures for stimulation parameters is required in order to guarantee reproducibility of results. Further rigorous studies are required to better understand the role that stimulation waveforms shapes play in affecting and causing neuromodulation outcomes.

2.7.2. Deep Brain Stimulation

We found there is an interest in the DBS field for finding the optimal parameters for a given neurostimulation outcome. The effects of stimulation parameters in sections of the brain have been previously studied, and several studies looked at the question of what waveforms are best for energy-efficient neurostimulation. We can conclude that the next step should be taken in the direction of in vivo experimentation. The specific effects of different waveforms on the brain subnetworks has not been addressed, and the effect of using efficient stimulation waveforms has not been thoroughly studied.

2.7.3. Vagus Nerve Stimulation

We found that the field of stimulation parameter effects is topic of interest in VNS studies. We found that studies in this area focus on finding optimal parameters for specific VNS effects. While optimal parameters were found in some cases [93, 94, 96], another application showed no evidence of optimal parameters being available in all cases [97]. However, none of the studies mentioned above looked at stimulation waveform effects on VNS outcome. This may have been due to the lack of VNS devices available that had features to test different VNS waveforms. A novel device with multiple waveform capabilities is required for research on the effects of stimulation waveforms.

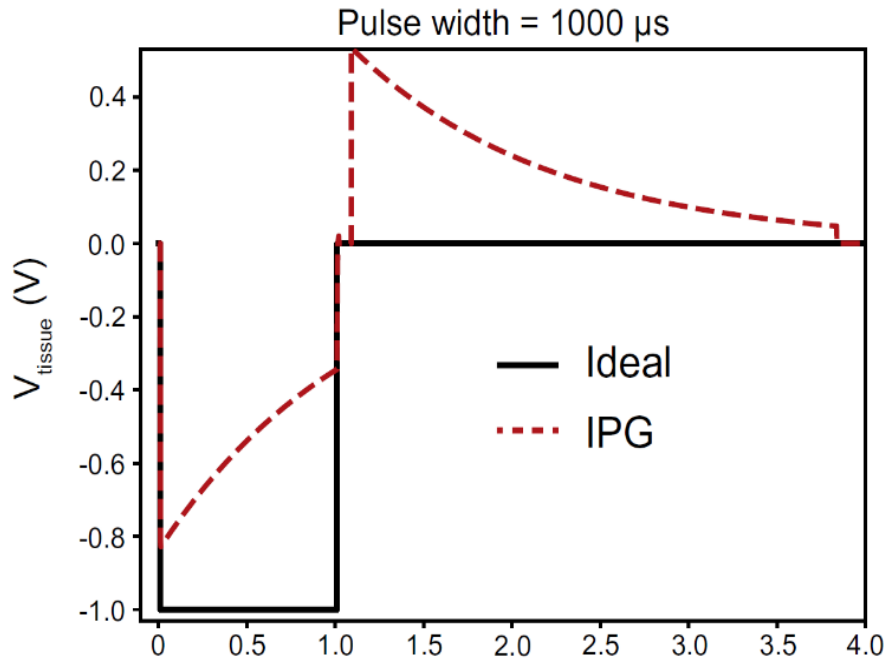


Figure 2.8. Tissue voltage waveform comparison between ideal implantable pulse generator (Ideal), and an adjusted implantable pulse generator model (IPG). Adapted from Lempka [63]. Reprinted from *Clinical Neurophysiology* with permission from Elsevier.

2.7.4. Electro-Acupuncture

We propose that EA in some acupoints should be studied in a similar fashion to other neurostimulation fields due to the evidence showing some acupuncture points as areas of high nerve ending density [103] and lying on nerve pathways [102]. Acupuncture treatments show effects on afferent nerve fibers [104], and neurobiological mechanisms [105]. Studies are still being conducted to help elucidate the role of acupuncture and neural mechanisms [106]. We can conclude that EA is a form of electrical neurostimulation of peripheral nerve fibers, and the field would benefit from the rigorous parametric stimulation studies that have been performed in TES, DBS, and VNS.

2.7.5. Need for Studies Investigating Stimulation Parameters and Waveforms

The analysis performed on TES methodologies shows evidence that stimulation waveform is integral at determining neurostimulation effects in this type of stimulation. The precise

mechanisms that explain these effects are still a subject of debate. The different neuromodulatory effects observed with different stimulation waveforms warrant more systematic studies with standardized reporting procedures for stimulation parameters to guarantee reproducibility of results.

The literature showed interest in the study of optimal parameters for DBS, VNS, and EA. The effects of different waveforms in DBS have not been explained yet, specifically with relation to the effect on brain subnetworks. The question of optimal stimulation waveforms is also a topic that should be studied. The effects of different waveforms may help in explaining why optimal parameters are available in some applications of VNS [93, 94, 96], but not all applications [97]. This requires development of VNS devices that can apply various VNS waveforms. It was also found that the neurostimulation field would benefit from considering EA as a neurostimulation method. We found many correlations between conventional neurostimulation targets and EA stimulation targets. EA research would benefit from rigorous parametric studies similar to the ones performed in TES, DBS, and VNS.

3. PULSE GENERATION CIRCUIT FOR NOVEL STIMULATION WAVEFORMS

3.1. Introduction

Neuromodulation is the active tuning of neural plasticity via electrical stimulation, and has been demonstrated present at the cellular, tissue, and brain level. Electrical stimulation parameters such as waveform, amplitude, and stimulation frequency have been shown to affect neuromodulation properties, however, the effects of waveform shape on neuromodulation have not been studied. To enable research with novel waveforms a passive pulse generator circuit capable of producing output pulses inspired by nature is presented and characterized. A circuit analytical expression is derived from the circuit, and shown to be of the same type to mathematical functions for excitatory post-synaptic potential (EPSP) and inhibitory post-synaptic potentials (IPSP). The analytical expression allows for the design of pulse parameters such as maximum amplitude voltage, time for peak amplitude, and stimulation duration. The circuit is shown to operate at variable output stimulation frequencies, and an expression is derived in order to determine the limit of the output stimulation frequency. This circuit can be designed for specific applications that will be addressed in later chapters.

As previously mentioned, square or rectangular [31, 40], exponential, ramp [41], sinusoidal [26, 42, 43], triangle, and Gaussian [44, 45] waveforms have been studied for their effects in neurostimulation. We have not found in the literature any devices specifically designed to output signals with shapes of naturally occurring waveforms such as EPSPs and IPSPs, and there have been few *in-vivo* or *in-vitro* studies verifying the effects of signals with novel shapes. Studies have shown a lack of sufficient evidence on the neuromodulation and neuroplasticity mechanisms affected by stimulation waveforms [24, 25, 27], such that there is a need for novel stimulation waveforms to determine the effects and capabilities of electrical stimulation. Thus, in this chapter

we present the design and implementation of a device that generates novel waveforms for neurostimulation purposes.

3.2. Review of State-of-the-Art

Neurostimulator design research has focused on complex systems and integrated circuit (IC) implementations with high flexibility in the system performance [111-119]. These devices are complex electronic circuits comprised by large amounts of components, and thus require significant expertise in electronic design to understand and use properly. We analyzed previously reported technology for its potential use for stimulation waveform research. A device was previously designed to fit in a micro-sized package, and is limited to only one signal type that varied directly with input power [111]. There was no mention in the paper of a methodology to alter the width and amplitude of the output signal, nor in the original theory paper describing the stimulation system [120]. Additionally, the control of the frequency of stimulation was built-in to the chip. We found that the system presented could be improved by introducing voltage regulation and allowing for a more flexible stimulation frequency control. The BION microstimulator family had a similar approach, and they had programmable output signal control [121]. However, these devices had a complicated fabrication process and their implementation led to dangerous patient outcomes during clinical trials with devices breaking after implantation. The complexity of the circuit was substantial, and design iterations from one stimulator to the next required significant time and revision. We learned from this approach and found that simpler circuit design allows for a more reliable design and implementation. The work performed in [115] showed the need for a more flexible design process that allows for the stimulator design to be tailored to the electrodes and load. This system was also limited in that there is only one type of output signal, and this signal has to be carefully controlled using a complex control circuit to allow the device to be viable.

Novel neurostimulator approaches are still required and are being developed. Seo have explored using ultrasonic power and communications in neurorecorders, with neurostimulators and complete neural interfaces being a logical next step [122]. Qian explored the possibility of using new types of waveforms by implementing carrier waves with stimulation signals [123]. Van Dongen and Serdijin described a neural stimulator design that utilizes an inductor to deliver charge to a load, in contrast with the typical capacitor [117]. Khalifa recently presented work on distributed neurostimulators as a necessary approach for neurostimulator design [119]. Distributed neurostimulators can be used for peripheral nerve stimulation and electro-acupuncture [124].

The pulse generator presented in this work has constant output pulses, a small component count, and is composed only of passive components. Khalifa used a similar methodology to design their system [119]. Our strategy departs from the norm by focusing on generating a pulse using only passive components and control, and each combination of components gives a unique output pulse (Figure 3.1).

The role of the stimulation waveform on neuromodulation has not been extensively explored. In this work, we present a novel pulse generator and characterize its operation. The pulse width and amplitude can be designed by choosing the circuit components of the generator, and the pulse frequency is determined by the input source. The general goal of this work is to aid in neuroscience and neurostimulator research in the field of neuromodulation by providing a pulse generator circuit with a novel stimulation waveform inspired by nature.

3.3. Circuit for Pulse Generation

3.3.1. Pulse Generator Circuit Development

We implement a circuit that has simple control relying only on the input power signal timing to determine when stimulation occurs. The design of this circuit is simple when compared to other

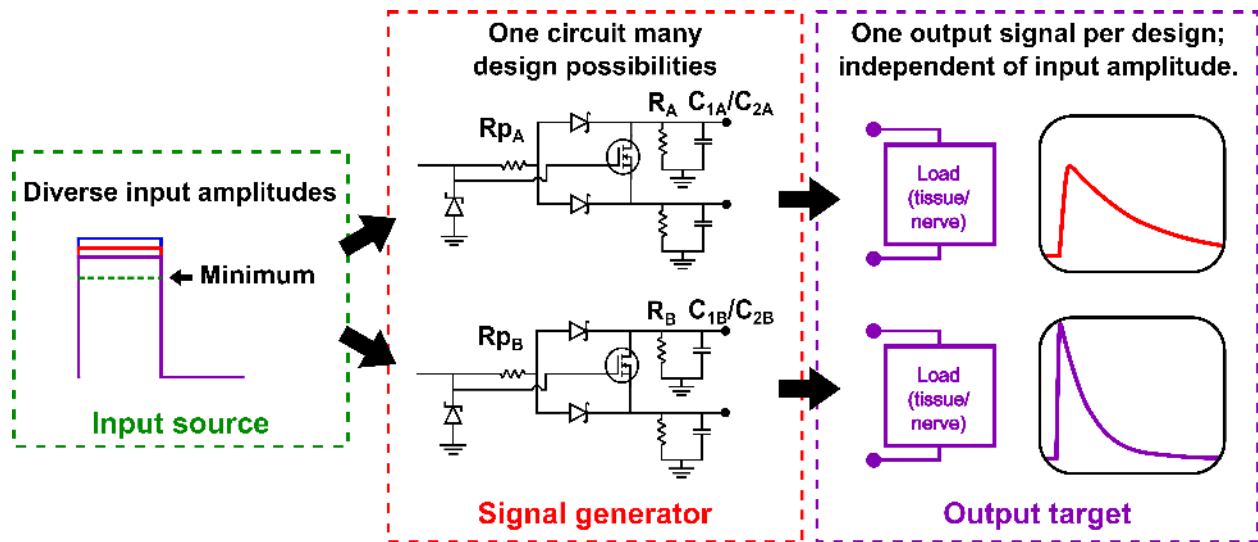


Figure 3.1. Overview of an envisioned circuit that allows different pulse outputs depending on circuit design. Outline of varying output pulses according to unique circuit parameters. The device is controlled by pulsing an input signal to the system. The input signal is processed by the pulse generator to generate the output pulse. The output pulse will be consistent as long as minimum power is supplied.

systems in terms of circuitry, operation, and waveform design adjustment. The resulting pulse generator can generate a unique waveform according to the passive design components used in the circuit (Figure 3.1). Output pulses are generated when the input is turned on and then off sequentially. Two output pins are set to a voltage, and then they are discharged at different rates via two capacitors C_1 and C_2 . This disparity in discharge rates causes the voltage across the tissue between the two electrodes to vary, thus causing stimulation. The output is also connected in parallel to resistors R , which allow passive charge balancing via a direct path to ground. The device ground is isolated from the tissue in this implementation. Grounding with respect to the tissue is not required because the output signal is generated by the variation in voltages between the two output electrodes, and not by reference to the device ground. This method contrasts with the previously described literature where digital control circuits are employed to provide control of the output signal. We use a circuit with outputs that can be accurately designed in order to facilitate the pulse design according to specific requirements. Passive components are used because they

allow a simple design and benchtop implementation for verification of the pulse outputs. The output of the circuit is regulated such that the output is not dependent on variations on the input source, as long as the input supplies a minimum power to generate the output pulse. Finally, the component count is minimized to promote simplicity, and avoid redundancy in the circuit.

The circuit implements regulation of the output voltage in two methods: the input voltage is regulated via a zener diode, and the output pulse amplitude can be modified via a resistor (R_p) placed before the RC branches. The R_p resistor effectively forms a voltage divider with the resistors (R) in the RC branches. Design of the maximum output pulse amplitude is achieved by varying the R_p resistor without affecting the transient response of the RC branches.

3.3.2. Safety and Failure Modes

As shown in Figure 3.1, the pulse generation circuit consists of two resistor-capacitor (RC) branches that generate output pulses, and this voltage is used as the stimulation across the load tissue. These RC branches are isolated from each other and the input through diodes, while still being connected through the load. The layout of the circuit is designed to be inherently safe. The diodes can fail to stay either shorted or open circuit. In the case that diodes fail into a short, then no signal would be seen by the load, as the terminals across the load would be connected to the same node. If the diodes fail into open circuit, then there would also be no output at the load since the output would be isolated from the input. It is unlikely that the diodes would fail in different modes, since the diode anodes are connected to the same node. A transistor connects the two RC branches in order to attenuate the charging phase voltage by providing a current path between the RC branches only during the charging phase. The transistor operates in saturation mode when input voltage is applied, thus it is only turned on when power is supplied to the circuit. In case of transistor failure into a short circuit, then there would be no signal at the load since the terminals across the load would be shorted together. The output electrodes can be driven at high voltage

safely because the electrode voltage is in reference to the device ground. The device does not have to be grounded in the target tissue. This feature allows high voltage to be used if desired because the tissue will not be affected by the high voltage, and will only be affected by the difference in voltages generated by the RC branches.

3.3.3. Signal Generator Operation

The signal generator has four distinct phases of operation: the charging phase, the charged phase, the discharging phase, and the unpowered phase, which are outlined in Figure 3.2. Two phases are important to calculate the pulse: a charging phase when power is supplied to the input, and a discharging phase when power is disconnected.

During the charging phase, the input voltage is isolated and applied separately across each capacitor by diodes. The capacitors are charged to a fixed voltage. This voltage is determined by the voltage regulator and the voltage divider between R_p and R resistors. There is a negligible output signal during the charging phase due to the attenuator. The effect of this output signal is reduced with the MOSFET connecting the RC branches, and via passive charge balancing through the resistors R . The charged phase begins once the capacitors are fully charged, and there is no output signal during this phase. Upon triggering the discharging phase by disconnecting the input power, the capacitors are discharged at different rates, making it possible to utilize the discharging potential difference across the capacitors to produce a pulse signal. The last unpowered phase consists of no input signal and no output signal from the circuit. It is important to note that the output pulse is timed by the input signal, which allows external control of the signal generator.

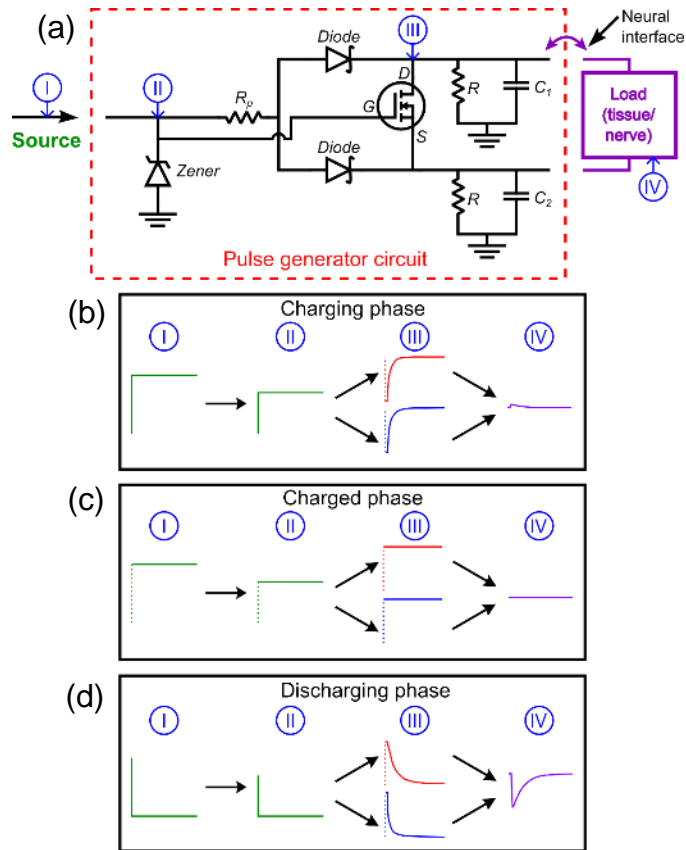


Figure 3.2. Overview of pulse generator circuitry and pulse generation phases: (a) circuit of proposed pulse generator for neurostimulation; (b) charging phase where two RC circuits store the energy that will be delivered as the output signal; (c) charged phase where the input signal is still on, and the two RC branch circuits yield 0 output signal, and (d) discharging phase where the input signal is turned off, thus causing the two RC branch circuits to discharge and generate the output signal. The last phase is when the signal generator is unpowered, with no signals across the circuitry (not shown). The pulse generator circuitry in (a) consists of an input power source (I), an input voltage regulation circuit (II), RC branches to generate output signal (III), and a load connected to the output (IV).

3.3.4. Pulse Design Considerations

Pulse signal parameters that have to be chosen for a given application are waveform, amplitude, width or duration, and output stimulation frequency [28, 125]. In our circuit, components in the RC branches (R , C_1 , and C_2) determined the rate-of-rise and decay, the amplitude, and the shape of the output waveform. Different C_1 and C_2 values were chosen in order to accentuate the potential difference between the RC branches. Thus, by varying the capacitances and resistances, it is possible to generate unique output pulse waveforms with different amplitude,

duration, and shape. The input resistor R_p affects only the amplitude of the signal by the voltage divider formed with the R resistor.

Other considerations can be taken with respect to the stimulation signal waveform. Signal waveforms can be mono- or biphasic. Biphasic signals can be symmetric or asymmetric, and charge-balanced or imbalanced. Waveform phase refers to the stimulation signal polarity, or if the waveform becomes positive, negative, or both during one stimulation cycle. Waveform phase symmetry means that the positive and negative phases are identical. Charge balancing is known to reduce probable injury caused to the target tissue due to charge accumulation [126], however, charge imbalanced or monophasic signals have shown safe and effective results in clinical studies with transcranial pulsed current stimulation applications [127, 128], and transcranial magnetic stimulation [25, 129, 130]. Asymmetric signals have shown selective activation of nerves with a long, small amplitude negative signal followed by faster, large amplitude positive signal [40, 131]. Our signal design was directed constitutes monophasic and asymmetric signals. The stimulator circuit and pulse design has inherent safety advantages however; these features make the device a charge-delivery based device. The charge delivered can be calculated if the load tissue characteristics are known. The variability in signal design allows for different charge densities according to each individual design, and this is dependent on electrode selection and interface. Charge density requirements have to be met for each application with the use of this stimulator. Depending on the waveform, the signal is considered effective only when it is above a certain amplitude [44]. This effect is taken into consideration in the circuit analysis when finding the signal stimulation width or duration.

3.4. Circuit Analysis

3.4.1. Overview of Circuit Analysis

We developed an analytical expression to find useful parameters from the output pulse. These parameters are peak amplitude (v_{max}), peak time (t_{peak}), and stimulation duration (δ_{stim}), as illustrated in Figure 3.3. When the circuit is powered and cycled through all four phases, it generates one pulse during the discharging phase. The discharging phase begins when the input signal is disconnected, such that control of the output is achieved by turning on and then off the input. Ideally, there is no signal during the charging, charged, and unpowered phases of operation. We focus our analysis on the charged and discharging phases of the circuit.

Analysis of the circuit gives us the output function of the circuit, and this in turn allows us to approximate the design parameters previously mentioned. The analysis of the signal generator consists of two parts: finding the charged phase capacitor voltage, and then the discharging phase output pulse waveform.

3.4.2. Charged Phase Capacitor Voltage

The capacitor voltage is rising during the charging phase. Then, in the charged phase, the capacitors are fully charged and act like open circuits. The charged phase circuit model is shown in Figure 3.4(a).

The input voltage is supplied by the source. The voltage regulator is providing a voltage V_{reg} , and the diodes are in forward bias with a voltage V_f . There is a voltage divider between R_p and R . The value of interest is the voltage across the resistors R , which is the voltage to which the capacitors are charged V_{cap} . We found V_{cap} by solving the voltage divider between R_p and R such that

$$V_{cap} = (V_{reg} - V_f) \frac{0.5R}{0.5R + R_p}. \quad (1)$$

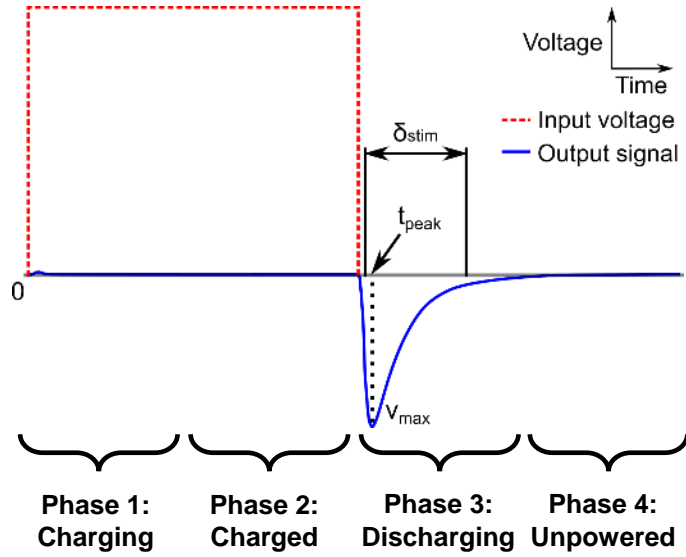


Figure 3.3. An example input and output signal. The discharging phase has peak amplitude (v_{max}), peak time (t_{peak}), and stimulation duration (δ_{stim}).

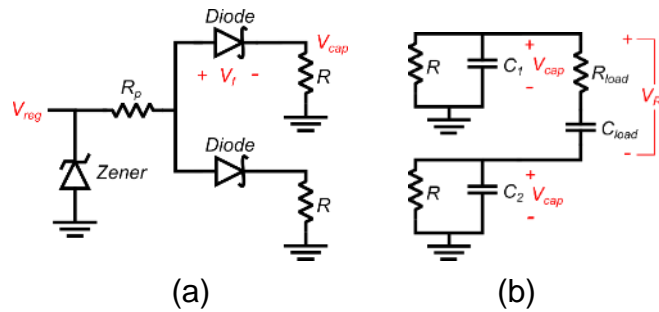


Figure 3.4. Circuit models for analysis: (a) charged phase circuit with capacitors C_1 and C_2 charged to V_{cap} , (b) discharging phase circuit, V_{cap} is the initial voltage of C_1 and C_2 .

The value of V_{cap} is only determined by the resistor values (R_p and R) and is the initial condition for the discharging phase discussed in the following section.

3.4.3. Discharging Output Waveform

At the start of the discharging phase, the diodes are in reverse bias, effectively acting as an open circuit. The RC branches of the circuit are connected only through the load during the discharging phase. The load is modeled using a modified Randles model that is a resistor and capacitor in series [115, 117, 132] (Figure 3.4(b)). The capacitor represents the electrode-electrolyte double layer capacitance, and bulk capacitance of the tissue.

During the discharging phase, the voltage is supplied only by the capacitors that are each charged to voltage V_{cap} . The discharging phase output pulse (v_{R_L}) is a function of R , C_1 , C_2 , R_L , C_L , and V_{cap} . We can apply a simplification where we can relate the separate RC time constants of the RC branches. We obtain this ratio by defining $\kappa = RC_1/RC_2 = C_1/C_2$. Thus, we obtain an expression for the output voltage waveform across the load tissue (R_L):

$$v_{R_L}(t) = \frac{V_{cap}(\kappa - 1)}{C_L^2 C_2 R_L^2 R \kappa} \left(\frac{e^{r_1 t} (C_L R_L r_1 + 1)^2}{(r_1 - r_2)(r_1 - r_3)(r_1 - r_4)} - \frac{e^{r_2 t} (C_L R_L r_2 + 1)^2}{(r_1 - r_2)(r_2 - r_3)(r_2 - r_4)} \right. \\ \left. + \frac{e^{r_3 t} (C_L R_L r_3 + 1)^2}{(r_1 - r_3)(r_2 - r_3)(r_3 - r_4)} - \frac{e^{r_4 t} (C_L R_L r_4 + 1)^2}{(r_1 - r_4)(r_2 - r_4)(r_3 - r_4)} \right), \quad (2)$$

where V_{cap} is the voltage to which C_1 and C_2 are initially charged. We also have r constants that are the roots of a polynomial defined by the values of the design parameters. We can compare the output function (2) from our circuit with previously reported model functions for EPSPs and IPSPs [133]:

$$h_i(t) = B(e^{-b_1 t} - e^{-b_2 t}) \quad (3)$$

and

$$h_e(t) = A(e^{-a_1 t} - e^{-a_2 t}), \quad (4)$$

where (3) is the IPSP waveform, and (4) is the EPSP waveform, and $a_2 > a_1$ and $b_2 > b_1$. The A and B are constants derived from the EPSP and IPSP recordings from biological data. They are used in the mathematical model presented by Lopes da Silva et al.. [133]. These A and B constants are comparable to our circuit component constants in (2), and in both cases the constants modify the amplitude of the signal. The exponential terms in (2) also have the same form as the exponential terms of (3) and (4). It can also be observed that the exponential terms r are actually negative. Thus, we can say that our circuit output pulse shown in (2) is of the same shape as naturally occurring EPSP and IPSP signals.

Knowing (2) we can define the operational parameters of the circuit: pulse peak time, t_{peak} , the pulse peak amplitude, v_{max} , and the discharging pulse duration, δ_{stim} . The pulse peak for the discharging signal can be found by taking the output signal expression (2) and taking its derivative, which is set equal to 0. The pulse peak amplitude can be evaluated using the value of t_{peak} and evaluating (2) at that value such that

$$v_{max} = v_{R_L}(t_{peak}). \quad (5)$$

Using (5) it is possible to design circuit components according to pulse amplitude requirements. However, it is hard to determine the effects of r in (3) explicitly, due to the complexity of the terms. Since the r constants appear in the exponential terms of (2), it is thought that these constants are a form of time constant for the circuit, playing a significant role in determining δ_{stim} . It can be seen that they directly determine t_{peak} in (2). The pulse duration can be defined as the amount of time it takes for the pulse to rise from 0 ($v_{R_L}(0) = 0$) up to a pulse peak (v_{max}), and then decay until it reaches 0 ($v_{R_L}(\infty) = 0$). However, we choose to take the pulse duration to be the time the pulse is above a fraction of the amplitude [44]. This is represented with the factor α , and can be modified as necessary. We use the value of (5) to find the time t_{stim} when the output signal is a fraction of v_{max} denoted by

$$v_{R_L}(t_{stim}) = \alpha v_{max}. \quad (6)$$

There are two solutions to (6). We take the difference between these two solutions to determine δ_{stim} in the following manner

$$\delta_{stim} = t_{decay} - t_{rise}, \quad (7)$$

where t_{rise} is the value of (6) as the pulse increases in magnitude, and t_{decay} is the value of (6) as the pulse decreases in magnitude.

3.5. Power Analysis

3.5.1. Overview of Power Analysis

Power analysis is important to understand in what ways the circuit can be optimized for applications that rely on low power consumption such as implantable, wearable, or portable devices. In this section we discuss the ideal power consumption of the device, and which elements in the circuit affect the power consumption of the pulse generator. We organize our analysis according to the operating phases of the circuit: charging, charged, and discharging. We show that the most power efficient strategy is to shorten the length of the charged phase, and lower the effective series resistance (ESR) of the current path to the RC branches. Our analysis is validated with digital simulation in software TINA-TI version 9.3.100.244 (DesignSoft, Budapest, Hungary).

3.5.2. Ideal Charging Case

The charging phase consists of raising the input and regulator voltages to their nominal operating level, and charging the capacitors in the RC branches to then discharge them to generate the output waveform. To estimate the power, we must know how long the capacitors will be charging for. We can observe that the resistance along current path to the capacitors is ESR of the source, regulator, and the R_p resistor in series with the ESR of the diodes. We call this resistance R_{input} . We assume the ESR of the attenuation MOSFET to be 0 for the ideal case. The R resistors form a parallel network with each other, R_{par} , with R_{input} , and are parallel to the capacitors. The equivalent circuit is shown in Figure 3.5. The time constant of the capacitors during the charging phase can be approximated by

$$\tau = \frac{(R_{input}R_{pal})}{R_{input}+R_{pal}}(C_1 + C_2), \quad (8)$$

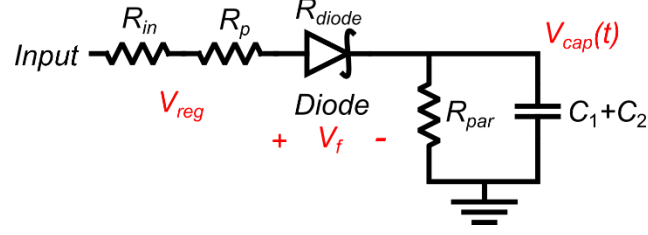


Figure 3.5. Charging phase equivalent circuit for power analysis. R_{input} is equal to the series resistance comprised of R_{in} , R_p , and R_{diode} .

and the time required to charge the capacitors can be approximated to 3τ .

The total power is equivalent to the power consumed by the R_p resistor, diodes, R resistors, and the power required to charge capacitors C_1 and C_2 . The R_{diode} voltage is known, and the capacitor $V_{cap}(t)$ follows the capacitor charging equation with V_{cap} from (1) as the charging voltage. The maximum current drawn by the circuit is V_{cap}/R_{par} and follow the capacitor current equation

$$I_{in}(t) = \frac{V_{cap}}{R_{par}} e^{-\frac{t}{\tau}}, \quad (9)$$

and we can determine all the currents and voltages to calculate the time-varying power consumption of the circuit.

The total power required to charge the capacitors depends on the C_1 , C_2 , and V_{cap} values. Part of the power dissipated will always be consumed in the resistors in the pulse generator circuit. Power consumption can be reduced by targeting ideal conditions where the ESR of the diodes and attenuation MOSFET are minimized. Power consumption during the charging phase is not affected by the load conditions if the attenuation MOSFET ESR is very small. Reductions in the power consumption include increasing the values of the R resistors, although this also affects the output function as shown in (2), so optimization can be performed with the signal requirements as constraints. Lowering the value of C_1 plus C_2 also reduces power consumed during the charging phase and lowers the rate constant, reducing the duration of the charging phase. However, the capacitors similarly affect the output signal and should be optimized with that consideration.

Increasing R_p reduces power consumption overall, however, it has the detrimental effect of reducing V_{cap} thus directly changing the output signal amplitude. Overall, the power consumption of the charging phase falls as the capacitors are charged and reduces to a minimum constant power when the capacitors are fully charged. The trends were simulated and can be observed in Figure 3.6. The circuit components for the simulations were $R = 1000 \Omega$, $R_p = 100 \Omega$, $C_1 = 27 \text{ nF}$, and $C_2 = 250 \text{ nF}$, with a 5V monopolar square wave input at 1 kHz with 50Ω ESR. Root-mean-square (RMS) value of the power consumption during all four phases of operation was 29.88 mW. RMS power consumption during the charging phase only (3τ , 95 μs) was 69.77 mW.

3.5.3. Charged and Discharging Phase Analysis

Power consumption during the charged phase is the power consumed by the R_p resistor, diodes, and R resistors. However, as soon as the capacitors are charged, the discharging phase can be initiated. The charged phase can be set to any arbitrary length of time in order to reduce power consumption. A simulation was performed with a monopolar square wave input with the pulse limited to 3τ or 96 μs , and the RMS power consumption was found to be 20.39 mW showing a reduction of 31.7%. For this reason, it is recommended that the charged phase duration be reduced to approximately 3τ via smart control methods that would prevent any excess power be consumed during this phase.

The discharging phase does not involve input power consumption, so it does not consume input power. The amount of power delivered to the load is the same function as (2), and can be optimized in the same manner. Increasing the amplitude of (2) will directly increase the power.

3.6. Characterization Procedures of the Pulse Generator

The circuit was constructed to verify the correct operation, and circuit analytical results were compared with measured outputs. Output pulses (v_{R_L}), and voltages were captured using a Keysight EDUX1002A oscilloscope (Keysight Technologies, Santa Rosa, California, USA). The

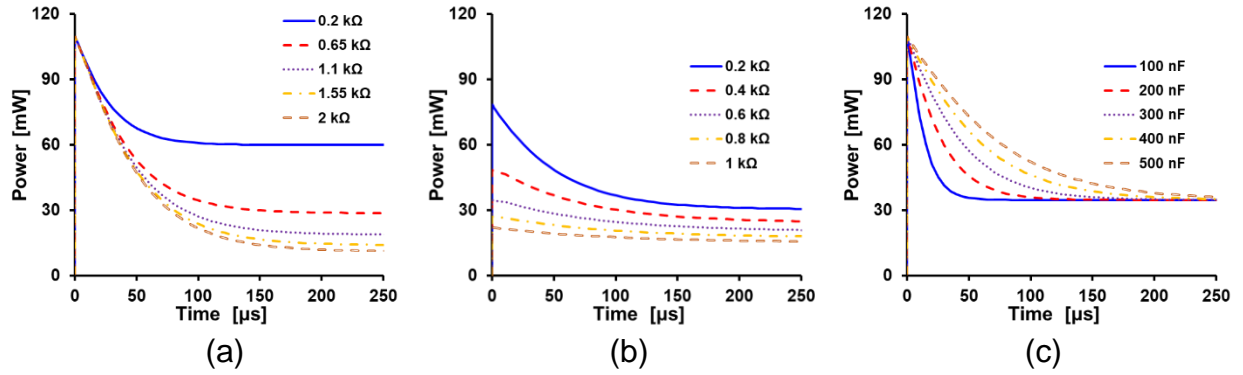


Figure 3.6. Simulations of component effects on input power consumption: (a) varying R , (b) varying R_p , and (c) varying $C_1 + C_2$.

pulse was obtained by measuring the voltage of each capacitor separately, and then subtracting one signal from the other. The deviation was calculated as the percent difference between the measured experimental values and circuit analytical expression results, divided by the measured experimental values.

First, the circuit operation was verified by capturing the input pulse, the regulated voltage, the capacitor voltage, and the output pulse was found by calculating the difference between the capacitor signals. Subsequently, characterization was performed to verify the accuracy of the analytical expressions and parameter functions by characterization with various components. The values of the circuit components tested are listed in Table 3.1.

Human internal resistance values have been measured at 0.43-0.56 kΩ, and the electrode resistance values have been reported to vary between 0.5 kΩ and 1.5 kΩ [134, 135]. The effect of R_L and C_L was characterized to understand the effect of load impedance on output. Load resistance values tested from 500 Ω to 2.7 kΩ [117], and load capacitance values tested are 27 to 150 nF [115]. R was characterized in order to better understand the effect of varying R on δ_{stim} and the v_{max} . The R_p characterization was performed to verify that modifying R_p only changes v_{max} . It is not necessary to increase C_1 with respect to C_2 as the pulse generator RC branch circuits are symmetric, and doing so would generate pulses with the same shape but opposite polarity. The

Table 3.1. Circuit characterization components.

Component	Value
R_L [k Ω]	0.5, 1, 2, 2.7
C_L [nf]	27, 50, 100, 150
R [k Ω]	0.5, 1, 2, 2.7
R_p [k Ω]	0, 0.5, 1
C_1 [nF]	27
C_2 [nF]	27, 250, 560, 1120
Input voltage [V]	6

R_L , C_L , R , R_p and C_2 were varied for the characterization results.

output pulse frequency was characterized by driving the output pulses at increasing frequencies until the pulse peak v_{max} breaks down. The output of the circuit was measured in 1X phosphate-buffered saline solution (PBS). Two 100 μm thick steel acupuncture needles were dipped 5 mm into the solution, and separated by 5 mm distance and used as the output electrodes of the circuit, and the C_2 and R characterization procedures were repeated. The largest output of the circuit was used to estimate the values of C_L and R_L of the PBS solution using Matlab software (Mathworks, Natick, MA). The circuit is designed to not be limited by choice of electrode, and the needles were chosen for ease of use.

The input pulses were generated with an arbitrary function generator (GW Instek AFG 2225, Good Will Instrument Co., Ltd., New Taipei City 236, Taiwan). These input pulses were obtained by programming the pulse setting of the function generator with 50 Hz frequency and 6 V amplitude. The frequency was varied from 20 Hz – 2.5 kHz for the signal generation frequency limit characterization only. The zener diode used as regulator had a 5.1 V of zener breakdown voltage. These characterization results were used to verify the accuracy of t_{peak} , v_{max} , and V_{cap} , by comparing with the results of the circuit analysis in the previous section.

3.7. Measured Results

3.7.1. Analytical Expression Characterization and Validation

The circuit was verified to operate according to the design (Figure 3.7). The four phases of

the circuit operation can be observed, and the state of each section of the circuit (1 - 4 in Figures 3.3 and 3.7) was measured to compare with the expected outcome.

The characterization results when C_2 was increased are shown in Figure 3.8. The component values are $C_1 = 27$ nF, $R = 1$ k Ω , $R_p = 0.5$ k Ω , load capacitance 100 nF, and load resistance 1 k Ω . The deviation between measured and calculated values for t_{peak} is 3.2% to 18.6%, for v_{max} is less than 1.04%, for δ_{stim} is 6.67% to 27% and for V_{cap} is 0.17% to 0.35%. Figure 3.9 shows results where R is increased. The component values are $C_1 = 27$ nF, $C_2 = 250$ nF, $R_p = 0.5$ k Ω , load capacitance 100 nF, and load resistance 1 k Ω . The deviation between measured and calculated values for t_{peak} is 0.5% to 48%, for v_{max} is 0.27% to 3.78%, for δ_{stim} is 3.89% to 20.5%, and for V_{cap} is 1.89% to 6.86%. Figure 3.10 shows results where R_p was increased. The component values are $C_1 = 27$ nF, $C_2 = 250$ nF, $R = 1$ k Ω , load capacitance 100 nF, and load resistance 1 k Ω . The deviation between measured and calculated values for t_{peak} is 1.72% to 33.7%, for v_{max} is 5.28% to 11%, for δ_{stim} is 2.74% to 20.47%, and for V_{cap} is 3.97% to 10.95%. A significant component of the error can be attributed to measurement instability of the oscilloscope, which can be observed in the measured output.

The measured output signal is shown to match the analytical expression output in Figures 3.8, 3.9 and 3.10. Deviation in the maximum output voltage v_{max} was calculated to range from 0.27% to 11% across all characterization tests. The measured and analytical expression values for t_{peak} had deviations of 1.72% to 48%, and for δ_{stim} was 2.74% to 20.5%. The deviation in the measurements stems partially from the oscilloscope signal stability, which contained significant

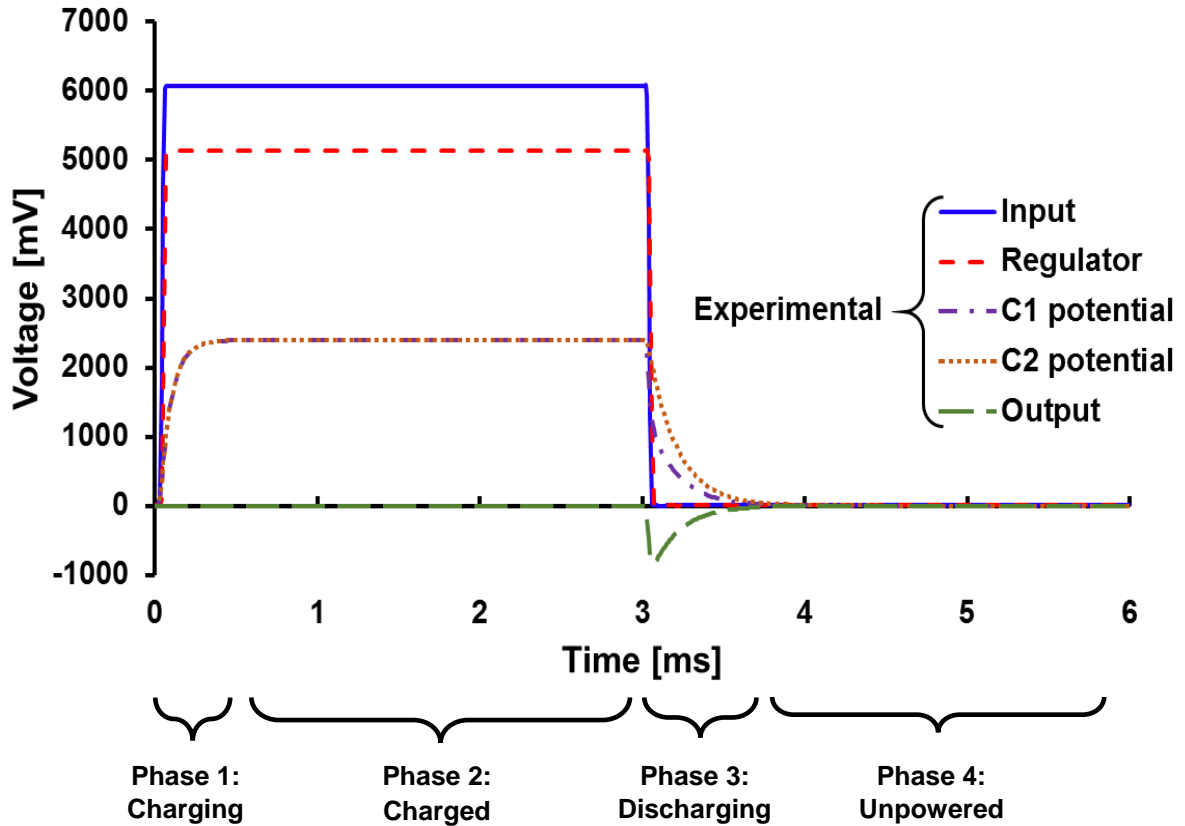


Figure 3.7. Circuit output showing circuit voltages and four operational phases.

high-frequency noise. The t_{peak} and v_{max} , and δ_{stim} are difficult to acquire exactly, as a sample may be collected with a slight increase or decrease in amplitude from the actual values for t_{peak} , δ_{stim} , and v_{max} . The practical effect of the large measured t_{peak} deviation is minimal, as it can be observed in Figures. 3.6, 3.7, and 3.8 that the mathematical model waveform closely follows the measured experimental waveform. The V_{cap} calculation also matched the measured results, with a deviation of 0.17% to 10.95%. The mathematical model of the circuit can thus be said to be accurate and reliable when designing to meet a given output pulse requirement.

The output pulse was shown to increase in amplitude (v_{max}), duration (δ_{stim}), and peak time (t_{peak}) as C_2 is increased, or as κ is decreased (Figure 3.8). This follows from the mathematical relationship previously established in (2). Investigation of (2) shows that as κ decreased in magnitude, the numerator increases which yields a larger amplitude v_{max} and an overall larger

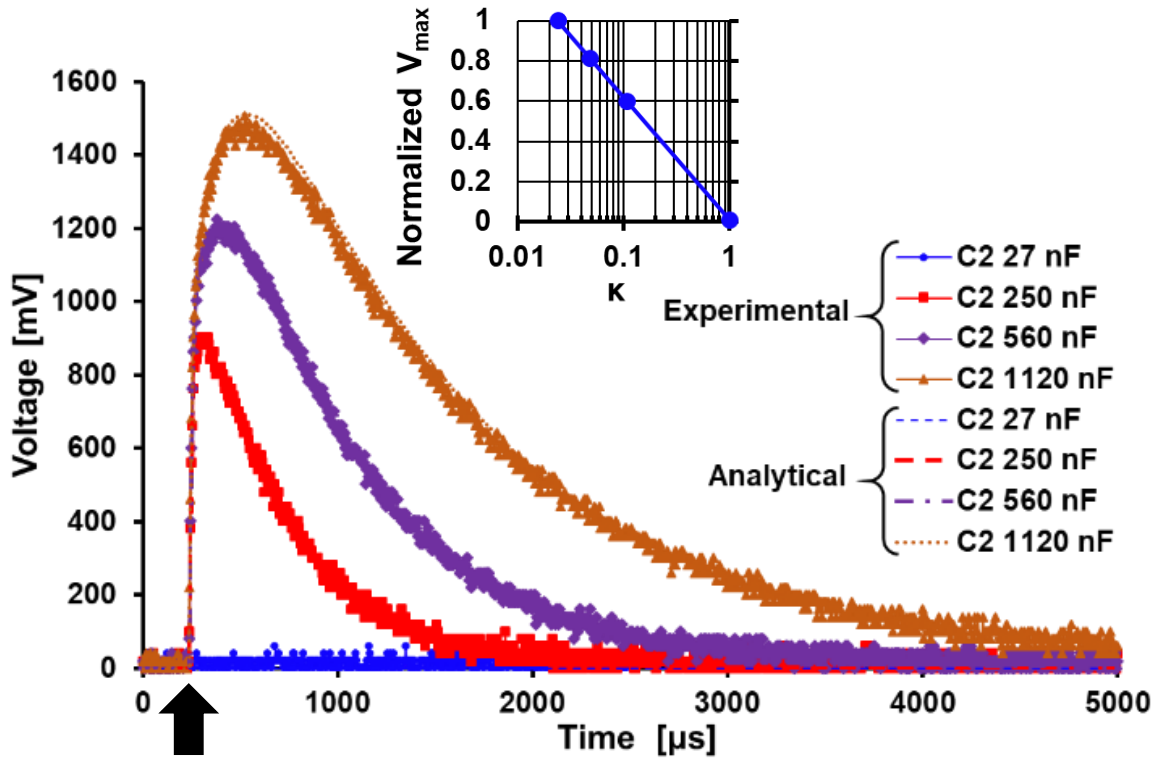


Figure 3.8. Characterization results for increasing C_2 or as κ is decreased. Normalized magnitude of v_{max} against κ (inset). The design component values are $C_1 = 27$ nF, $R = 1$ k Ω , $R_p = 0.5$ k Ω , load capacitance 100 nF, and load resistance 1 k Ω . The deviation between measured and calculated values for t_{peak} is 3.2% to 18.6%, for v_{max} is less than 1.04%, for δ_{stim} is 6.67% to 27% and for V_{cap} is 0.17% to 0.35%. Arrow indicates signal start.

signal. The special case where C_1 is equal to C_2 (κ equals 1) can also be seen in the $\kappa - 1$ term where the output signal (v_{R_L}) becomes 0 for all time. The value κ is a representation of the different time constants of each RC branch. In the special case that κ equals 1, it can also be shown conceptually that both RC branches share the same time constant and thus the pulse becomes 0 across the load. The κ constant is useful to relate the time constant of both RC branches. The expression (2) also holds when C_1 is exchanged with C_2 , and it can be shown by evaluation that the constant parts of the expression are identical but opposite in sign when this change is performed. This means that when the capacitors are exchanged, the same output signal is generated except it has opposite polarity.

A similar trend as the one previously mentioned for κ can be seen when R is increased (Figure

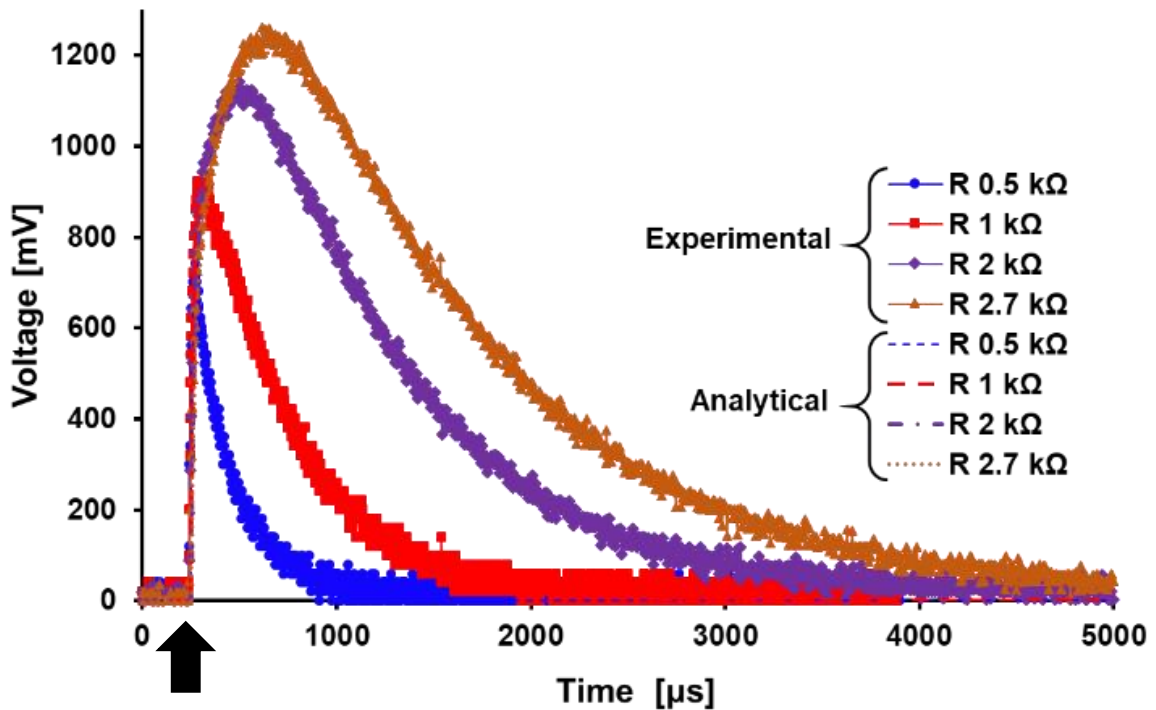


Figure 3.9. Circuit output signal with increasing R . The design component values are $C_1 = 27$ nF, $C_2 = 250$ nF, $R_p = 0.5$ k Ω , load capacitance 100 nF, and load resistance 1 k Ω . The deviation between measured and calculated values for t_{peak} is 0.5% to 48%, for v_{max} is 0.27% to 3.78%, for δ_{stim} is 3.89% to 20.5%, and for V_{cap} is 1.89% to 6.86%. Arrow indicates signal start.

3.9). This trend also follows the mathematical relationship previously established in (2), whereas R is increased, the denominator decreases much faster than the numerator, which yields a larger signal. This is similar to how C_2 affects the output signal. This effect can be seen in the measured outputs where the signals become narrower with R values less than R_p , and wider with R values greater than R_p .

R_p varies the maximum amplitude of the output signal without changing the rate-of-rise or rate-of-decay (Figure 3.10). In summary, the design components R , R_p , C_1 , and C_2 allow for tuning of the output signal amplitude, duration, and location of the peak.

3.7.2. Output Frequency Characterization

The circuit is also able to operate at different output stimulation frequency levels. The output pulse is shown up to 1 kHz (Figure 3.11). The output stimulation frequency (f_{stim}) was

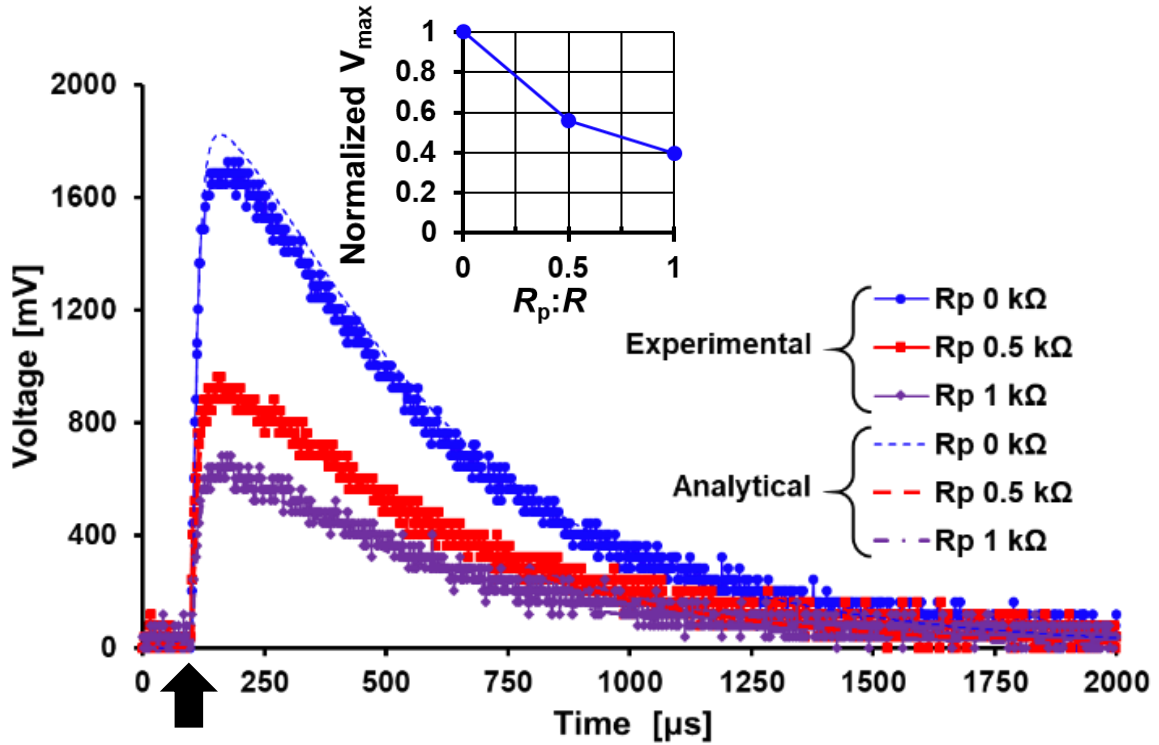


Figure 3.10. Characterization results of circuit output pulse with increasing R_p . Normalized magnitude of v_{max} against $R:R_p$ ratio (inset). The design component values are $C_1 = 27$ nF, $C_2 = 250$ nF, $R = 1$ k Ω , load capacitance 100 nF, and load resistance 1 k Ω . The deviation between measured and calculated values for t_{peak} is 1.72% to 33.7%, for v_{max} is 5.28% to 11%, for δ_{stim} is 2.74% to 20.47%, and for V_{cap} is 3.97% to 10.95%. Arrow indicates signal start.

approximated from the experimental data. According to the four phases of operation, the capacitors must first be charged completely during the charging phase before a signal can be generated during the discharging phase. The duration of the charged and unpowered phases can be reduced by control of the input signal such that they do not appear in the output signal. From the measurement of a low frequency pulse, an expression was derived to approximate the output stimulation frequency limit. First, the charging time of the capacitors, t_{charge} , is approximated by measuring the duration of the charging phase, which in this case was approximately 500 μ s. The experimentally derived f_{stim} becomes

$$f_{stim} = \frac{1}{2t_{charge}}. \quad (10)$$

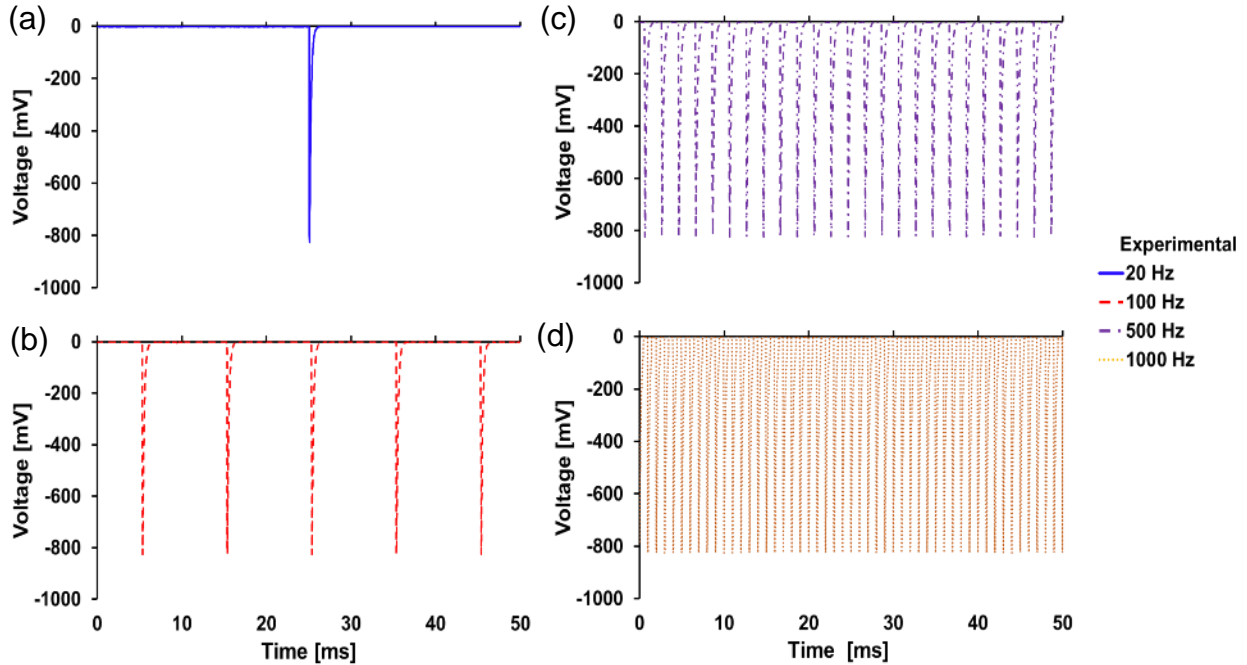


Figure 3.11. Measured results for the circuit with a variable output pulse frequency: (a) 20 Hz, (b) 100 Hz, (c) 500 Hz, and (d) 1000 Hz.

This expression allows us to approximate the f_{stim} that a circuit can operate at with given circuit components. The circuit components were $R_L = 1 \text{ k}\Omega$, $R_p = 0.5 \text{ k}\Omega$, $R = 1 \text{ k}\Omega$, $C_1 = 27 \text{ nF}$, and $C_2 = 250 \text{ nF}$. The circuit is shown to have a reliable output stimulation frequency variability that is dependent on the width of the charging phase. An exact expression for f_{stim} was not derived in this work. The circuit was tested at frequencies of up to 2.5 kHz, and the circuit operated normally up to 1.6 kHz, where a drop of 1% is seen in v_{max} . The signal was considered to break down when the v_{max} amplitude of the output signal lowered by more than 1% at a given f_{stim} . The circuit was tested at frequencies of up to 2.5 kHz.

3.7.3. Load Characterization

The effects of a model load were characterized by varying the load resistance and capacitance (Figures 3.12 and 3.13). From (2) we can see that the output pulse decreases with increasing load capacitance, and increases in increasing load resistance.

The characterization when the load capacitance is varied is shown in Figure 3.12. The design

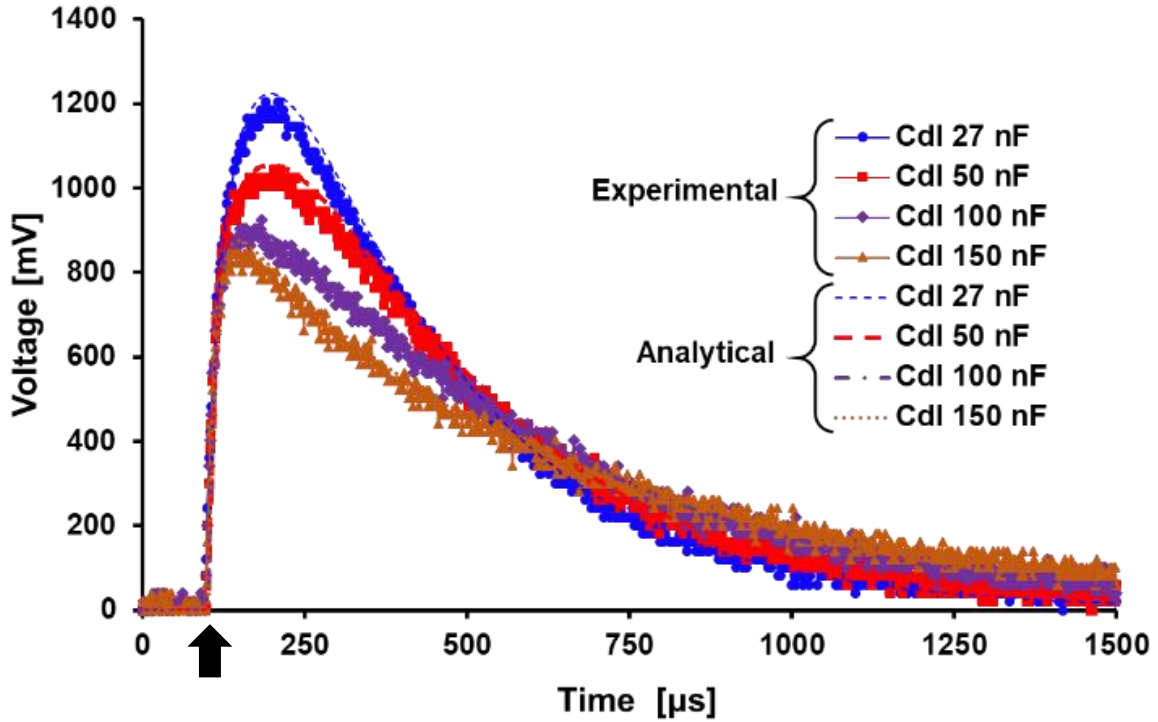


Figure 3.12. Characterization results for increasing load capacitance. The design component values are $C_1 = 27$ nF, $C_2 = 250$ nF, $R = 1$ k Ω , $R_p = 0.5$ k Ω , and load resistance 1 k Ω . The deviation between measured and calculated values for t_{peak} is 5.56% to 10.91%, for v_{max} is 0.94% to 3.86%, for δ_{stim} is 3.92% to 13.98% and for V_{cap} is 4.48% to 4.95%. Arrow indicates signal start.

component values are $C_1 = 27$ nF, $C_2 = 250$ nF, $R = 1$ k Ω , $R_p = 0.5$ k Ω , and load resistance 1 k Ω .

The deviation between measured and calculated values for t_{peak} is 5.56% to 10.91%, for v_{max} is 0.94% to 3.86%, for δ_{stim} is 3.92% to 13.98% and for V_{cap} is 4.48% to 4.95%. The characterization results when the load resistance is varied are shown in Figure 3.13. The design component values are $C_1 = 27$ nF, $C_2 = 250$ nF, $R = 1$ k Ω , $R_p = 0.5$ k Ω , and load capacitance 100 nF. The deviation between measured and calculated values for t_{peak} is 6% to 32.94%, for v_{max} is 0.20% to 5.01%, for δ_{stim} is 8.86% to 20.2% and for V_{cap} is 4.95% to 5.81%. The load conditions affect both the t_{peak} and v_{max} , however the signal width δ_{stim} affected in a different manner. Since δ_{stim} depends on v_{max} in our definition, the output width is affected according to our analytical expression. Observation of the measured results suggests that variations in load resistance do not significantly affect the signal after the time point t_{peak} , and the effects of the resistive load on the tail end of the signal are

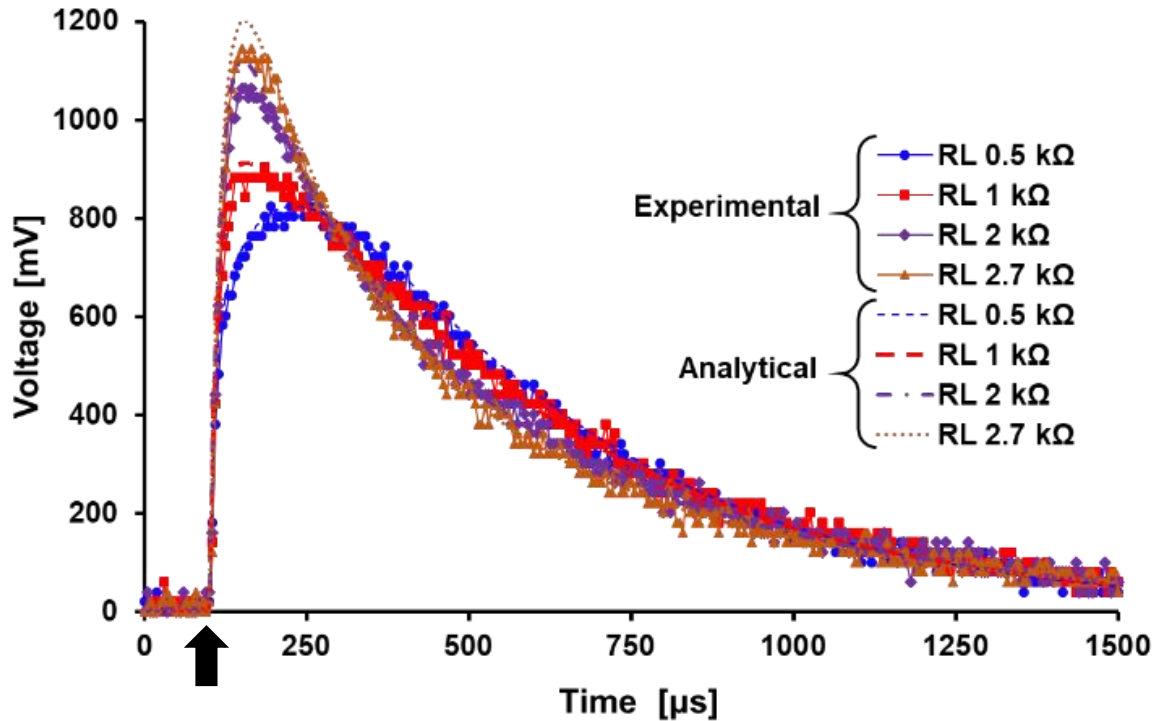


Figure 3.13. Characterization results for increasing load resistance. The design component values are $C_1 = 27$ nF, $C_2 = 250$ nF, $R = 1$ k Ω , $R_p = 0.5$ k Ω , and load capacitance 100 nF. The deviation between measured and calculated values for t_{peak} is 6% to 32.94%, for v_{max} is 0.20% to 5.01%, for δ_{stim} is 8.86% to 20.2% and for V_{cap} is 4.95% to 5.81%. Arrow indicates signal start.

minimal.

3.7.4. Phosphate-Buffered Saline Solution Measurements

The design of the circuit has to take into account the target application load conditions. The circuit output was measured when PBS solution was used as the load instead of the circuit model load. The largest signal of each data set (1120 nF for C_2 characterization, and 2.7 k Ω for R characterization) was used to estimate the component values of the circuit model load, and these values were then used to calculate the output of the circuit for the other component values used for characterization. The load component values were estimated to be $C_L = 410$ nF and $R = 600$ Ω for the C_2 characterization (Figure 3.14), and $C_L = 310$ nF and $R = 580$ Ω for the R characterization (Figure 3.15). The characterizations performed in PBS solution load showed the same trends as the electrical model load characterization.

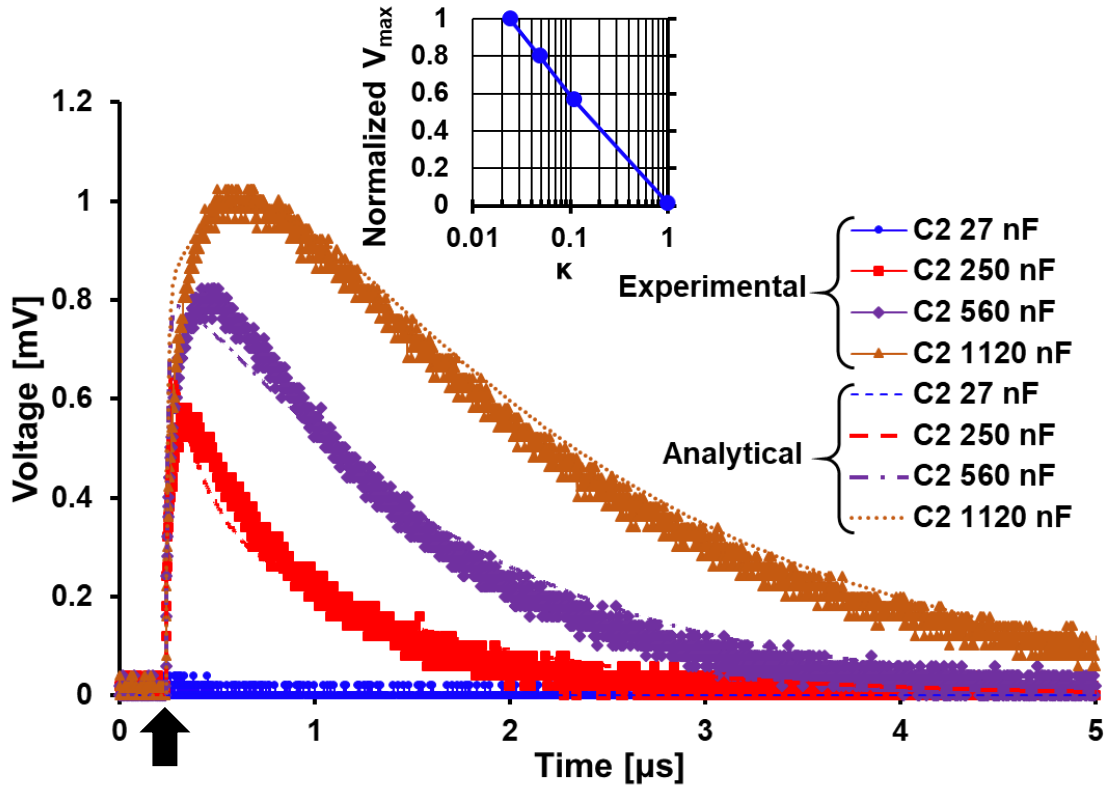


Figure 3.14. Characterization results for increasing C_2 in PBS solution. The design component values are $C_1 = 27$ nF, $R = 1$ k Ω , and $R_p = 0.5$ k Ω . The deviation between measured and calculated values for t_{peak} is 8.9% to 75%, for v_{max} is 3.5% to 11.8%, and for δ_{stim} is 25.7% to 61%. Arrow indicates signal start.

The characterization for C_2 in PBS solution load had design component values $C_1 = 27$ nF, $R = 1$ k Ω , and $R_p = 0.5$ k Ω . The deviation between measured and calculated values for t_{peak} is 8.9% to 75%, for v_{max} is 3.5% to 11.8%, and for δ_{stim} is 25.7% to 61%. The output signal in PBS solution can be estimated using the output expressions of the circuit and one measurement. The characterization for R in PBS solution load had the design component values $C_1 = 27$ nF, $C_2 = 250$ nF, and $R_p = 0.5$ k Ω . The deviation between measured and calculated values for t_{peak} is 9.67% to 69%, for v_{max} is 1% to 15.3%, and for δ_{stim} is 15.5% to 48.7%. The measured output was observed to be similar to the analytical expression output however; there were time domain discrepancies that led to a high deviation of t_{peak} values. This indicates that the load model based on the simplified Randles equivalent circuit is incomplete, and can be improved with a better model of the electrode-

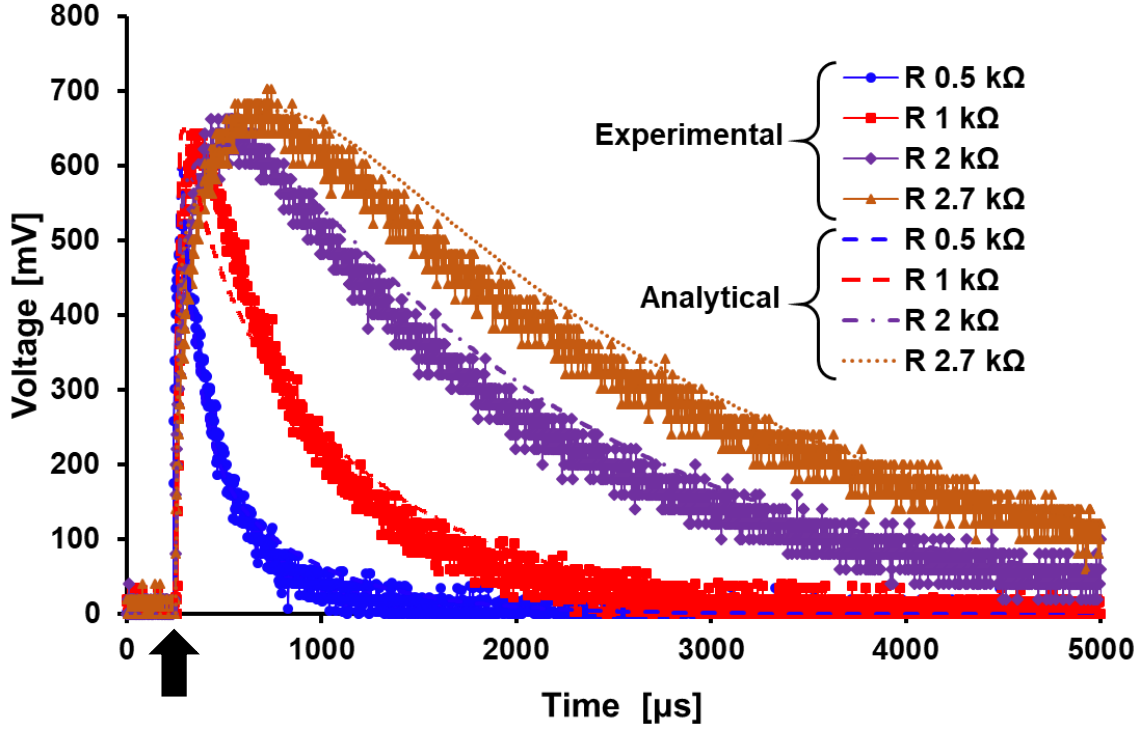


Figure 3.15. Characterization results for increasing R in PBS solution. The design component values are $C_1 = 27$ nF, $C_2 = 250$ nF, and $R_p = 0.5$ k Ω . The deviation between measured and calculated values for t_{peak} is 9.67% to 69%, for v_{max} is 1% to 15.3%, and for δ_{stim} is 15.5% to 48.7%. Arrow indicates signal start.

electrolyte interface. The measured results and analytical expression output show good agreement overall, and the expected stimulation pulse in future applications can be estimated if the expected C_L and R_L are found.

The charge delivered to the load can be approximated with the output expression

$$Q_{stim} = \int_{t_{rise}}^{t_{decay}} I_{load}(t) dt, \quad (11)$$

where the current across the load is defined by the voltage across the load and the electrode parameters.

Power consumption analysis of the circuit is not the focus of this work, however, the target application should be considered when designing the circuit. Laboratory studies that focus on analyzing *in-vitro* tissue responses to diverse waveforms will have different power requirements

than *in-vivo* studies with wearable devices such as transcranial electrical stimulation (TES) and functional electrical stimulation (FES). Studies related to effects of waveforms *in-vitro* have less strict power requirements when compared to portable devices *in-vivo*.

3.8. Conclusions and Improvements for Circuit

A novel passive pulse generator circuit with EPSP-shape waveforms has been presented and characterized. A circuit analysis was presented, and the results were compared to previous literature [133] showing output shape inspired by EPSP and IPSP waveform functions. The signal generator operation and circuit analytical expressions were verified by characterizing an assembled circuit. The analytical expression results and the experimental measured results showed good agreement in both benchtop and PBS solution measurements that confirms that the circuit expressions are accurate for the pulse generator. In terms of signal design, v_{max} , t_{peak} , and δ_{stim} increased as κ was decreased; and t_{peak} and δ_{stim} increased and v_{max} decreased as R was increased. Furthermore, the pulse generator outputs a unique shape for each design component combination, allowing for the design of the pulse when given a required amplitude and duration. The circuit was shown to operate with a variable output stimulation frequency.

An expression for the limit of the output stimulation frequency was derived from the measured results of the signal generator waveform. The device is independent of tissue interface methodology, and was designed as a pulse generator that can be coupled with different power sources and neural interface mechanisms for application-specific purposes. Power consumption of the circuit should be considered when designing a circuit for a specific application. Studies related to effects of waveforms *in-vitro* will have less strict power requirements when compared to portable devices *in-vivo*. Knowing the electrode type and target tissue (muscle, nerve, brain slices) an application-specific circuit could be designed using the analytical circuit expressions. It is envisioned that this system can have modular applications as a research tool for generation of

EPSP- and IPSP-shaped signals in studies of stimulation waveforms such as transcranial electrical stimulation (TES), deep brain stimulation (DBS), and studies on complex response of brain subnetworks or brain slices.

There are other variations of the circuit which must be considered in future work. For example, the circuit can be designed to provide a square-wave signal by choosing resistors R of different values, and omitting the balance transistor, but this characterization and analysis are out of the scope of the present work. Additionally, if the transistor is removed then the output pulse becomes biphasic, as the charging and discharging phase output signals are opposite in sign. It is envisioned that this device would allow for comprehensive neurostimulation systems where several distinct stimulation signals are required to stimulate different nervous locations or different tissues such as muscle and nerves. Moreover, it provides a simple solution for scientists looking to study the effects of novel waveforms on neuromodulation and plasticity. The simplicity of the circuit allows for easy inclusion of the pulse generator in larger systems as a modular unit for neurostimulation purposes or other applications.

Current work for improvement of the signal generator involves utilizing two circuits in tandem to generate a biphasic signal. Additional improvements include implementation of a closed-loop feedback circuit to regulate the output pulse according to changing load conditions, and this may be necessary for long-term applications. Smart control to minimize power consumption, and choosing design components to optimize power are also tasks that should be explored. Collaborative projects with *in-vitro* and *in-vivo* stimulation studies could be implemented in order to demonstrate the applicability of this circuit in neurostimulation. The effectiveness of our passive charge balancing method via continuous grounding should be verified with further studies on tissue damage. Applications being considered include transcutaneous

electrical nerve stimulation (TENS), transcutaneous pulsed current stimulation (tPCS), and control of biological function through vagal nerve stimulation. Future research lies with *in-vivo* stimulation studies to identify the effects of EPSP and IPSP shaped stimulation pulses. An implantable device would have to take into consideration the size of the passive devices on the circuit, as these may be large depending on the implant location. For some applications such as VNS this may not be an issue, but for other applications such as DBS size must be carefully considered. Improvements to the model to find the charge density provided by the signal generator with a given neural interface are also possible.

The following chapter presents a design project that provides a neurostimulator solution for EA applications, and verifies operation of the circuit in an EA animal study.

4. WEARABLE SMARTPHONE-COMPATIBLE ELECTRO-ACUPUNCTURE NEUROSTIMULATOR FOR ENHANCED CLINICAL AND SCIENTIFIC OUTCOMES

4.1. Introduction

Acupuncture is a growing field in western medicine that can be used to treat a plurality of conditions because it taps into nerve pathways and motor control areas. Electro-acupuncture (EA) is a method for applying acupuncture stimulation using electrical stimulation machines. Significant challenges are present in the clinical and research fields of electro-acupuncture because results typically depend on the experience of the acupuncturist, and electro-acupuncture stimulators are large, cumbersome, and have analog settings; making it difficult to report and later reproduce results across research and clinical applications. An electro-acupuncture stimulator was developed that is wearable and programmable via smartphone in order address these issues. The system was programmed via smartphone app, and shown to control output voltage and output frequency. The system was verified to operate as an electro-acupuncture stimulator by incorporating it into an electro-acupuncture study. In this chapter we cover the design process involved to develop a wearable stimulator enhanced with smartphone control and Bluetooth connectivity.

4.2. Acupuncture Background and Design Problem

Acupuncture is a method for treating conditions through stimulation of specific points in the body that lie on nerve pathways, lymphatic pathways, or motor control areas [99, 102, 103, 105, 106, 136, 137]. Stimulation can be performed through various methodologies, and electro-acupuncture has increased in interest due to the ease of use of electrical stimulation machines. EA is a growing field with diverse medical applications [100]. Medical conditions treated include pain management, cancer symptoms, musculoskeletal, neurological, obstetric, gastrointestinal, cardiovascular, and surgical anesthesia [51, 101, 138-140]. While many studies have been

conducted, significant challenges remain in the scientific study of medical applications of EA [141-143].

One of the problems with scientific studies of EA is that acupuncture techniques and stimulation parameters can differ depending on clinician experience, personal preference, and individual pain tolerance [108]. Additionally, commercial EA stimulation machines are large and heavy which requires the patient – human or animal – to remain relatively motionless during treatment [124]. This can cause undesired stress responses in animals, or require sedation of the animal. Both of these options fundamentally change the physiological condition of the patient and can affect the outcome of the experimental procedure. From the clinician and scientist point of view, EA machines are not designed for modern experimental conditions that take advantage of computational power of smartphones or computers. A solution is desired that tackles these problems, and provides a better approach for clinicians and scientists alike [144, 145].

The features of the system discussed in this chapter are outlined in Figure 4.1. The EA stimulator is designed to be worn by the patient during treatment, and is controlled via a smartphone with Bluetooth connection. The small size and wearable feature of the device allow the patient to move around and resume normal activities during treatment. This feature is especially important in veterinary applications to reduce stress on the animal. The smartphone control of the device allows for precise adjustment of stimulation pulse voltage and frequency. This can be combined with smartphone data processing capabilities to allow easy logging of patient and treatment data.

In this chapter we discuss the circuit and smartphone app design of the system. We also use the device in an EA animal study to verify the correct operation as an EA stimulation machine.

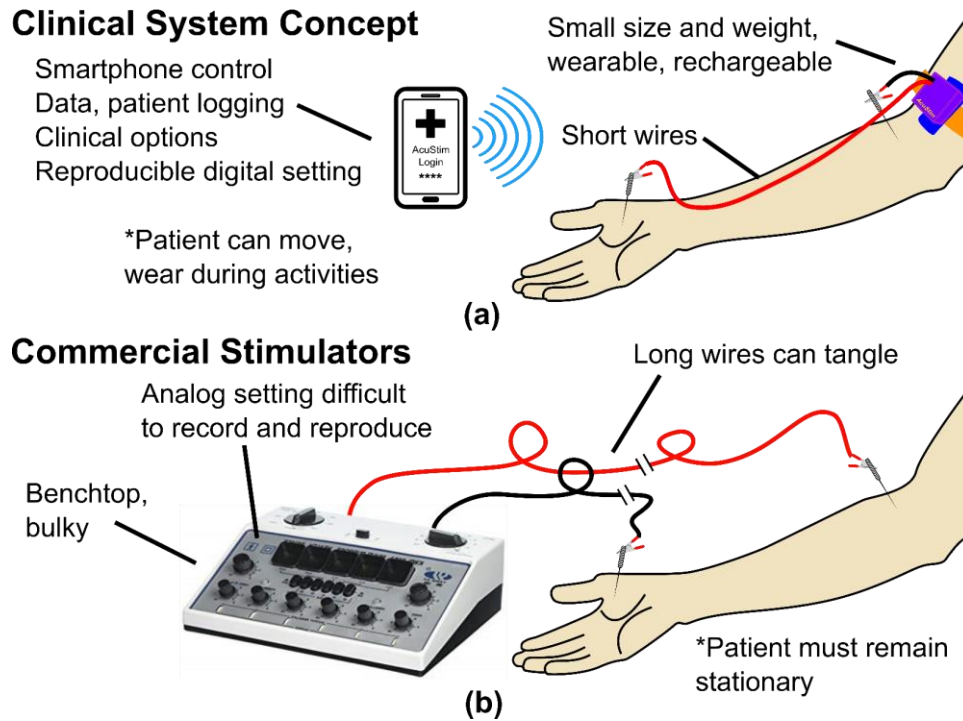


Figure 4.1. Comparison between features of proposed system, and problems with current commercial stimulators: (a) main features of proposed system, and (b) problems with commercial stimulators tackled by our system concept.

4.3. Design of Electro-Acupuncture Circuit

4.3.1. Overview of Circuit Design

The circuit organization is shown in Figure 4.2. Power input is a 3.7 V lithium polymer battery connected to a battery charger module. Power is then delivered to the Bluetooth module, boost converter circuit, and microprocessor unit. The microprocessor relays device information to the user smartphone via the Bluetooth module, which is used for bidirectional communication. The microprocessor then controls the output voltage level of the device via the boost controller, and sets the frequency of stimulation with the high-voltage (HV) switch. The stimulator is based on the pulse generator circuit presented in Chapter 3, and is improved by adding a boost converter for input power, and the output is controlled by an HV switch. A bipolar wire clip connects the output of the stimulator to acupuncture needles which are inserted in acupoints for treatment. Stimulation

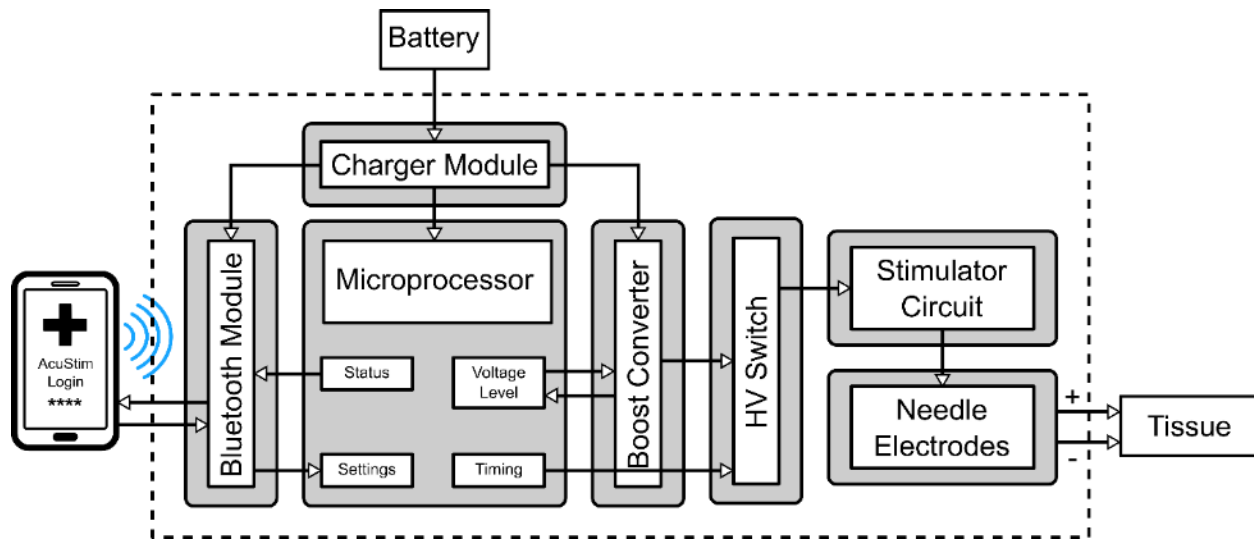


Figure 4.2. Electro-acupuncture circuit design.

output design was performed with consultation with a veterinary acupuncturist from the Louisiana State University School of Veterinary Medicine (LSU-SVM).

4.3.2. Output Pulse Generator Circuit

A commercial electro-acupuncture device output was analyzed, and the maximum power level output used by the acupuncturist was found to be 3 V across a 1 k Ω load with an approximate duration of 400 μ s. Thus, we chose our design to have a maximum output voltage of at least 4 V, and duration of at least 500 μ s with a 1 k Ω load. Stimulation pulse design is detailed in Chapter 3 for resistive and capacitive loads. The improved circuit is shown in Figure 4.3. The boost converter was designed to supply up to 18 V to the HV switch. The boost converter output level is controlled via a (PWM) signal from the microprocessor. The HV switch is timed by the microprocessor. The microprocessor is also used to control LEDs for visual indication. The machine we tested had 8 independent channel outputs, here we focus on the development of a single channel first to ensure correct operation.

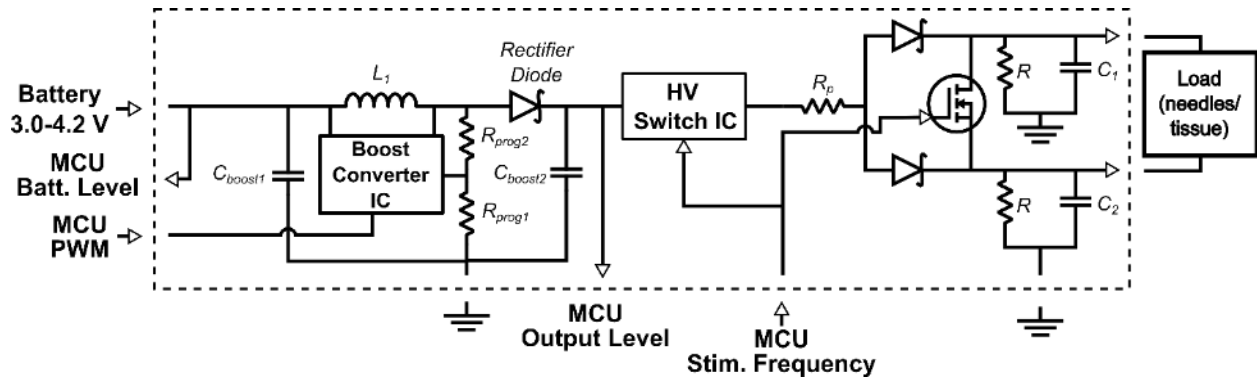


Figure 4.3. Stimulation pulse output circuits showing boost converter and HV switch layout, and microprocessor I/O.

4.3.3. Printed Circuit Board and Case

The veterinary acupuncturist was also consulted for the case design of the EA stimulator. Device size must be optimized for the device to be wearable. The circuits were implemented in a PCB that is attached vertically to a microprocessor pin-out board and Bluetooth module (Figure 4.4(a)). The dimensions of the device with case were 56 mm x 35 mm x 41 mm, with a weight of 75 grams. A 500 mAh 3.7 V lithium polymer battery was used for this system.

We also investigated the clinical setting and discussed with clinicians about usage of the device in order to determine typical requirements for battery life, pulse characteristics, interface type, and case design. Minimum battery life is 30 minutes for a typical EA treatment session, however, a charge should last at least one day of treatment sessions. Each device is used for approximately one 30 minute treatment session per hour, which results in 4.5 hours of usage. Output voltage should go up to a minimum of 3 V across a 1 k Ω load, and duration should be 500 μ s. Stimulation frequency should be variable, and the most commonly used frequencies lie between 2 Hz and 100 Hz [100, 107]. The interface type preferred was 2 mm banana plug jack bipolar alligator clips that clamp on the acupuncture needles (Figure 4.4(b)).

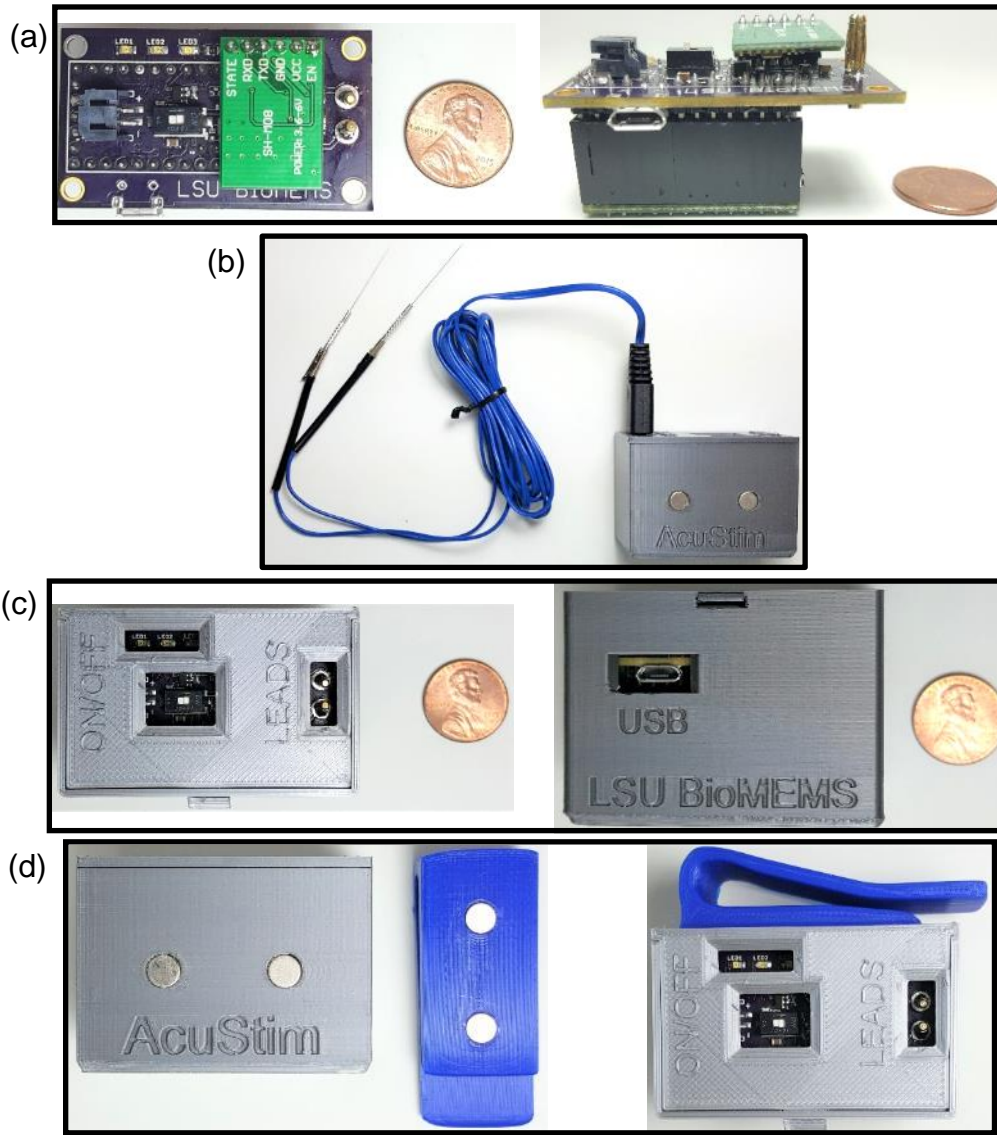


Figure 4.4. Design of PCB and case: (a) picture of system PCB, (b) 2 mm banana plug for electrode interface with acupuncture needles as electrodes, (c) LEDs for visual status indication, recessed ON/OFF switch, and USB charging port, and (d) magnetic attachment to belt clip.

The wearable case design required that the settings would not accidentally be altered during treatment, and that the device would not tangle and break the electrodes, device, or harm the patient. The case was designed to have 3 LEDs for visual status indication to the user (charging, done charging, and device status), and one recessed main power switch with a charging port on the side (Figure 4.4(c)). The settings can only be changed in the app used by the clinician. The

case attaches to a belt clip via neodymium magnets such that if tangling of wires or impact to the case occurs the case detaches safely from the belt clip. (Figure 4.4(d)).

4.3.4. Smartphone App Design

A smartphone application was developed to control the EA stimulator. We used Bluetooth Low Energy (BLE) protocol because of its reduced energy consumption. The main screen shows all the control buttons and the current values of the voltage output, stimulation frequency and duration of stimulation (Figure 4.5). The user simply changes the values of the parameters and presses the “Start” button to commence stimulation. The BLE device was configured as server, so that the smartphone makes requests to the device for updating the stimulation parameters. Once treatment is started, the EA stimulator will operate independently of the smartphone in case Bluetooth connection is lost, and will carry out stimulation for the duration set during the programming. Chapter 5 discusses software and hardware requirements in detail.

4.4. Measurement Results and Discussion

4.4.1. Smartphone Control of the Output Voltage

The device was connected to acupuncture needle clips, and voltage was measured across a 1 k Ω load (Figure 4.6(a)). The output voltage was controlled via the smartphone, and continuously measured to verify operation of the voltage control (Figure 4.6(b)). The present output level is also shown in the app to allow for repeatability and consistency across patients or treatments. Precise controllability of output levels allows for repeatable experimental procedures, and for repeatable and reliable treatment conditions. This type of recording and repeatability, in addition to the stimulation pulse characteristics developed previously by our group are necessary for proper reporting of electro-acupuncture results [142].

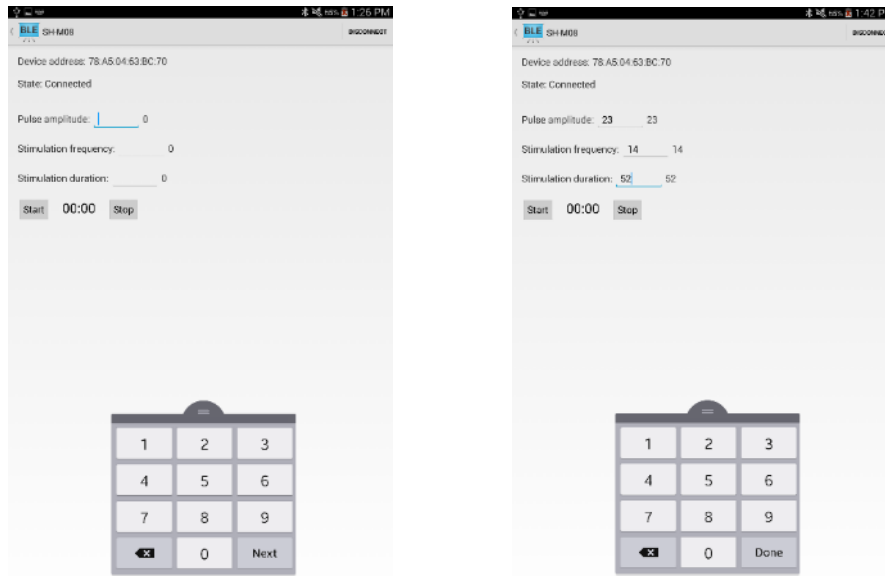


Figure 4.5. Smartphone app images.

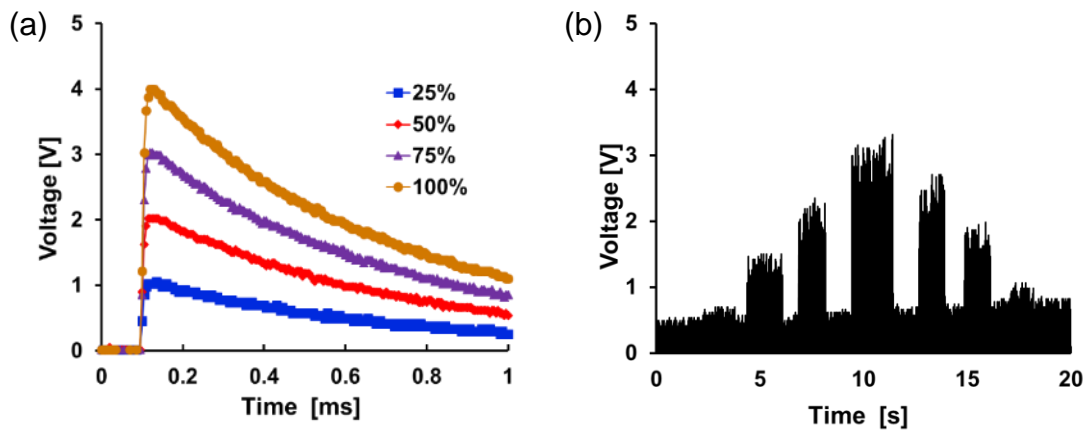


Figure 4.6. Output voltage measurements using smartphone control via Bluetooth: (a) range of voltage levels, (b) continuous measurement of variable output voltage.

4.4.2. Smartphone Control of Stimulation Frequency

Stimulation frequency was also measured with outputs across a 1 k Ω load (Figure 4.7). The stimulation frequency was controlled via the smartphone, and the current setting is reflected in the app. Controllability of stimulation frequency is integral for research and clinical applications of EA devices [108, 142].

In the veterinary setting, animals must be physically restrained or sedated to allow for EA treatment, the placement of needles, and to maintain proximity to benchtop devices [124, 145].

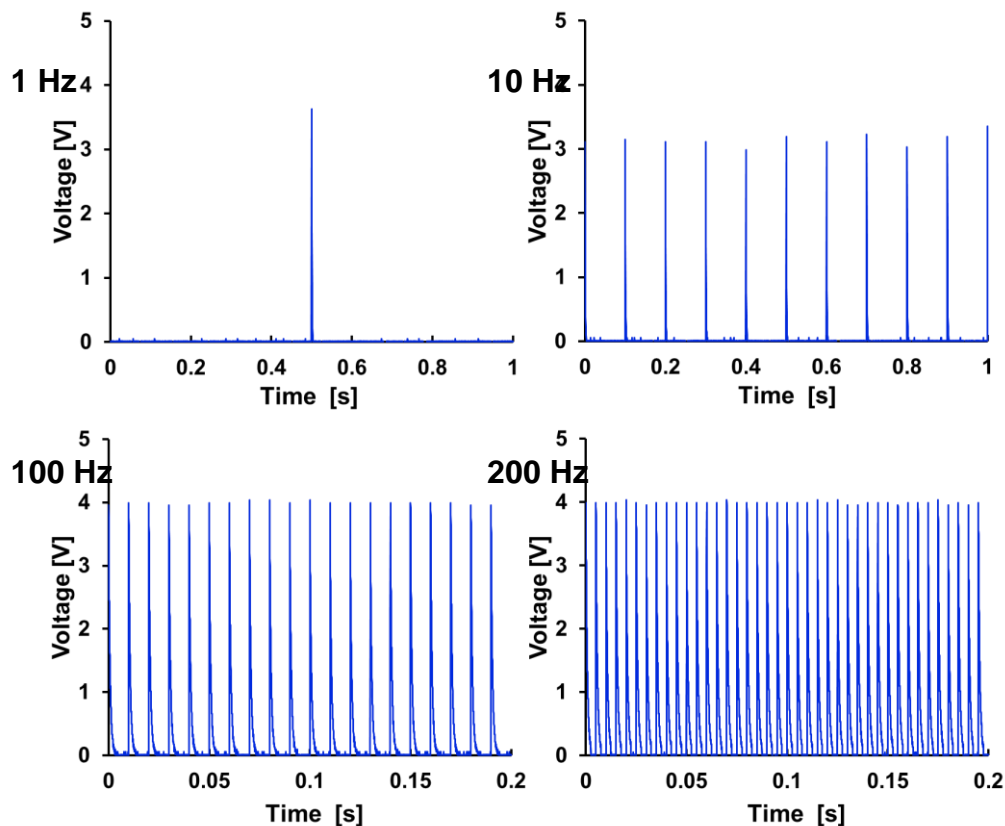


Figure 4.7. Stimulation measurements using smartphone control via Bluetooth over a range of stimulation frequencies: 1 Hz, 10 Hz, 100 Hz, and 200 Hz.

Our wearable approach provides a solution for these issues. Veterinary patients have the additional problem that sedation and holding may cause unwanted hormone release, and this may affect the outcome of treatment. Wearable operation solves these issues by allowing patients to move freely while receiving treatment, and also to move to a different location during treatment. Additionally, wearable devices allow for new treatment methodologies such as take-home EA prescription treatment. In this case the device would be programmed at the clinic, and then the patient can take it home for treatment over several days. The use of a smartphone also allows for novel features not available in other commercial EA devices such as: secure user login, patient logging, treatment logging, multiple device connectivity, and take-home device programming. Our approach is

comparable with the system presented in [145], where we take advantage of the ubiquity of mobile devices to provide enhanced features for the clinician.

4.4.3. Measurements in Phosphate-Buffered Saline Solution

The circuit output was measured using 1X phosphate-buffered saline (PBS) solution with steel acupuncture needles as electrodes (Figure 4.8). The needles were immersed 5 mm into the solution, and separated 5 mm. The output leads were directly clipped onto the acupuncture needles, and the output voltage was varied using the smartphone app set to 25% – 100%. Other types of neural interface electrodes can be utilized, and the system is not limited to one type or another. The output waveform characteristics in an electrochemical load such as PBS can be approximated using the analytical expressions detailed in Chapter 3. The overall shape of the signal was maintained with the PBS load, and the output control followed a similar linear trend when increasing the output voltage using the smartphone app.

4.4.4. Battery Life

The device was powered by a 500 mAh 3.7 V lithium polymer battery. The system was set to output stimulation at maximum output level and 150 Hz stimulation frequency across a 1 k Ω load with no stop in stimulation. Battery was charged to 4.2 V. The battery voltage was periodically measured, and found to last 300 minutes (6 hours) before it was discharged and device turns off. This duration is sufficient for the expected use of one day of treatment in a clinical setting (approximately 4.5 hours of stimulation). The battery life can be extended via microprocessor and Bluetooth low-power settings, which were not implemented in this test.

4.4.5. Animal Experiment Validation

The system was utilized in an EA study at the LSU-SVM. The animal study protocol was approved by the Institutional Animal Care and Use Committee (IACUC) of LSU-SVM. The

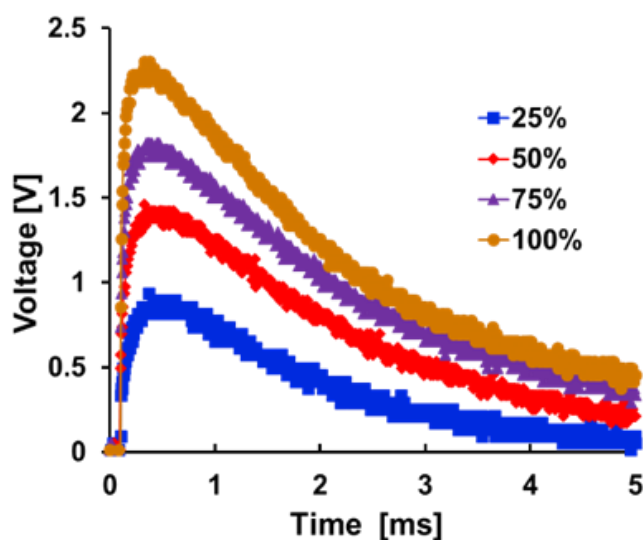


Figure 4.8. Output voltage measurement with acupuncture needles as electrodes and PBS 1X as load.

randomized animal study was performed to determine if EA applied to GV26 and GV1-b (Weijian) could be used to lower the dosage amount of atipamezole hydrochloride required for post-surgery anesthesia recovery. 35 cats were anesthetized using ketamine, dexmedetomidine, and butorphanol tartrate in 1.25:1:1.25 ml ratio mixed with 1.5 ml saline. Dosage of the anesthesia was 20 $\mu\text{g}/\text{kg}$. The manufacturer recommended full dose of atipamezole hydrochloride is equal to the dosage of anesthesia, or 20 $\mu\text{g}/\text{kg}$ in our case [146]. 3 groups of cats were treated using one quarter dose atipamezole hydrochloride and EA (12 cats), one quarter dose atipamezole hydrochloride and dry needling (10 cats), or one half dose atipamezole hydrochloride and no acupuncture (13 cats). The time to recover from anesthesia was recorded.

The recovery time for dexmedetomidine reversal with atipamezole hydrochloride in cats has previously been reported [147]. Sedation and analgesic effects were clinically and statistically reduced in 5 minutes, and full recovery was observed at 15 minutes. Dosage in the study was 40 $\mu\text{g}/\text{kg}$ dexmedetomidine, and 200 $\mu\text{g}/\text{kg}$ atipamezole hydrochloride, or a 5-fold increase in atipamezole hydrochloride compared to our method.

The animal experiments were used to verify correct operation of the device in EA applications. The 1/4 dose atipamezole hydrochloride treatments alone should not be effective in recovering the cats from anesthesia however, when coupled with dry needling (DN) and EA it can be seen they have similar effectiveness to using a 1/2 dose (Figure 4.9). These results are comparable with the manufacturer effectiveness results and previous studies [146, 147]. Additionally, these results also support conclusions found by Shmalberg [107], who performed an experiment where they stimulate GV26 to increase anesthesia recovery. The comparable performance between treatments was expected, however, it can be seen that EA treatment had less error and matched the 1/2 dose results better than the DN treatment. This is because application of DN treatment has a dependency on clinician skill and consistency. Due to the short amount of time required for treatments to be effective, it was difficult to see if the DN needle placement was initially correct, or if modification was required. EA shows more consistent results as it is less dependent on user skill, and this is desirable for consistency in research and clinical purposes [108, 142, 144]. The probability of the variances between the two 1/4 dose groups to be statistically significant was calculated to be 0.0534 via F-test, so we cannot conclusively say that the variances are different. However, we cannot draw conclusions beyond the fact that the EA device has comparable results to DN treatment because of limitations to the design of the study. A future study would need to have an additional control group with 1/4 dose and no treatment, so that results can be directly compared between treatment groups with and without EA. The additional control group will allow for direct comparison of the efficacy of acupuncture methods with atipamezole hydrochloride. This group would be needed to properly determine if acupuncture treatment has a significant effect over simply using a smaller dose, as the results stand it is not possible to make this conclusion from the data.

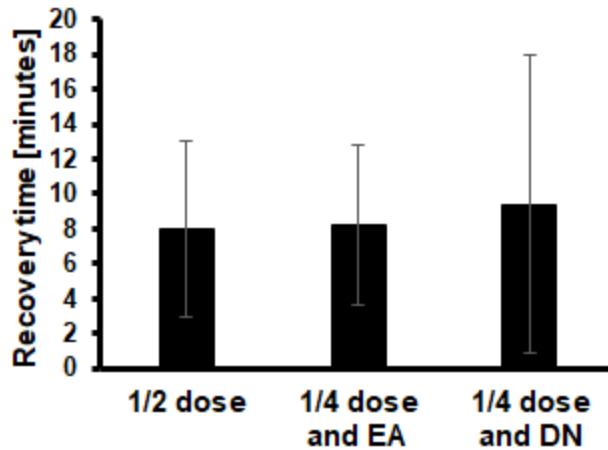


Figure 4.9. Animal experimental results of using reduced doses of atipamezole hydrochloride and acupuncture for anesthesia recovery.

4.5. 2-Channel Implementation

4.5.1. 2-Channel Implementation Requirements

EA is typically performed on several acupoints simultaneously. Therefore, it is desirable to have a device that outputs independently controlled signals on multiple channels. The machine that we analyzed had 8 output channels, here we will show a 2-channel implementation, and the hardware requirements to enable more channels. The block diagram with multiple channels is shown in Figure 4.10.

Each channel requires independent voltage amplitude control, frequency output, and stimulation duration. Voltage amplitude is controlled at the boost converter via the duty cycle of 1 PWM signal from the microprocessor. This PWM signal must have frequency greater than 10 kHz and less than 100 kHz because of the chip that we have chosen. The output frequency is controlled via the frequency of 1 PWM signal with fixed 50% duty cycle. This frequency is 1-200 Hz for EA applications. Thus, each channel requires two independent PWM signals, one with variable duty cycle, and one with variable frequency. Each channel also requires a pulse generator circuit which determines the output signal waveform. This waveform can be kept the same for each channel, or modified such that different channels have different waveforms.

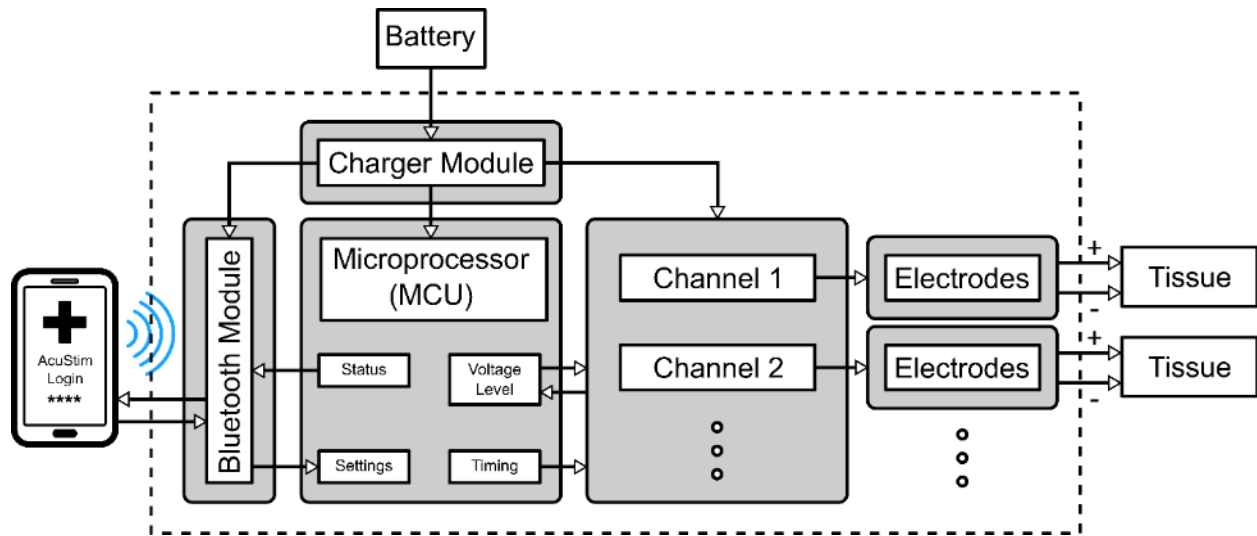


Figure 4.10. Multi-channel device block diagram.

We chose a Teensy 3.2 microprocessor interface board with a MK20DX256VLH7 Cortex M4 processor (Arm, Cambridge, United Kingdom) because of the shield-type interfacing for fast prototype iteration, and because hardware can be programmed in C++ through the Arduino environment. Additionally, this processor is inexpensive and well-known in the industry, and can be configured for diverse applications. The manufacturer also has different models of the same architecture which would be compatible with the same high-level programming, thus allowing for different devices to be configured based on one processor family.

The Teensy 3.2 board implements PWM on 12 digital pins, and all pins can have individual duty cycle which allows all of them to be used for output amplitude control. The board utilizes 3 independent timers which can be programmed to individual frequencies. These timers are tied to specific pins, with one timer tied to 8 pins, and the other two timers tied to 2 pins each. The timers are required to generate the variable frequency PWM signal. With this board and processor it is possible to implement a design with a maximum of 2 channels using hardware timers alone. The Arduino environment allows for one more channel to be implemented using a software timer that can output a third variable frequency PWM signal. The microprocessor also comes in a model

variant with 6 PWM timers, and this device would allow for a 6 channel device to be possible. In general, the number of channels is limited to the number of hardware timers available, and also limited to the number of pins controlled by these timers. Dedicated PWM drivers can also be used, such as the PIC12F1571 (Microchip, Chandler, Arizona), which would provide 3 more timers per chip.

4.5.2. Printed Circuit Board and Case for 2-channel

A PCB with 2-channels was designed in a shield configuration for vertical interfacing with the microcontroller board and the Bluetooth module (Figure 4.11(a)). The case for this device was 55 mm x 48 mm x 30 mm. Testing was performed using a 2000 mAh 3.7 V lithium polymer battery. The case, leads, and collar clip are shown in Figure 4.11(b).

4.5.3. 2-channel Operation Verification

The device was tested to operate in single-channel, and simultaneous 2-channel mode with independent voltage and frequency control. Output with either channel 1, channel 2, or simultaneous output is shown in Figures 4.12(a). The calculated output of the oscilloscope probes that represents the channel 1 and channel 2 is shown in Figure 4.12(b). Channel 1 was set to 4V output amplitude and 100 Hz frequency, and channel 2 was set to 2.5 V output with 50 Hz frequency. The independent stimulation duration timer was also tested and found to be working properly. However, an issue with the previously used 500 mAh 3.7V battery and power supply was found. A drop in maximum amplitude voltage was seen when both channels were set to output simultaneously. This is because the battery supplies power simultaneously to both circuits. A 30 uF capacitor bank was used as a decoupling capacitor, but this issue was still present. Using the 2000 mAh battery showed no problem. Further revision to the power supply, such as a larger decoupling capacitor or bigger battery, would allow for this issue to be resolved.

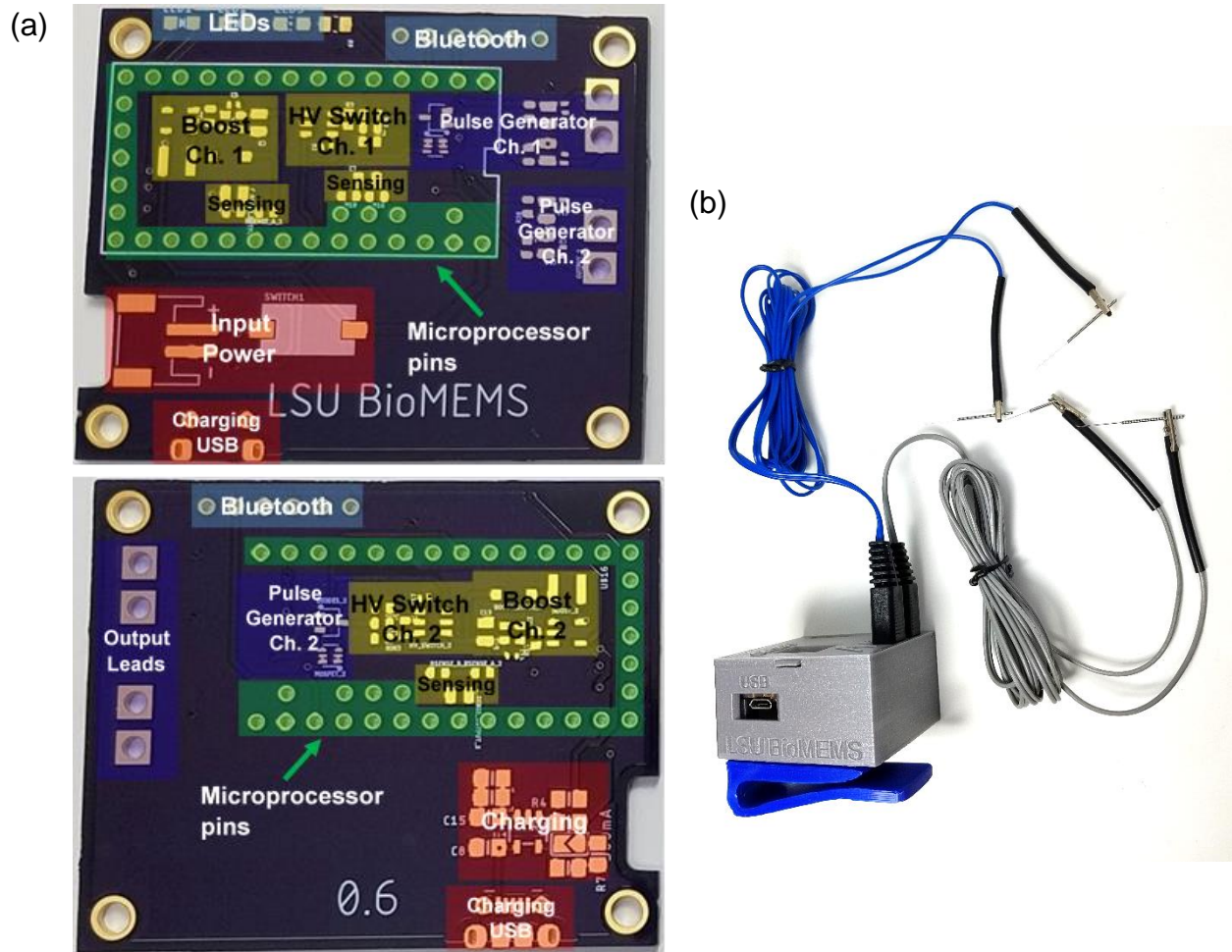


Figure 4.11. 2-channel device design: (a) PCB design showing circuit blocks, and (b) device with leads and collar clip.

4.6. Conclusions

The field of EA treatment and research has been slowed down due to a lack of modern treatment devices that allow for precise controllability and reproducibility. Stimulation machines are large and cumbersome which in turn leads to difficult clinical conditions and research problems. For clinicians this means that treatment protocols are hard to reproduce within the same patient, and animals have to be restrained or sedated in the case of veterinary patients. Stress that

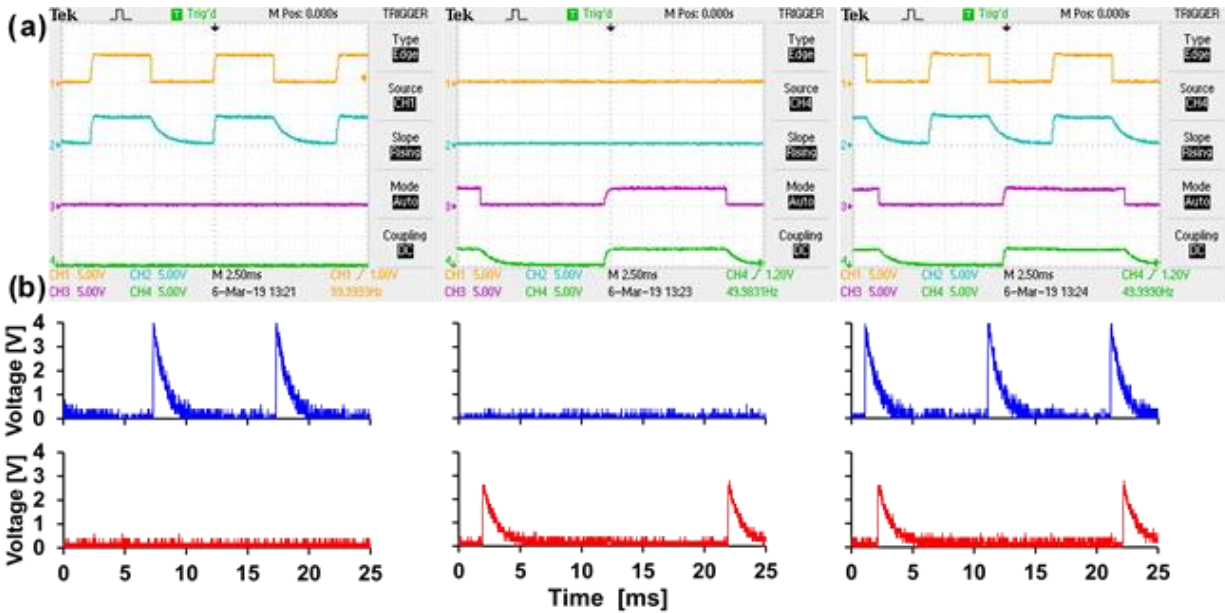


Figure 4.12. Oscilloscope voltage measurements and calculated 2-channel system output: (a) channel 1 only on left, channel 2 only on middle, and both channels on right; and (b) calculated output.

arises from restraining has an impact on the outcome of EA treatment. These problems can be tackled by designing EA stimulation machines with the clinician and patient in mind.

An EA stimulator system was designed in order to address these problems. The system is shown to operate via Bluetooth connection with a smartphone, and its output voltage control, stimulation frequency control, and battery life are characterized. The output of the device was measured in PBS solution using acupuncture needles as electrodes. The device is used in an EA animal study to verify its capability for EA stimulation, and it is shown to have less user error than dry needle acupuncture. A significant advantage of the device lies in its connectivity to a smartphone. The smartphone is used to monitor device status and output settings. This feature allows for treatment protocols to be easily reproduced by other scientists and clinicians. A 2-channel implementation of the device was shown and the independent 2-channel operation was demonstrated. The requirements per channel are also outlined for further implementations with

more channels. This approach could also benefit from dedicated PWM driver ICs such that each driver can allow for more output channels.

The device may be utilized in further clinical research to enhance patient outcomes in electro-acupuncture treatment, help implement reporting standards of electro-acupuncture research, and provide novel smartphone features for the clinician such as patient logging, data logging, take-home programmable prescriptions, and clinical access security.

The smartphone can also be used to implement secure access for doctors, and allow them to store their patient data and treatment data in the device. Novel applications include programming of at-home EA treatment. Further work in this area consists of implementing these smartphone features for the device, implementing additional output channels, and investigating possibilities for the device to be used in further EA research and clinical treatment.

5. ARDUINO SOFTWARE AND HARDWARE AND ANDROID STUDIO SOFTWARE

5.1. Introduction

The pulse generator presented in chapter 3 was used in the design of a stimulator device in chapter 4. The main components of the device are the power source, microcontroller, Bluetooth module, boost converter, high-side switch, and the pulse generator. The microcontroller receives commands from the user via the Bluetooth module, and then controls the output according to the user settings. The Teensy 3.2 microcontroller interface board was chosen due to the 3 PWM hardware timers of the microprocessor, adequate digital pin-out, and ease of programming in the Arduino environment. This board is also easily interfaced via serial connection to the Bluetooth low-energy module, which handles communication with the smartphone. The smartphone app is programmed in Android via Android Studio because mobile device communications to the system can be performed via Bluetooth in this environment. The software architecture is shown in Figure 5.1. In this chapter we will discuss the primary requirements and outcomes of the software developed for the correct operation of the stimulator presented in chapter 4.

5.2. Arduino Programming

The Teensy 3.2 microcontroller board can be programmed in the Arduino environment. The primary functions that the microcontroller must perform are: amplitude control, frequency control, start/stop stimulation on a timer, and receive and execute commands from the user. Other functions include monitoring the battery voltage, the output amplitude, and relay device status information by blinking a LED.

5.2.1. Amplitude Control

The amplitude control is performed by adjusting the output of a boost converter by varying the duty cycle of a PWM signal. The boost converter output voltage follows the PWM duty cycle

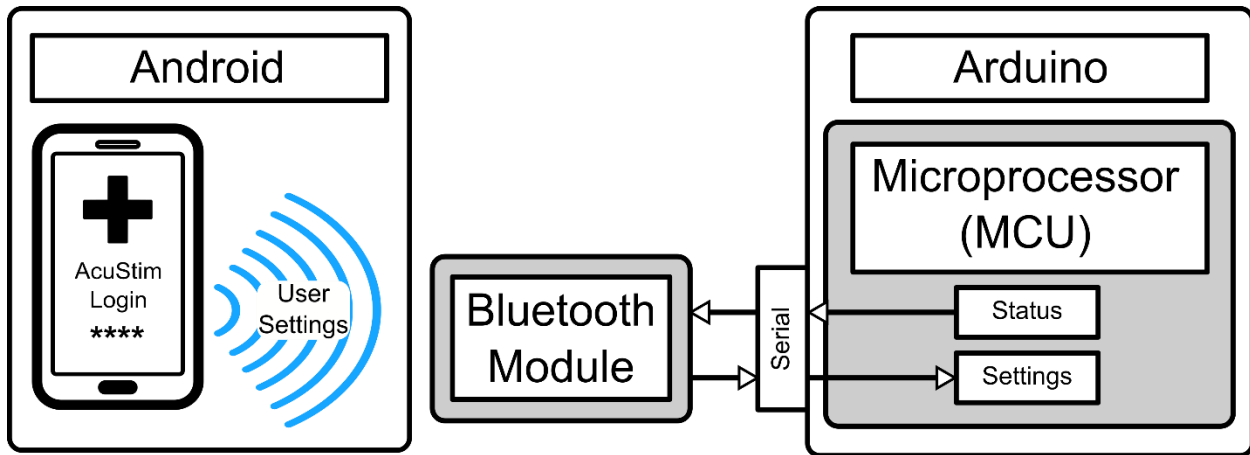


Figure 5.1. Software and hardware block diagrams showing serial communications between the microprocessor and Bluetooth module, and wireless communications between the smartphone and Bluetooth module.

in a linear relationship. When the duty cycle is 0, the boost converter performs no regulation and the output voltage follows the battery voltage level minus the forward voltage of the boost converter diode. This gives the boost converter an operating range of 3 V – 18 V, because the boost converter is programmed with resistors to output a maximum of 18 V. This value is chosen because the high-side switch has a maximum input voltage rating of 18 V.

In order to properly control the boost converter, the PWM signal must have a frequency greater than 10 kHz. A frequency of 35156.25 Hz is chosen because it is the ideal PWM frequency that maintains correct operation with a duty cycle resolution of 10 bits for this microprocessor. In this way, the PWM duty cycle can be expressed in 1024 steps. This gives about 15 mV resolution at the boost converter, an around 4 mV resolution at the stimulation output. In practical application, the output voltage has a resolution of 100 steps corresponding to one hundred percent, and the 1024 steps are mapped to 100 steps when the user inputs a value between 0 – 100. The PWM output pins are initialized with these settings in the Arduino code when the device is turned on.

The Teensy 3.2 microcontroller has 3 hardware timers that control PWM outputs. This is useful in the case of 2-channel or multi-channel implementations, because one timer can be

dedicated to the amplitude control, and we use the timer that controls 8 PWM pins such that the amplitude of up to 8 channels can be controlled using this board. There are limitations, however, when considering frequency control of output channels.

5.2.2. Frequency Control

The stimulation frequency is set via a PWM signal with varying frequency. This PWM signal is fixed at 50% duty cycle, but requires different frequencies for each output channel. For this reason, a multi-channel implementation requires several hardware PWM timers. One timer is needed for the amplitude control of all the channels, and then one more timer is needed for every channel utilized. The PWM signal is used to control the on/off switching of the high-side switch that controls the power delivery to the pulse generator circuitry.

The frequency control is implemented by initializing one digital pin and then changing the frequency output. EA applications do not require stimulation frequency beyond 150 Hz, making this application suitable for software implemented PWM. This method was not pursued because it is very susceptible to bugs and glitches when the microprocessor is busy. A software implemented PWM requires that the microprocessor follow a strict timing to switch a digital pin high and low when necessary. If the microprocessor is busy parsing incoming user settings or commands, sending messages, or reading device voltages then it could miss the timing window to update the PWM pins, leading to unreliable outputs. The alternative would be to have the microprocessor to stop watching interrupts and incoming messages, which would greatly reduce the number of features that the device can implement. The Teensy microcontroller has hardware timing circuitry that takes commands from the control logic and then produces the PWM output without requiring any more processing cycles from the device.

There is one software implementation of PWM that we can use without sacrificing microprocessor capability, which is the `tone()` function. This function uses the microprocessor

control logic timer to calculate the output PWM frequency, which allows 1 more frequency control signal to be easily implemented in any digital pin. This function was used in the 2-channel implementation of the device.

5.2.3. Stimulation Timer

The stimulation timer is implemented using a timer library called Metro. This library allows for any number of timers to be started, and the microprocessor periodically polls them to see if they have expired. This implementation is ideal for features that do not require fast timing reliability (in the microseconds range), such as the starting and stopping of stimulation, and blinking of the on-board LED.

5.2.4. Bluetooth Communications

The Bluetooth (BT) communications are performed via serial protocol with the BT module. The BT module chip has an option to be directly controlled with commands from the microprocessor, but it is not necessary in this case as the communications are handled simply as a serial device with no programming required. The BT programming feature would allow the device to go into low power mode more efficiently, which would save battery power.

The microprocessor receives a message from the BT module, which is then parsed to obtain the user command that was sent from the smartphone. The message is encoded in a simple manner. The first character denotes the user setting to update, or the command to execute, and the next three characters represent the data. For example, the message “a55” tells the microprocessor to set the output amplitude for channel 1 to 55%. The messages contain codes for which channel to update, and then which setting to update in that channel. A different code is used for starting and stopping stimulation of a chosen channel. The settings are stored in a temporary memory that is reset after each message is processed to prevent settings from colliding.

5.2.5. Arduino Advantages

One of the advantages of using the Arduino environment and supporting microprocessor interfacing boards is that software can be easily modified to be used with processors of different capabilities by performing intelligent software design. Each software file is started with the placeholder names of the required pins for correct operation of each channel and readout of the battery and output voltages. This small section is the main part required to be modified to have the rest of the software to be compatible with a board. Other sections would be modified if features are added or removed accordingly.

Another advantage of the Arduino environment is that the microprocessor interfacing boards are open-source. Knowing the board architecture and design allows for smaller dedicated boards to be developed according to each specific application if mass manufacturing is a desired option. These smaller boards would have the circuits required for the correct operation of a specific application or device.

5.3. Android Programming

5.3.1. Introduction

The Android programming mainly focuses around designing app layouts and then writing code in Java to functionalize them. App layouts are the different interactive graphical user interfaces (GUI) that are displayed by the app, and which are used as the means for exchange of information with the user. The layouts are the app foreground tasks, while the background tasks consist of preparing and sending commands, parsing incoming messages, and creating the Bluetooth connection.

5.3.2. Layouts

The main usage for the layouts is to give the user an easy to use interface with which to control the settings of the EA stimulator and send commands to it. The layout for the 2-channel

implementation can be seen in Figure 5.2. The layout allows for the user to input the pulse amplitude, stimulation frequency, and the stimulation duration for both channels. The user can then start and stop stimulation for each channel. The layout also displays the current stimulation settings of the device, the Bluetooth connectivity, and a timer that shows how much time has elapsed since the stimulation was started. The Stop button stops stimulation and the stimulation timer. The user stimulation settings are sent to the device as soon as the user updates them in the layout.

5.3.3. Preparing and Sending Commands

Once the user has updated a stimulation setting on the layout, the app reads the values in the background and prepares a message to send to the device via Bluetooth. The app first creates a string data with the command prefix and the data values that were input by the user, and then sends the string via Bluetooth using generic attribute profile (GATT) characteristics. Characteristics comprise many different types of data that can be exchanged quickly between the app and Bluetooth device. In this case, the characteristic used is called string. For example, when the user types in that they want a pulse amplitude of 75% on channel 1, the app creates the string “a75” and sends it to the microprocessor. The microprocessor interprets the character “a” as the command to update channel 1 output amplitude, and sets the value to 75%. After performing the command the microprocessor sends the current device settings to the app via Bluetooth.

5.3.4. Parsing Incoming Messages

The system updates the device settings to the app every time it receives a command. The message sent includes the pulse amplitude, stimulation frequency, and stimulation duration of the channels. The app parses this message, and stores the settings in memory. Then the layout is updated to show the current settings of the device to the user. The message is received by the app as a string containing all the device data separated by end line symbols ($\backslash n$). The app separates the



Figure 5.2. Android layout for 2-channel device. The user can set stimulation parameters, read current stimulation parameter settings, and start and stop stimulation.

data and then reads each data one by one extracting the value of the settings. This communication is performed using Bluetooth GATT characteristics.

5.3.5. Bluetooth Connection

The Bluetooth connection is handled by libraries available for use in Android Studio. The code handles establishing communications with a peripheral device, and then sending and receiving messages to the peripheral device. Bluetooth communication is handled with GATT characteristics protocols. The communications software is provided by Google (Google, Inc., Mountain View, CA, USA) and can be used as-is to transmit messages between Bluetooth devices. The communication software is open source and can be found online on GitHub.com under the name “BluetoothLeService.java”.

5.4. Conclusions

In this chapter we describe the software development performed to control the EA stimulator system. The architecture of the software involves using Arduino to control the pulse generator

using the microcontroller, and then the microcontroller communicates with the smartphone using a Bluetooth module. The smartphone app is written in the Android environment.

The Arduino software and hardware requirements for multi-channel implementations were presented and discussed. The amount of channels in a device using the current design is limited by the number of hardware timers for PWM outputs in the microcontroller. One hardware timer with multiple PWM outputs is needed for amplitude control of all channels. One hardware timer is then needed for frequency control in each channel. The number of hardware timers can be increased using dedicated PWM driver ICs which would then be controlled by the microcontroller.

The communications protocol between the microcontroller and smartphone via the Bluetooth module was presented. The microcontroller receives commands from the smartphone in a specific format, and this message is interpreted to extract the command and data values. The microcontroller then sends the device status to the smartphone.

The smartphone app is written in the Android platform. The app provides the user interface to allow the user to view and change stimulation settings, and also prepares messages to send to the microcontroller via Bluetooth. The app also establishes and maintains Bluetooth connectivity with the Bluetooth module. Finally, the app receives device status messages from the microcontroller, interprets them, and updates the device status for the user to view.

6. SUMMARY AND CONCLUSIONS

The main objective of this work was to develop a neurostimulation device that implements technology that allows novel research in the field. Neurostimulation is a growing field that shows promise to provide novel treatment methodologies in medical intervention. Conditions that have shown response to neurostimulation treatment include Alzheimer's, Parkinson's, epilepsy, and various conditions related to vagus nerve stimulation. The optimal stimulation methodologies are required in order for neurostimulation treatments to be effective. It was found that the stimulation waveform plays a significant role in the outcomes of neurostimulation, and that there was little scientific research that discussed or focused on this aspect. Additionally, we found a consensus in the literature that reporting standards of the neurostimulation parameters and waveforms are key for scientific reproducibility and verification of results. In this work we focus on making a small contribution to the field by proposing and testing a neurostimulation device that allows neurostimulation with waveforms with similar shape to EPSPs. Specifically, the contributions can be listed as:

- Identification of the need for scientific research focusing on stimulation waveform and parameters.
- Development of a neurostimulator that implements novel waveforms for various design application targets.
- Implementation of the neurostimulator for electro-acupuncture targets.

The chapters are summarized in the following sections.

6.1. Review of Neurostimulation Literature Focusing on Waveforms and Parameters

Chapter 2 focuses on reviewing the literature in the neurostimulation field with a focus on identifying correlations between outcomes and waveform shapes. Studies that discuss stimulation

parameters are also reviewed. The fields reviewed are: transcranial electrical stimulation (TES), deep brain stimulation (DBS), vagal nerve stimulation (VNS), and electro-acupuncture (EA).

There are three main methodologies in TES according to stimulation waveform: transcranial direct current stimulation (tDCS), transcranial alternating current stimulation (tACS), and transcranial random noise stimulation (tRNS). We found different neuromodulatory mechanisms have been proposed to be responsible for the effects seen in each method:

- promotion of long-term potentiation (LTP), or long-term depression (LTD) for tDCS [32, 33],
- modulation of brain oscillations for tACS [34],
- and repetitive opening of sodium channels in tRNS [35].

There are several scientific studies that could benefit from scrutinizing the stimulation waveform effects. There is significant interest in finding the optimal stimulation parameters for eliciting various effects on the nerve and subnetwork level. The analysis of literature on DBS and VNS also led to the conclusion that the study of optimal stimulation parameters including stimulation waveform is important. The literature for EA studies showed that it is still a young field with many questions left to be studied. We could conclude that EA stimulation is a form of neurostimulation depending on which acupoints are stimulated, and their proximity to nerves and nerve endings. The body of knowledge would benefit from studies that look at EA from a neurostimulation perspective. Our review leads us to conclude that the following topics of study will benefit neurostimulation research:

- Comprehensive parametric studies that include standardized methodological reporting. To aid in this approach we suggest utilizing graphical figures to show the stimulation pulse parameters and settings.

- Consideration of complete electrical models for neurostimulation studies that include pulse generator circuits and tissue capacitance.
- Study of effects of various stimulation pulse waveforms and their effects on stimulation outcomes, specifically related to waveforms with different time rate of change.
- Consideration of certain types of electro-acupuncture treatments as peripheral nerve stimulation protocols.

6.2. A Pulse Generation Circuit for Novel Stimulation Waveforms

In chapter 3 we show the development and design of a circuit that generates signals inspired by EPSP waveform shapes. The analytical equations are derived and plotted against measured results, showing excellent agreement. The analytical expressions allows for the design of pulse parameters according to different application requirements.

The circuit design components are characterized to see their effects on the output pulse waveform. R_p allows for direct amplitude output control, varying C_2 with respect to C_1 allows for the pulse width to be controlled, varying R also allows for control of the signal width. C_2 and R also affect output pulse width, but to a lesser extent than R_p . The output signal can be driven at any frequency that complies with equation (10). This circuit allows for application-specific design. Chapter 4 discusses a special application of the pulse generation circuit designed for electro-acupuncture.

6.3. Wearable Smartphone-Compatible Electro-Acupuncture Neurostimulator for Enhanced Clinical and Scientific Outcomes

In chapter 4, a special application of the pulse generator for electro-acupuncture (EA) is presented. A review of state-of-the-art showed EA neurostimulation could benefit from a wearable device that can be controlled remotely, as through a smartphone. These improvements are more pronounced in veterinary applications, where animal stress could be reduced during treatment.

A boost converter is used as the input source for the neurostimulation circuit, and the input to the neurostimulation circuit is controlled by a high-side switch. A microprocessor controls the boost converter via PWM, and the timing of the high-side switch. The microprocessor interfaces with a Bluetooth module that allows for the system to communicate with a smartphone via an app. The system is powered via a 3.7 V 500 mAh battery that is connected to the system through a charger module that allows recharging. The system was implemented in a printed-circuit-board (PCB) and a 3D-printed case was designed for the device.

The device is verified to show smartphone control of the output amplitude, stimulation frequency, and duration of stimulation. The device was included in an EA animal study to verify its correct operation. This device may be utilized for veterinary clinical applications, and for novel uses such as take-home prescription treatments. The device is also implemented in a 2-channel configuration, and each channel is shown with independent output amplitude, frequency, and stimulation duration.

6.4. Arduino and Android Studio Software

In chapter 5, the software requirements are presented and their relationship to the hardware requirement. The Arduino environment is easy to use for prototyping applications, and the open-source nature of the Teensy microcontroller interface board allows the project to be taken further using optimized boards for specific applications.

The hardware requirements for multiple channels are discussed, with their implications on software design with PWM control. The requirements for the output amplitude, stimulation frequency, and stimulation duration control are described. In general, the first output channel requires two hardware PWM timers, and each subsequent channel requires an additional hardware timer. The Bluetooth communications protocol is based on strings being exchanged between the

microcontroller and smartphone. These strings carry command and data from the smartphone to the microcontroller, and the device status from the microcontroller to the smartphone.

The Android app development is outlined. First a description of the layouts used for GUI, then the methodology for sending messages from the app to the microcontroller is described. The methodology for parsing the incoming status messages is then described. The Bluetooth connectivity software from Google Inc. is given.

7. SUGGESTIONS FOR FUTURE WORK

A number of improvements have been considered for the work presented. The following sections describe directions where this work could be taken.

7.1. Biphasic Signal Generation

Charge-balancing is an important aspect of neurostimulation devices in order to prevent accumulation of charge at the tissue level. Other technologies implement active charge-balancing which typically consist of measuring the charge imbalance, and providing a balancing electrical signal after the stimulation signal has been delivered. There are also passive charge-balancing methodologies such as connecting the outputs to ground via a switch, or having a path to ground from the output. Another common way to provide charge-balancing is to have symmetrical positive and negative waveforms (biphasic signal) delivered during stimulation. There is a possibility to enable this feature in our neurostimulator via digital output control, where the stimulation signal is delivered to the output electrodes in one polarity, and then the output electrodes are isolated and the electrode polarity is reversed. One way to possibly accomplish this would be through a multiplexer circuit used to manage the output. Another possible way to implement this would be to use two identical circuits to drive one output in tandem, with each circuit providing the positive and negative polarity signal.

7.2. Improvements to Electro-Acupuncture Stimulator System

The system proposed in this work has several improvements that will help the clinical adoption, and research experience with the device.

7.2.1. App Design Improvements

There are several features that should be added to the app in order to provide incremental improvements to the device. These features would help the experience of the user when using the device. Improvements for the app include:

- Secure clinical login.
- Take-home prescription programming.
- Patient, treatment, and data logging.
- Device identification for use with multiple devices.

The secure clinical login is required for use in the clinic to prevent unwanted use of the device. Additionally, this feature should prevent other Bluetooth devices from accessing the stimulation device and control it.

The take-home prescription programming should be implemented as a novel application. This feature would allow a clinician to program the device to deliver EA treatment whenever the device is turned on, and automatically shut off when treatment is finished. This option would have to be coupled with specialized mid-term EA electrodes, such that the user could easily apply the stimulation.

Logging features are welcome for the device to be used for research purposes as they allow for data to be stored and retrieved easily during treatments. Smartphone or tablet devices should allow for other features such as pictures and notes for patients, and treatment logs that allow clinicians or researchers to see previous applied treatments per patient.

Device identification should also be included so one smartphone can control several stimulator devices simultaneously. This allows for not only performing stimulation with multiple devices, but also for devices with multiple specifications (different outputs, longer battery, different stimulation waveforms).

7.2.2. Stimulator Multi-Channel and Low-Power Operation

The stimulator is presented with two stimulation outputs. EA applications typically require several stimulation outputs for applying electrical stimulation to 6 or 7 acupoints. The first channel

requires two hardware PWM timers from the microprocessor, and each subsequent channel requires one more hardware timer for the frequency control. The PWM timer can be used for several PWM controls, as long as duty cycle can be individually controlled. The HV switch requires individually controlled frequencies. The first output requires two timers, and each output above that requires one or two more timers. This limitation requires specific microprocessor capabilities, which should be considered in future iterations of the stimulator circuit. A possible implementation could retain the same microprocessor, and utilize dedicated PWM driver ICs to provide hardware timers for the channel outputs.

The microprocessor has several low-power operation modes that can be applied to lower power consumption and increase battery life, and these should be considered when designing the software package for the device.

7.2.3. Objective Metrics for Comparing Stimulation Waveforms

Stimulation parameters are a field with active research in many applications. DBS, VNS, TES, FES, and implantable devices are some of the applications with significant developments in recent years. In some cases such as the research presented by Marshall [37], Eggert [39], and Sahlem [38] the signal waveforms are different but current density is kept constant across the studies. The disparaging results of the studies given that the current density is kept constant but the waveforms are different, this indicates that the waveforms probably have an effect on the outcomes. However, the scientific literature has not developed yet a widely recognized metric or conclusively decided which parameters are most important to compare stimulation waveforms.

A starting point for studying these parameters could be to keep current density constant across signal waveforms. A second parameter could be to have a constant integral of the temporal pattern of stimulation. Within these bounds the stimulation waveforms may be better compared, but the applicability of fixing these two parameters should be further studied.

7.2.4. Animal Studies with Electro-Acupuncture

Further animal studies should be pursued. Additional potential projects include: horse anesthesia recovery post-surgery, outcome of EA treatment for animals that can roam and move around during treatment, comparison of EA outcomes with varying EPSP waveforms, and outcomes of patients that have take-home prescription treatments. Other possibilities should be considered for novel applications that take advantage of the wireless programming and initiation of stimulation.

APPENDIX A: CAT STUDY PROTOCOL IACUC APPROVAL



School of
Veterinary Medicine

October 10, 2017

Institutional Animal Care
And Use Committee

Dr. Ronald Koh
Veterinary Clinical Sciences
LSU School of Veterinary Medicine

Division of
Laboratory Animal Medicine

Dear Dr. Koh:

Louisiana State University
200 College Street
Baton Rouge, LA 70803

Protocol number 17-026 entitled, "Effect of Acupuncture on Recovery from General Anesthesia in Cats" lists you as the principal investigator.

504-388-7900
Fax: 504-388-2540

I am happy to inform you that the above protocol is approved by the IACUC as of September 20, 2017, and remains valid until September 19, 2020. This approval authorizes the use of 80 client-owned cats.

Thank you.

Sincerely,

A handwritten signature in black ink, appearing to read "Anderson F. da Cunha", is written over a circular stamp or seal.

Anderson F. da Cunha, MV, MS, DACVA
Chair

Dbd



APPENDIX B: FIGURE PERMISSIONS

Figures 2.1 and 2.4

Figures 2.1 and 2.4 are used under the CC BY 4.0 Attribution 4.0 International license with permission to copy and redistribute the material in any medium or format. The material may also be remixed, transformed, and built upon for any purpose, even commercial. Attribution was given in the in-text figure captions.

The license requires a link be provided to read the terms of the license, which can be found below:

<https://creativecommons.org/licenses/by/4.0/>

Figure 2.5

3/18/2019

Copyright Clearance Center



Confirmation Number: 11799676
Order Date: 03/18/2019

Customer Information

Customer: Jose Parodi Amaya
Account Number: 3001422267
Organization: Louisiana State University
Email: aquilesblazer@hotmail.com
Phone: +1 (225) 281-7540
Payment Method: Invoice

This is not an invoice

Order Details

Journal of Neural Engineering

Billing Status:
N/A

Order detail ID: 71854730
ISSN: 1741-2552
Publication Type: e-Journal
Volume:
Issue:
Start page:
Publisher: IOP Publishing
Author/Editor: Institute of Physics (Great Britain)

Permission Status: **Granted**
Permission type: Republish or display content
Type of use: Thesis/Dissertation
Order License Id: 4552120229823

Requestor type: Academic institution
Format: Print, Electronic
Portion: image/photo
Number of images/photos requested: 1
The requesting person/organization: Jose Aquiles Parodi/Louisiana State University
Title or numeric reference of the portion(s): Figure 2.
Title of the article or chapter the portion is from: Energy-efficient waveform shapes for neural stimulation revealed with genetic algorithm
Editor of portion(s): n/a
Author of portion(s): Amorn Wongsarnpigoon, Warren M. Grill
Volume of serial or monograph: 7
Issue, if republishing an article from a serial: 4
Page range of portion: 15
Publication date of portion: August 2010
Rights for: Main product
Duration of use: Current edition and up to 5 years
Creation of copies for the disabled: yes

<https://www.copyright.com/printOrder.do?id=11799676>

1/2

3/18/2019

Copyright Clearance Center

With minor editing privileges	yes
For distribution to	Worldwide
In the following language(s)	Original language of publication
With incidental promotional use	no
Lifetime unit quantity of new product	Up to 499
Title	Neurostimulator with Waveforms Inspired by Nature for Wearable Electro-Acupuncture
Institution name	Louisiana State University
Expected presentation date	Aug 2019

Note: This item was invoiced separately through our **RightsLink service**. [More info](#)

\$ 0.00

Total order items: 1

Order Total: \$0.00


[About Us](#) | [Privacy Policy](#) | [Terms & Conditions](#) | [Pay an Invoice](#)

Copyright 2019 Copyright Clearance Center

Figure 2.6

3/18/2019

Copyright Clearance Center



Note: Copyright.com supplies permissions but not the copyrighted content itself.

1
PAYMENT
2
REVIEW
3
CONFIRMATION

Step 3: Order Confirmation

Thank you for your order! A confirmation for your order will be sent to your account email address. If you have questions about your order, you can call us 24 hrs/day, M-F at +1.855.239.3415 Toll Free, or write to us at info@copyright.com. This is not an invoice.

Confirmation Number: 11799681
Order Date: 03/18/2019

Payment Information

Jose Parodi Amaya
 Louisiana State University
aquilesblazer@hotmail.com
 +1 (225) 281-7540
 Payment Method: n/a

If you paid by credit card, your order will be finalized and your card will be charged within 24 hours. If you choose to be invoiced, you can change or cancel your order until the invoice is generated.

Order Details

Journal of Neural Engineering

<p>Order detail ID: 71854742 Order License Id: 4552121043986 ISSN: 1741-2552 Publication Type: e-Journal Volume: Issue: Start page: Publisher: IOP Publishing Author/Editor: Institute of Physics (Great Britain)</p>	<p>Permission Status: ✔ Granted Permission type: Republish or display content Type of use: Thesis/Dissertation</p> <p>Requestor type: Academic institution</p> <p>Format: Print, Electronic</p> <p>Portion: image/photo</p> <p>Number of images/photos requested: 1</p> <p>The requesting person/organization: Jose Aquiles Parodi/Louisiana State University</p> <p>Title or numeric reference of the portion(s): Figure 8.</p> <p>Title of the article or chapter the portion is from: Evaluation of novel stimulus waveforms for deep brain stimulation</p>
--	--

<https://www.copyright.com/printCoiConfirmPurchase.do?operation=defaultOperation&confirmNum=11799681&showTCCitation=TRUE>

1/8

Editor of portion(s)	n/a
Author of portion(s)	TJ Foutz, CC McIntyre
Volume of serial or monograph	7
Issue, if republishing an article from a serial	6
Page range of portion	20
Publication date of portion	December 2010
Rights for	Main product
Duration of use	Current edition and up to 5 years
Creation of copies for the disabled	yes
With minor editing privileges	yes
For distribution to	Worldwide
In the following language(s)	Original language of publication
With incidental promotional use	no
Lifetime unit quantity of new product	Up to 499
Title	Neurostimulator with Waveforms Inspired by Nature for Wearable Electro-Acupuncture
Institution name	Louisiana State University
Expected presentation date	Aug 2019

Note: This item will be invoiced or charged separately through CCC's **RightsLink** service. [More info](#)

\$ 0.00

Total order items: 1

This is not an invoice.

Order Total: 0.00 USD

3/18/2019

RightsLink Printable License

**JOHN WILEY AND SONS LICENSE
TERMS AND CONDITIONS**

Mar 18, 2019

This Agreement between Louisiana State University -- Jose Parodi Amaya ("You") and John Wiley and Sons ("John Wiley and Sons") consists of your license details and the terms and conditions provided by John Wiley and Sons and Copyright Clearance Center.

License Number	4552131384227
License date	Mar 18, 2019
Licensed Content Publisher	John Wiley and Sons
Licensed Content Publication	NEUROMODULATION: TECHNOLOGY AT THE NEURAL INTERFACE
Licensed Content Title	High-Resolution Multi-Scale Computational Model for Non-Invasive Cervical Vagus Nerve Stimulation
Licensed Content Author	Antonios P. Mourdoukoutas, Dennis Q. Truong, Devin K. Adair, et al
Licensed Content Date	Oct 27, 2017
Licensed Content Volume	21
Licensed Content Issue	3
Licensed Content Pages	8
Type of use	Dissertation/Thesis
Requestor type	University/Academic
Format	Print and electronic
Portion	Figure/table
Number of figures/tables	1
Original Wiley figure/table number(s)	Figure 1
Will you be translating?	No
Title of your thesis / dissertation	Neurostimulator with Waveforms Inspired by Nature for Wearable Electro-Acupuncture
Expected completion date	Aug 2019
Expected size (number of pages)	1
Requestor Location	Louisiana State University 1855 Brightside Dr Apt L6 Baton Rouge, LA 70820 United States Attn: Louisiana State University
Publisher Tax ID	EU826007151
Total	0.00 USD
Terms and Conditions	

TERMS AND CONDITIONS

This copyrighted material is owned by or exclusively licensed to John Wiley & Sons, Inc. or one of its group companies (each a "Wiley Company") or handled on behalf of a society with

Figure 2.8

3/18/2019

RightsLink Printable License

ELSEVIER LICENSE TERMS AND CONDITIONS

Mar 18, 2019

This Agreement between Louisiana State University -- Jose Parodi Amaya ("You") and Elsevier ("Elsevier") consists of your license details and the terms and conditions provided by Elsevier and Copyright Clearance Center.

License Number	4552130368811
License date	Mar 18, 2019
Licensed Content Publisher	Elsevier
Licensed Content Publication	Clinical Neurophysiology
Licensed Content Title	Characterization of the stimulus waveforms generated by implantable pulse generators for deep brain stimulation
Licensed Content Author	Scott F. Lempka, Bryan Howell, Kabilar Gunalan, Andre G. Machado, Cameron C. McIntyre
Licensed Content Date	Apr 1, 2018
Licensed Content Volume	129
Licensed Content Issue	4
Licensed Content Pages	12
Start Page	731
End Page	742
Type of Use	reuse in a thesis/dissertation
Intended publisher of new work	other
Portion	figures/tables/illustrations
Number of figures/tables/illustrations	1
Format	both print and electronic
Are you the author of this Elsevier article?	No
Will you be translating?	No
Original figure numbers	Figure 8(a)
Title of your thesis/dissertation	Neurostimulator with Waveforms Inspired by Nature for Wearable Electro-Acupuncture
Publisher of new work	Louisiana State University
Expected completion date	Aug 2019
Estimated size (number of pages)	1
Requestor Location	Louisiana State University 1855 Brightside Dr Apt L6 Baton Rouge, LA 70820 United States Attn: Louisiana State University

<https://s100.copyright.com/AppDispatchServlet>

1/6

REFERENCES

- [1] K. Famm, B. Litt, K. J. Tracey, E. S. Boyden, and M. Slaoui, "Drug discovery: a jump-start for electroceuticals," *Nature*, vol. 496, no. 7444, pp. 159-161, Apr. 2013.
- [2] G. Sinha, "Charged by GSK investment, battery of electroceuticals advance," *Nature Medicine*, vol. 19, no. 6, p. 654, June 2013.
- [3] A. Majid, *Electroceuticals: Advances in Electrostimulation Therapies*. Cham, Switzerland: Springer, 2017.
- [4] Y. Tufail, A. Matyushov, N. Baldwin, M. L. Tauchmann, J. Georges, A. Yoshihiro, S. I. H. Tillery, and W. J. Tyler, "Transcranial Pulsed Ultrasound Stimulates Intact Brain Circuits," *Neuron*, vol. 66, no. 5, pp. 681-694, June 2010.
- [5] K. Deisseroth, "Optogenetics," *Nature Methods*, vol. 8, no. 1, pp. 26-29, Jan. 2011.
- [6] B. Guleyupoglu, P. Schestatsky, F. Fregni, and M. Bikson, "Methods and Technologies for Low-Intensity Transcranial Electrical Stimulation: Waveforms, Terminology, and Historical Notes," in *Textbook of Neuromodulation*, H. Knotkova, D. Rasche, Eds. New York, NY: Springer, 2015, pp. 7-16.
- [7] P. Bailey and F. Bremer, "A sensory cortical representation of the vagus nerve: with a note on the effects of low blood pressure on the cortical electrogram," *Journal of Neurophysiology*, vol. 1, no. 5, pp. 405-412, Sept. 1938.
- [8] O. Aquilina, "A brief history of cardiac pacing," *Images in Paediatric Cardiology*, vol. 8, no. 2, pp. 17-81, Apr. 2006.
- [9] P. A. Merton and H. B. Morton, "Stimulation of the cerebral cortex in the intact human subject," *Nature*, vol. 285, no. 5762, p. 227, May 1980.
- [10] S. Reardon, "Electroceuticals spark interest," *Nature*, vol. 511, no. 7507, p. 18, July 2014.
- [11] D. Reato, A. Rahman, M. Bikson, and L. C. Parra, "Low-intensity electrical stimulation affects network dynamics by modulating population rate and spike timing," *The Journal of Neuroscience*, vol. 30, no. 45, pp. 15067-15079, Nov. 2010.
- [12] M. B. Hoppa, G. Gouzer, M. Armbruster, and T. A. Ryan, "Control and plasticity of the presynaptic action potential waveform at small CNS nerve terminals," *Neuron*, vol. 84, no. 4, pp. 778-789, Nov. 2014.
- [13] A. L. Orsborn, H. G. Moorman, S. A. Overduin, M. M. Shanechi, D. F. Dimitrov, and J. M. Carmena, "Closed-loop decoder adaptation shapes neural plasticity for skillful neuroprosthetic control," *Neuron*, vol. 82, no. 6, pp. 1380-1393, June 2014.

- [14] K. V. Shenoy and J. M. Carmena, "Combining decoder design and neural adaptation in brain-machine interfaces," *Neuron*, vol. 84, no. 4, pp. 665-680, Nov. 2014.
- [15] N. Bostrom and A. Sandberg, "Cognitive enhancement: methods, ethics, regulatory challenges," *Science and Engineering Ethics*, vol. 15, no. 3, pp. 311-341, Sept. 2009.
- [16] H. M. Schambra, M. Abe, D. A. Luckenbaugh, J. Reis, J. W. Krakauer, and L. G. Cohen, "Probing for hemispheric specialization for motor skill learning: a transcranial direct current stimulation study," *Journal of Neurophysiology*, vol. 106, no. 2, pp. 652-661, Aug. 2011.
- [17] T. Sasaki, N. Matsuki, and Y. Ikegaya, "Effects of Axonal Topology on the Somatic Modulation of Synaptic Outputs," *The Journal of Neuroscience*, vol. 32, no. 8, pp. 2868-2876, Feb. 2012.
- [18] T. Sasaki, N. Matsuki, and Y. Ikegaya, "Action-potential modulation during axonal conduction," *Science*, vol. 331, no. 6017, pp. 599-601, Feb. 2011.
- [19] S. Boudkkazi, L. Fronzaroli-Molinieres, and D. Debanne, "Presynaptic action potential waveform determines cortical synaptic latency," *Journal of Physiology*, vol. 589, no. 5, pp. 1117-1131, Mar. 2011.
- [20] M. Fuenzalida, D. F. de Sevilla, and W. Buño, "Changes of the EPSP waveform regulate the temporal window for spike-timing-dependent plasticity," *The Journal of Neuroscience*, vol. 27, no. 44 pp. 11940-11948, Oct. 2007.
- [21] A. M. Kuncel and W. M. Grill, "Selection of stimulus parameters for deep brain stimulation," *Clinical Neurophysiology*, vol. 115, no. 11, pp. 2431-2441, Nov. 2004.
- [22] D. Magis and J. Schoenen, "Advances and challenges in neurostimulation for headaches," *The Lancet Neurology*, vol. 11, no. 8, pp. 708-719, Aug. 2012.
- [23] G. Cruccu, T. Z. Aziz, L. Garcia-Larrea, P. Hansson, T. S. Jensen, J.-P. Lefaucheur, B. A. Simpson, and R. S. Taylor, "EFNS guidelines on neurostimulation therapy for neuropathic pain," *European Journal of Neurology*, vol. 14, no. 9, pp. 952-970, Aug. 2007.
- [24] L. S. Chipchase, S. M. Schabrun, and P. W. Hodges, "Peripheral electrical stimulation to induce cortical plasticity: a systematic review of stimulus parameters," *Clinical Neurophysiology*, vol. 122, no. 3, pp. 456-463, Mar. 2011.
- [25] T. Kammer, S. Beck, A. Thielscher, U. Laubis-Herrmann, and H. Topka, "Motor thresholds in humans: a transcranial magnetic stimulation study comparing different pulse

- waveforms, current directions and stimulator types," *Clinical Neurophysiology*, vol. 112, no. 2, pp. 250-258, Feb. 2001.
- [26] N. Lang, J. Harms, T. Weyh, Roger N. Lemon, W. Paulus, J. C. Rothwell, and H. R. Siebner, "Stimulus intensity and coil characteristics influence the efficacy of rTMS to suppress cortical excitability," *Clinical Neurophysiology*, vol. 117, no. 10, pp. 2292-2301, Oct. 2006.
- [27] I. R. Cassar, N. D. Titus, and W. M. Grill, "An improved genetic algorithm for designing optimal temporal patterns of neural stimulation," *Journal of Neural Engineering*, vol. 14, no. 6, 066013 (14pp), Nov. 2017.
- [28] N. S. Davidovics, G. Y. Fridman, B. Chiang, and C. C. Della Santina, "Effects of biphasic current pulse frequency, amplitude, duration, and interphase gap on eye movement responses to prosthetic electrical stimulation of the vestibular nerve," *IEEE Transactions on Neural Systems and Rehabilitation Engineering*, vol. 19, no. 1, pp. 84-94, Feb. 2011.
- [29] A. K. Ahuja, M. R. Behrend, M. Kuroda, M. S. Humayun, and J. D. Weiland, "An in vitro model of a retinal prosthesis," *IEEE Transactions on Biomedical Engineering*, vol. 55, no. 6, pp. 1744-1753, June 2008.
- [30] P. H. Gorman and J. T. Mortimer, "The effect of stimulus parameters on the recruitment characteristics of direct nerve stimulation," *IEEE Transactions on Biomedical Engineering*, vol. BME-30, no. 7, pp. 407-414, July 1983.
- [31] W. M. Grill and J. T. Mortimer, "The effect of stimulus pulse duration on selectivity of neural stimulation," *IEEE Transactions on Biomedical Engineering*, vol. 43, no. 2, pp. 161-166, Feb. 1996.
- [32] G. Kronberg, M. Bridi, T. Abel, M. Bikson, and L. C. Parra, "Direct current stimulation modulates LTP and LTD: activity dependence and dendritic effects," *Brain Stimulation*, vol. 10, no. 1, pp. 51-58, Jan. 2017.
- [33] R. C. Kadosh, S. Soskic, T. Iuculano, R. Kanai, and V. Walsh, "Modulating Neuronal Activity Produces Specific and Long-Lasting Changes in Numerical Competence," *Current Biology*, vol. 20, no. 22, pp. 2016-2020, Nov. 2010.
- [34] T. Neuling, S. Rach, and C. S. Herrmann, "Orchestrating neuronal networks: sustained after-effects of transcranial alternating current stimulation depend upon brain states," *Frontiers in Human Neuroscience*, vol. 7, 161 (12pp), Apr. 2013.
- [35] A. Antal and C. S. Herrmann, "Transcranial alternating current and random noise stimulation: possible mechanisms," *Neural Plasticity*, vol. 2016, 3616807 (12pp), Apr. 2016.

- [36] B. C. Carter, A. J. Giessel, B. L. Sabatini, and B. P. Bean, "Transient sodium current at subthreshold voltages: activation by EPSP waveforms," *Neuron*, vol. 75, no. 6, pp. 1081-1093, Sep. 2012.
- [37] L. Marshall, H. Helgadóttir, M. Mölle, and J. Born, "Boosting slow oscillations during sleep potentiates memory," *Nature*, vol. 444, no. 7119, pp. 610-613, Nov. 2006.
- [38] G. L. Sahlem, B. W. Badran, J. J. Halford, N. R. Williams, J. E. Korte, K. Leslie, M. Strachan, J. L. Breedlove, J. Runion, D. L. Bachman, T. W. Uhde, J. J. Borckardt, M. S. George, "Oscillating square wave transcranial direct current stimulation (tDCS) delivered during slow wave sleep does not improve declarative memory more than sham: a randomized sham controlled crossover study," *Brain Stimulation*, vol. 8, no. 3, pp. 528-534, May 2015.
- [39] T. Eggert, H. Dorn, C. Sauter, M. A. Nitsche, M. Bajbouj, and H. Danker-Hopfe, "No effects of slow oscillatory transcranial direct current stimulation (tDCS) on sleep-dependent memory consolidation in healthy elderly subjects," *Brain Stimulation*, vol. 6, no. 6, pp. 938-945, Nov. 2013.
- [40] C. C. McIntyre and W. M. Grill, "Extracellular stimulation of central neurons: influence of stimulus waveform and frequency on neuronal output," *Journal of Neurophysiology*, vol. 88, no. 4, pp. 1592-1604, Oct. 2002.
- [41] A. Wongsarnpigoon, J. P. Woock, and W. M. Grill, "Efficiency analysis of waveform shape for electrical excitation of nerve fibers," *IEEE Transactions on Neural Systems and Rehabilitation Engineering*, vol. 18, no. 3, pp. 319-328, June 2010.
- [42] G. S. Pell, Y. Roth, and A. Zangen, "Modulation of cortical excitability induced by repetitive transcranial magnetic stimulation: influence of timing and geometrical parameters and underlying mechanisms," *Progress in Neurobiology*, vol. 93, no. 1, pp. 59-98, Jan. 2011.
- [43] B. B. Barth, C. S. Henriquez, W. M. Grill, and X. Shen, "Electrical stimulation of gut motility guided by an *in silico* model," *Journal of Neural Engineering*, vol. 14, no. 6, 066010 (13pp), Dec. 2017.
- [44] T. J. Foutz and C. C. McIntyre, "Evaluation of novel stimulus waveforms for deep brain stimulation," *Journal of Neural Engineering*, vol. 7, no. 6, 066008 (22pp), Dec. 2010.
- [45] A. Wongsarnpigoon and W. M. Grill, "Energy-efficient waveform shapes for neural stimulation revealed with a genetic algorithm," *Journal of Neural Engineering*, vol. 7, no. 4, 046009 (20pp), Aug. 2010.

- [46] A. Ciurea, J. Ciurea, and I. Opris, "Neuromodulation of Consciousness Disorders," in *Electroceuticals: Advances in Electrostimulation Therapies*, A. Majid, Ed. Cham, Switzerland: Springer, 2017, pp. 317-346.
- [47] B. Elsner, J. Kugler, M. Pohl, and J. Mehrholz, "Transcranial direct current stimulation (tDCS) for improving activities of daily living, and physical and cognitive functioning, in people after stroke," *Cochrane Database of Systematic Reviews*, vol. 3, CD009645 (187pp), Mar. 2016.
- [48] T. Wagner, J. Rushmore, U. Eden, and A. Valero-Cabre, "Biophysical foundations underlying TMS: Setting the stage for an effective use of neurostimulation in the cognitive neurosciences," *Cortex*, vol. 45, no. 9, pp. 1025-1034, Oct. 2009.
- [49] P. M. Rossini, D. Burke, R. Chen, L. G. Cohen, Z. Daskalakis, R. Di Iorio, V. Di Lazzaro, F. Ferreri, P. B. Fitzgerald, M. S. George, M. Hallett, J. P. Lefaucheur, B. Langguth, H. Matsumoto, C. Miniussi, M. A. Nitsche, A. Pascual-Leone, W. Paulus, S. Rossi, J. C. Rothwell, H. R. Siebner, Y. Ugawa, V. Walsh, U. Ziemann, "Non-invasive electrical and magnetic stimulation of the brain, spinal cord, roots and peripheral nerves: Basic principles and procedures for routine clinical and research application. An updated report from an I.F.C.N. Committee," *Clinical Neurophysiology*, vol. 126, no. 6, pp. 1071-1107, June 2015.
- [50] G. C. Albert, C. M. Cook, F. S. Prato, and A. W. Thomas, "Deep brain stimulation, vagal nerve stimulation and transcranial stimulation: An overview of stimulation parameters and neurotransmitter release," *Neuroscience & Biobehavioral Reviews*, vol. 33, no. 7, pp. 1042-1060, July 2009.
- [51] P. Li, S. C. Tjen-A-Looi, L. Cheng, D. Liu, J. Painovich, S. Vinjaramury, and J. C. Longhurst, "CME Article: Long-Lasting Reduction of Blood Pressure by Electroacupuncture in Patients with Hypertension: Randomized Controlled Trial," *Medical acupuncture*, vol. 27, no. 4, pp. 253-266, Aug. 2015.
- [52] Z.-Q. Zhao, "Neural mechanism underlying acupuncture analgesia," *Progress in Neurobiology*, vol. 85, no. 4, pp. 355-375, Aug. 2008.
- [53] A. J. Woods, A. Antal, M. Bikson, P.S. Boggio, A. R. Brunoni, P. Celnik, L. G. Cohen, F. Fregni, C. S. Herrmann, E. S. Kappenman, H. Knotkova, D. Liebetanz, C. Miniussi, P. C. Miranda, W. Paulus, A. Priori, D. Reato, C. Stagg, N. Wenderoth, M. A. Nitsche, "A technical guide to tDCS, and related non-invasive brain stimulation tools," *Clinical Neurophysiology*, vol. 127, no. 2, pp. 1031-1048, Feb. 2016.
- [54] D. J. Edwards, M. Cortex, S. Wortman-Jutt, D. Putrino, M. Bikson, G. Thickbroom, and A. Pascual-Leone, "Transcranial Direct Current Stimulation and Sports Performance," *Frontiers in Human Neuroscience*, vol. 11, 243 (4pp), May 2017.

- [55] K. Kitajo, T. Hanakawa, R. J. Ilmoniemi, and C. Miniussi, "A contemporary research topic: manipulative approaches to human brain dynamics," *Frontiers in Human Neuroscience*, vol. 9, 118 (3pp), Mar. 2015.
- [56] C. Saiote, Z. Turi, W. Paulus, and A. Antal, "Combining functional magnetic resonance imaging with transcranial electrical stimulation," *Frontiers in Human Neuroscience*, vol. 7, 435 (7pp), Aug. 2013.
- [57] A. R. Brunoni, M. A. Nitsche, N. Bolognini, M. Bikson, T. Wagner, L. Merabet, D. J. Edwards, A. Valero-Cabre, A. Rotenberg, A. Pascual-Leone, R. Ferrucci, A. Priori, P. Boggio, F. Fregni, "Clinical research with transcranial direct current stimulation (tDCS): challenges and future directions," *Brain Stimulation*, vol. 5, no. 3, pp. 175-195, July 2012.
- [58] N. Roche, M. Geiger, and B. Bussel, "Mechanisms underlying transcranial direct current stimulation in rehabilitation," *Annals of Physical and Rehabilitation Medicine*, vol. 58, no. 4, pp. 214-219, Sept. 2015.
- [59] W. Paulus, "Transcranial electrical stimulation (tES-tDCS; tRNS, tACS) methods," *Neuropsychological Rehabilitation*, vol. 21, no. 5, pp. 602-617, Aug. 2011.
- [60] M. A. Nitsche, M.-F. Kuo, W. Paulus, and A. Antal, "Transcranial direct current stimulation: protocols and physiological mechanisms of action," in *Textbook of Neuromodulation*, H. Knotkova, D. Rasche, Eds. New York, NY: Springer, 2015, pp. 101-111.
- [61] R. C. Kadosh, N. Levy, J. O'Shea, N. Shea, and J. Savulescu, "The neuroethics of non-invasive brain stimulation," *Current Biology*, vol. 22, no. 4, pp. R108-R111, Feb. 2012.
- [62] P. Marangolo, V. Fiori, M. A. Calpagnano, S. Campana, C. Razzano, C. Caltagirone, and A. Marini, "tDCS over the left inferior frontal cortex improves speech production in aphasia," *Frontiers in Human Neuroscience*, vol. 7, 539 (10pp), Sept. 2013.
- [63] S. F. Lempka, B. Howell, K. Gunalan, A. G. Machado, and C. C. McIntyre, "Characterization of the stimulus waveforms generated by implantable pulse generators for deep brain stimulation," *Clinical Neurophysiology*, vol. 129, no. 4, pp. 731-742, Apr. 2018.
- [64] B. Howell, L. E. Medina, and W. M. Grill, "Effects of frequency-dependent membrane capacitance on neural excitability," *Journal of Neural Engineering*, vol. 12, no. 5, 056015 (32pp), Sept. 2015.
- [65] W. M. Grill, "Model-based analysis and design of waveforms for efficient neural stimulation," *Progress in Brain Research*, vol. 222, in *Computational Neurostimulation*, S. Bestmann, Ed. Amsterdam, Netherlands: Elsevier, Sept. 2015, pp. 147-162.

- [66] M. Bikson, A. Rahman, and A. Datta, "Computational Models of Transcranial Direct Current Stimulation," *Clinical EEG and Neuroscience*, vol. 43, no. 3, pp. 176-183, Sept. 2012.
- [67] T. Kunze, A. Hunold, J. Haueisen, V. Jirsa, and A. Spiegler, "Transcranial direct current stimulation changes resting state functional connectivity: A large-scale brain network modeling study," *NeuroImage*, vol. 140, pp. 174-187, Oct. 2016.
- [68] J. Vosskuhl, R. J. Huster, and C. S. Herrmann, "BOLD signal effects of transcranial alternating current stimulation (tACS) in the alpha range: A concurrent tACS-fMRI study," *NeuroImage*, vol. 140, pp. 118-125, Oct. 2016.
- [69] R. F. Helfrich, T. R. Schneider, S. Rach, S. A. Trautmann-Lengsfeld, A. K. Engel, and C. S. Herrmann, "Entrainment of Brain Oscillations by Transcranial Alternating Current Stimulation," *Current Biology*, vol. 24, no. 3, pp. 333-339, Feb. 2014.
- [70] R. Kanai, W. Paulus, and V. Walsh, "Transcranial alternating current stimulation (tACS) modulates cortical excitability as assessed by TMS-induced phosphene thresholds," *Clinical Neurophysiology*, vol. 121, no. 9, pp. 1551-1554, Sept. 2010.
- [71] E. Santarnecchi, T. Muller, S. Rossi, A. Sarkar, N. R. Polizzotto, A. Rossi, and R. C. Kadosh, "Individual differences and specificity of prefrontal gamma frequency-tACS on fluid intelligence capabilities," *Cortex*, vol. 75, pp. 33-43, Feb. 2016.
- [72] M. Witkowski, E. Garcia-Cossio, B. S. Chander, C. Braun, N. Birbaumer, S. E. Robinson, and S. R. Soekadar, "Mapping entrained brain oscillations during transcranial alternating current stimulation (tACS)," *NeuroImage*, vol. 140, pp. 89-98, Oct. 2016.
- [73] N. Jaušovec, K. Jaušovec, and A. Pahor, "The influence of theta transcranial alternating current stimulation (tACS) on working memory storage and processing functions," *Acta Psychologica*, vol. 146, pp. 1-6, Feb. 2014.
- [74] A. Pahor and N. Jaušovec, "The effects of theta transcranial alternating current stimulation (tACS) on fluid intelligence," *International Journal of Psychophysiology*, vol. 93, no. 3, pp. 322-331, Sept. 2014.
- [75] D. Brignani, M. Ruzzoli, P. Mauri, and C. Miniussi, "Is transcranial alternating current stimulation effective in modulating brain oscillations?," *PloS one*, vol. 8, no. 2, e56589 (8pp), Feb. 2013.
- [76] A. Vossen, J. Gross, and G. Thut, "Alpha Power Increase After Transcranial Alternating Current Stimulation at Alpha Frequency (α -tACS) Reflects Plastic Changes Rather Than Entrainment," *Brain Stimulation*, vol. 8, no. 3, pp. 499-508, May 2015.
- [77] B. Lafon, S. Henin, Y. Huang, D. Friedman, L. Melloni, T. Thesen, W. Doyle, G. Buzsáki, O. Devinsky, L. C. Parra, A. A. Liu, "Low frequency transcranial electrical stimulation

- does not entrain sleep rhythms measured by human intracranial recordings," *Nature Communications*, vol. 8, no. 1, 1199 (14pp), Oct. 2017.
- [78] D. Terney, L. Chaieb, V. Moliadze, A. Antal, and W. Paulus, "Increasing human brain excitability by transcranial high-frequency random noise stimulation," *Journal of Neuroscience*, vol. 28, no. 52, pp. 14147-14155, Dec. 2008.
- [79] L. Chaieb, A. Antal, and W. Paulus, "Transcranial random noise stimulation-induced plasticity is NMDA-receptor independent but sodium-channel blocker and benzodiazepines sensitive," *Frontiers in Neuroscience*, vol. 9, 125 (9pp), Apr. 2015.
- [80] G. G. Ambrus, W. Paulus, and A. Antal, "Cutaneous perception thresholds of electrical stimulation methods: comparison of tDCS and tRNS," *Clinical Neurophysiology*, vol. 121, no. 11, pp. 1908-1914, Nov. 2010.
- [81] G. Prichard, C. Weiller, B. Fritsch, and J. Reis, "Effects of Different Electrical Brain Stimulation Protocols on Subcomponents of Motor Skill Learning," *Brain Stimulation*, vol. 7, no. 4, pp. 532-540, July 2014.
- [82] A. Snowball, I. Tachtsidis, T. Popescu, J. Thompson, M. Delazer, L. Zamarian, T. Zhu, and R. C. Kadosh, "Long-term enhancement of brain function and cognition using cognitive training and brain stimulation," *Current Biology*, vol. 23, no. 11, pp. 987-992, June 2013.
- [83] T. Popescu, B. Krause, D. B. Terhune, O. Twose, T. Page, G. Humphreys, and R. C. Kadosh, "Transcranial random noise stimulation mitigates increased difficulty in an arithmetic learning task," *Neuropsychologia*, vol. 81, pp. 255-264, Jan. 2016.
- [84] M. G. van Koningsbruggen, S. C. Ficarella, L. Battelli, and C. Hickey, "Transcranial random-noise stimulation of visual cortex potentiates value-driven attentional capture," *Social Cognitive and Affective Neuroscience*, vol. 11, no. 9, pp. 1481-1488, Sept. 2016.
- [85] J. Holmes, E. M. Byrne, S. E. Gathercole, and M. P. Ewbank, "Transcranial random noise stimulation does not enhance the effects of working memory training," *Journal of Cognitive Neuroscience*, vol. 28, no. 10, pp. 1471-1483, Oct. 2016.
- [86] N. Mammarella, A. Di Domenico, R. Palumbo, and B. Fairfield, "Self-generation and positivity effects following transcranial random noise stimulation in medial prefrontal cortex: a reality monitoring task in older adults," *Cortex*, vol. 91, pp. 186-196, June 2017.
- [87] J. Van Doren, B. Langguth, and M. Schecklmann, "Electroencephalographic effects of transcranial random noise stimulation in the auditory cortex," *Brain Stimulation: Basic, Translational, and Clinical Research in Neuromodulation*, vol. 7, no. 6, pp. 807-812, Nov. 2014.

- [88] A. Romanska, C. Rezlescu, T. Susilo, B. Duchaine, and M. J. Banissy, "High-frequency transcranial random noise stimulation enhances perception of facial identity," *Cerebral Cortex*, vol. 25, no. 11, pp. 4334-4340, Nov. 2015.
- [89] O. van der Groen and N. Wenderoth, "Transcranial random noise stimulation of visual cortex: stochastic resonance enhances central mechanisms of perception," *Journal of Neuroscience*, vol. 36, no. 19, pp. 5289-5298, May 2016.
- [90] S. E. Cooper, A. M. Kuncel, B. R. Wolgamuth, A. Rezai, and W. M. Grill, "A model predicting optimal parameters for deep brain stimulation in essential tremor," *Journal of Clinical Neurophysiology*, vol. 25, no. 5, pp. 265-273, Oct. 2008.
- [91] A. Wongsarnpigoon and W. M. Grill, "Effects of stimulation parameters and electrode location on thresholds for epidural stimulation of cat motor cortex," *Journal of Neural Engineering*, vol. 8, no. 6, 066016 (10pp), Nov. 2011.
- [92] D. Labar, L. Ponticello, B. Nikolov, S. Bellapu, and T. H. Schwartz, "Stimulation Parameters After Vagus Nerve Stimulator Replacement," *Neuromodulation*, vol. 11, no. 2, pp. 132-134, Apr. 2008.
- [93] M. S. Borland, W. A. Vrana, N. A. Moreno, E. A. Fogarty, E. P. Buell, P. Sharma, C. T. Engineer, and M. P. Kilgard, "Cortical Map Plasticity as a Function of Vagus Nerve Stimulation Intensity," *Brain Stimulation*, vol. 9, no. 1, pp. 117-123, Jan. 2016.
- [94] S. Ghani, J. Vilensky, B. Turner, R. S. Tubbs, and M. Loukas, "Meta-analysis of vagus nerve stimulation treatment for epilepsy: correlation between device setting parameters and acute response," *Child's Nervous System*, vol. 31, no. 12, pp. 2291-2304, Dec. 2015.
- [95] D. R. Hulsey, J. R. Riley, K. W. Loerwald, R. L. Rennaker II, M. P. Kilgard, and S. A. Hays, "Parametric characterization of neural activity in the locus coeruleus in response to vagus nerve stimulation," *Experimental Neurology*, vol. 289, pp. 21-30, Mar. 2017.
- [96] S. Manta, J. Dong, G. Debonnel, and P. Blier, "Optimization of vagus nerve stimulation parameters using the firing activity of serotonin neurons in the rat dorsal raphe," *European Neuropsychopharmacology*, vol. 19, no. 4, pp. 250-255, Apr. 2009.
- [97] S.-S. Kong, J.-J. Liu, T.-C. Hwang, X.-J. Yu, M. Zhao, M. Zhao, B. X. Yuan, Y. Lu, Y.-M. Kang, B. Wang, W.-J. Zang, "Optimizing the Parameters of Vagus Nerve Stimulation by Uniform Design in Rats with Acute Myocardial Infarction," *PLoS ONE*, Article vol. 7, no. 11, e42799 (10pp), Nov. 2012.
- [98] A. P. Mourdoukoutas, D. Q. Truong, D. K. Adair, B. J. Simon, and M. Bikson, "High-Resolution Multi-Scale Computational Model for Non-Invasive Cervical Vagus Nerve Stimulation," *Neuromodulation*, vol. 21, no. 3, pp. 261-268, Apr. 2018.

- [99] G. A. Ulett, S. Han, and J.-S. Han, "Electroacupuncture: mechanisms and clinical application," *Biological Psychiatry*, vol. 44, no. 2, pp. 129-138, July 1998.
- [100] Z. Lu, H. Dong, Q. Wang, and L. Xiong, "Perioperative acupuncture modulation: more than anaesthesia," *British Journal of Anaesthesia*, vol. 115, no. 2, pp. 183-193, Aug. 2015.
- [101] D. Mayor, "An exploratory review of the electroacupuncture literature: clinical applications and endorphin mechanisms," *Acupuncture in Medicine*, vol. 31, no. 4, pp. 409-415, Dec. 2013.
- [102] J. C. Longhurst, "Defining Meridians: A Modern Basis of Understanding," *Journal of Acupuncture and Meridian Studies*, vol. 3, no. 2, pp. 67-74, June 2010.
- [103] A.-H. Li, J.-M. Zhang, and Y.-K. Xie, "Human acupuncture points mapped in rats are associated with excitable muscle/skin–nerve complexes with enriched nerve endings," *Brain Research*, vol. 1012, no. 1-2, pp. 154-159, June 2004.
- [104] F. Kagitani, S. Uchida, and H. Hotta, "Afferent nerve fibers and acupuncture," *Autonomic Neuroscience*, vol. 157, no. 1, pp. 2-8, Oct. 2010.
- [105] K. J. Cheng, "Neurobiological Mechanisms of Acupuncture for Some Common Illnesses: A Clinician's Perspective," *Journal of Acupuncture and Meridian Studies*, vol. 7, no. 3, pp. 105-114, June 2014.
- [106] S. Quiroz-González, S. Torres-Castillo, R. E. López-Gómez, and I. Jiménez Estrada, "Acupuncture Points and Their Relationship with Multireceptive Fields of Neurons," *Journal of Acupuncture and Meridian Studies*, vol. 10, no. 2, pp. 81-89, Apr. 2017.
- [107] A. Goe, J. Shmalberg, B. Gatson, P. Bartolini, J. Curtiss, and J. F. X. Wellehan, "EPINEPHRINE OR GV-26 ELECTRICAL STIMULATION REDUCES INHALANT ANESTHETIC RECOVERY TIME IN COMMON SNAPPING TURTLES (CHELYDRA SERPENTINA)," *Journal of Zoo and Wildlife Medicine*, vol. 47, no. 2, pp. 501-507, June 2016.
- [108] H. M. Langevin, R. Schnyer, H. MacPherson, R. Davis, R. E. Harris, V. Napadow, P. M. Wayne, R. J. Milley, L. Lao, E. Stener-Victorin, J.-T. Kong, R. Hammerschlag, "Manual and Electrical Needle Stimulation in Acupuncture Research: Pitfalls and Challenges of Heterogeneity," *Journal of Alternative and Complementary Medicine*, vol. 21, no. 3, pp. 113-128, Mar. 2015.
- [109] H. Matsumoto and Y. Ugawa, "Adverse events of tDCS and tACS: A review," *Clinical Neurophysiology Practice*, vol. 2, pp. 19-25, Jan. 2017.
- [110] J. Clausen, "Bonding brains to machines: ethical implications of electroceuticals for the human brain," *Neuroethics*, vol. 6, no. 3, pp. 429-434, Dec. 2013.

- [111] S.-H. Cho, N. Xue, L. Cauller, W. Rosellini, and J.-B. Lee, "A SU-8-based fully integrated biocompatible inductively powered wireless neurostimulator," *Journal of Microelectromechanical Systems*, vol. 22, no. 1, pp. 170-176, Feb. 2013.
- [112] M. J. Kane, P. P. Breen, F. Quondamatteo, and G. ÓLaighin, "BION microstimulators: A case study in the engineering of an electronic implantable medical device," *Medical Engineering and Physics*, vol. 33, no. 1, pp. 7-16, Jan. 2011.
- [113] S. U. Rehman and A. M. Kamboh, "A CMOS micro-power and area efficient neural recording and stimulation front-end for biomedical applications," *Circuits, Systems, and Signal Processing*, vol. 34, no. 6, pp. 1725-1746, June 2015.
- [114] E. Noorsal, K. Sooksood, H. Xu, R. Hornig, J. Becker, and M. Ortmanns, "A neural stimulator frontend with high-voltage compliance and programmable pulse shape for epiretinal implants," *IEEE Journal of Solid-State Circuits*, vol. 47, no. 1, pp. 244-256, Jan. 2012.
- [115] W.-Y. Hsu and A. Schmid, "Compact, energy-efficient high-frequency switched capacitor neural stimulator with active charge balancing," *IEEE Transactions on Biomedical Circuits and Systems*, vol. 11, no. 4, pp. 878-888, Aug. 2017.
- [116] J. Vidal and M. Ghovanloo, "Towards a Switched-Capacitor based Stimulator for efficient deep-brain stimulation," in *Proceedings of the 32nd Annual International Conference of the IEEE Engineering in Medicine and Biology Society (IEEE EMBC 2010)*, Buenos Aires, Argentina, August 31 – September 4, 2010, pp. 2927-2930.
- [117] M. N. van Dongen and W. A. Serdijin, "A power-efficient multichannel neural stimulator using high-frequency pulsed excitation from an unfiltered dynamic supply," *IEEE Transactions on Biomedical Circuits and Systems*, vol. 10, no. 1, pp. 61-71, Feb. 2016.
- [118] F. Mounaim, M. Sawan, "Toward A Fully Integrated Neurostimulator With Inductive Power Recovery Front-End," *IEEE Transactions on Biomedical Circuits and Systems*, vol. 6, no. 4, pp. 309-318, Aug. 2012.
- [119] A. Khalifa, Y. Karimi, Q. Wang, S. Garikapati, W. Montlouis, M. Stanaćević, N. Thakor, R. Etienne-Cummings, "The Microbead: A Highly Miniaturized Wirelessly Powered Implantable Neural Stimulating System," *IEEE Transactions on Biomedical Circuits and Systems*, pp. 1-11, Mar. 2018. [Online] Available: IEEE Xplore.
- [120] M. Ghovanloo, "Switched-capacitor based implantable low-power wireless microstimulating systems," in *Proceedings of the 2006 IEEE International Symposium on Circuits and Systems (IEEE ISCAS 2006)*, Island of Kos, Greece, May 21-24, 2006, pp. 2197-2200.

- [121] T. K. Whitehurst, J. H. Schulman, K. N. Jaax, and R. Carbunaru, "The Bion Microstimulator and its Clinical Applications," in *Implantable Neural Prostheses 1*, 1st Edition, Elias Greenbaum and David Zhou, Eds., Springer-Verlag, New York, NY, 2009, pp. 253-273.
- [122] D. Seo, R. M. Neely, K. Shen, U. Singhal, E. Alon, J. M. Rabaey, J. M. Carmena, and M. M. Maharbiz, "Wireless recording in the peripheral nervous system with ultrasonic neural dust," *Neuron*, vol. 91, no. 3, pp. 529-539, Aug. 2016.
- [123] X. Qian, H.-W. Hao, B.-Z. Ma, X.-W. Wen, C.-H. Hu, L.-M. Li, R. Y. C. Lau, and X. Guo, "Programmable and implantable neurostimulator with novel stimulus waveforms for rat models," *Electronics Letters*, vol. 48, no. 17, pp. 1035-1036, Aug. 2012.
- [124] K. Song, L. Yan, S. Lee, J. Yoo, and H. J. Yoo, "A Wirelessly Powered Electro-Acupuncture Based on Adaptive Pulsewidth Monophasic Stimulation," *IEEE Transactions on Biomedical Circuits and Systems*, vol. 5, no. 2, pp. 138-146, Apr. 2011.
- [125] W. Zaraska, P. Thor, M. Lipiński, M. Cież, W. Grzesiak, J. Początek, and K. Zaraska, "Design and fabrication of neurostimulator implants—selected problems," *Microelectronics Reliability*, vol. 45, no. 12, pp. 1930-1934, Dec. 2005.
- [126] J. C. Lilly, J. R. Hughes, E. C. Alvord Jr, and T. W. Galkin, "Brief, noninjurious electric waveform for stimulation of the brain," *Science*, vol. 121, no. 3144, pp. 468-469, Apr. 1955.
- [127] A. Vasquez, A. Malavera, D. Doruk, L. Morales-Quezada, S. Carvalho, J. Leite, and F. Fregni, "Duration dependent effects of transcranial pulsed current stimulation (tPCS) indexed by electroencephalography," *Neuromodulation: Technology at the Neural Interface*, vol. 19, no. 7, pp. 679-688, Oct. 2016.
- [128] G. Alon, S. R. Roys, R. P. Gullapalli, and J. D. Greenspan, "Non-invasive electrical stimulation of the brain (ESB) modifies the resting-state network connectivity of the primary motor cortex: a proof of concept fMRI study," *Brain Research*, vol. 1403, pp. 37-44, July 2011.
- [129] V. Di Lazzaro, A. Oliviero, P. Mazzone, A. Insola, F. Pilato, E. Saturno, A. Accurso, P. Tonali, and J. Rothwell, "Comparison of descending volleys evoked by monophasic and biphasic magnetic stimulation of the motor cortex in conscious humans," *Experimental Brain Research*, vol. 141, no. 1, pp. 121-127, Nov. 2001.
- [130] V. Di Lazzaro, A. Oliviero, F. Pilato, E. Saturno, M. Dileone, P. Mazzone, A. Insola, P. A. Tonali, and J. C. Rothwell, "The physiological basis of transcranial motor cortex

- stimulation in conscious humans," *Clinical Neurophysiology*, vol. 115, no. 2, pp. 255-266, Feb. 2004.
- [131] C. C. McIntyre and W. M. Grill, "Selective microstimulation of central nervous system neurons," *Annals of Biomedical Engineering*, vol. 28, no. 3, pp. 219-233, Mar. 2000.
- [132] Y.-P. Lin *et al.*, "A Battery-Less, Implantable Neuro-Electronic Interface for Studying the Mechanisms of Deep Brain Stimulation in Rat Models," *IEEE Transactions on Biomedical Circuits and Systems*, vol. 10, no. 1, pp. 98-112, Feb. 2016.
- [133] F. H. Lopes da Silva, A. Hoeks, H. Smits, and L. H. Zetterberg, "Model of brain rhythmic activity. The alpha-rhythm of the thalamus," *Kybernetik*, vol. 15, no. 1, p. 27-37, May 1974.
- [134] C. R. Butson, C. B. Moks, and C. C. McIntyre, "Sources and effects of electrode impedance during deep brain stimulation," *Clinical Neurophysiology*, vol. 117, no. 2, pp. 447-454, Feb. 2006.
- [135] H. C. Lukaski, W. W. Bolonchuk, C. B. Hall, and W. A. Siders, "Validation of tetrapolar bioelectrical impedance method to assess human body composition," *Journal of Applied Physiology*, vol. 60, no. 4, pp. 1327-1332, Apr. 1986.
- [136] E. A. Tough, A. R. White, T. M. Cummings, S. H. Richards, and J. L. Campbell, "Acupuncture and dry needling in the management of myofascial trigger point pain: a systematic review and meta-analysis of randomised controlled trials," *European Journal of Pain*, vol. 13, no. 1, pp. 3-10, Jan. 2009.
- [137] W. Chapple, "Proposed Catalog of the Neuroanatomy and the Stratified Anatomy for the 361 Acupuncture Points of 14 Channels," *Journal of Acupuncture and Meridian Studies*, vol. 6, no. 5, pp. 270-274, Oct. 2013.
- [138] J. J. Mao, M. A. Bowman, S. X. Xie, D. Bruner, A. DeMichele, and J. T. Farrar, "Electroacupuncture Versus Gabapentin for Hot Flashes Among Breast Cancer Survivors: A Randomized Placebo-Controlled Trial," *Journal of Clinical Oncology*, vol. 33, no. 31, pp. 3615-3620, Nov. 2015.
- [139] M. A. Sahmeddini, M. H. Eghbal, M. B. Khosravi, S. Ghaffaripour, F. Janatmakan, and S. Shokrizade, "Electro-Acupuncture Stimulation at Acupoints Reduced the Severity Of Hypotension During Anesthesia in Patients Undergoing Liver Transplantation," *Journal of Acupuncture and Meridian Studies*, vol. 5, no. 1, pp. 11-14, Feb. 2012.
- [140] H.-W. Liu, M.-C. Liu, C.-M. Tsao, M.-H. Liao, and C.-C. Wu, "Electro-acupuncture at 'Neiguan'(PC6) attenuates liver injury in endotoxaemic rats," *Acupuncture in Medicine*, vol. 29, no. 4, pp. 284-288, Nov. 2011.

- [141] A. C. Ahn and Ø. G. Martinsen, "Electrical Characterization of Acupuncture Points: Technical Issues and Challenges," *The Journal of Alternative and Complementary Medicine*, vol. 13, no. 8, pp. 817-824, Oct. 2007.
- [142] J. Hubacher, R. C. Niemtow, M. D. Corradino, J. C. Y. Dunn, and D. H. Ha, "Standards for Reporting Electroacupuncture Parameters," *Medical Acupuncture*, vol. 28, no. 5, pp. 249-255, Oct. 2016.
- [143] R. Zhang, A. H. Andersen, P. A. Hardy, E. Forman, A. Evans, Y. Ai, J. Yue, G. Yue, D. M. Gash, R. Grondin, Z. Zhang, "Objectively measuring effects of electro-acupuncture in parkinsonian rhesus monkeys," *Brain Research*, vol. 1678, pp. 12-19, Jan. 2018.
- [144] J. French, D. Bardot, E. Graczyk, A. Hess-Dunning, J. L. Lujan, M. Moynahan, W. Tan, R. Triolo, A. Zbrzeski, "The need for understanding and engaging the patient as consumer of products developed by neural engineering," *Journal of Neural Engineering*, vol. 15, no. 4, 040201 (2pp), June 2018.
- [145] K. Song, H. Lee, S. Hong, H. Cho, U. Ha, and H.-J. Yoo, "A Sub-10 nA DC-Balanced Adaptive Stimulator IC With Multi-Modal Sensor for Compact Electro-Acupuncture Stimulation," *IEEE Transactions on Biomedical Circuits and Systems*, vol. 6, no. 6, pp. 533-541, Dec. 2012.
- [146] *Antisedan(R)*. Espoo, Finland: Orion Corporation, April 2014, [Online]. Available: https://www.zoetisus.com/locale-assets/dog/product/antisedan/asset/antisedan_pi.pdf. [Accessed: April 4, 2019].
- [147] M. Granholm, B. C. McKusick, F. C. Westerholm, and J. C. Aspegrén, "Evaluation of the clinical efficacy and safety of dexmedetomidine or medetomidine in cats and their reversal with atipamezole," *Veterinary Anaesthesia and Analgesia*, vol. 33, no. 4, pp. 214-223, July 2006.

VITA

Jose Aquiles Parodi Amaya is a native of Tegucigalpa, Honduras who came to Baton Rouge in 2009 to study electrical engineer. Aquiles has spent ten years developing his professional research and engineering skills at Louisiana State University. He has worked in the BioMEMS laboratory since 2013 with pioneering work in better understanding neurostimulation technology. Teaching is one of his passions and he was a teaching assistant for several courses in the Division of Electrical and Computer Engineering. He also enjoyed helping other students by working as a tutor from 2010 until 2016. Aquiles will join his wife Maria Quinones in Orlando, Florida, and hopes to work in industry or as a professor one day.